elektronisches
dokument
ULB Sachsen-Anhalt

Dynamics of quantum systems driven by half-cycle electromagnetic pulses

Dissertation

zur Erlangung des akademischen Grades

doctor rerum naturalium (Dr. rer. nat.)

vorgelegt der

Mathematisch-Naturwissenschaftlich-Technischen Fakultät
(mathematisch-naturwissenschaftlicher Bereich)
der Martin-Luther-Universität Halle-Wittenberg

von Herrn Alex Matos Abiague
geb. am: 6 December 1969 in Santiago de Cuba, Cuba

Gutachter:
1. PD. Dr. Jamal Berakdar
2. Prof. Dr. Volker Engel
3. Prof. Dr. Wolfram Hergert

Halle/Saale, 12 Oktober 2004

urn:nbn:de:gbv:3-000008160
[http://nbn-resolving.de/urn/resolver.pl?urn=nbn%3Ade%3Agbv%3A3-000008160]

Within the framework of the present Thesis, the following papers have been published:

1. A. Matos-Abiague and J. Berakdar, Controlling the orientation of polar molecules by half-cycle pulses, Chem. Phys. Lett., **382**, 475 (2003).

2. A. Matos-Abiague and J. Berakdar, Sustainable orientation of polar molecules induced by half-cycle pulses, Phys. Rev. A **68**, 063411 (2003).

3. A. Matos-Abiague and J. Berakdar, Ultrafast control of electron motion in quantum well structures, Appl. Phys. Lett. **84**, 2346 (2004).

4. A. Matos-Abiague and J. Berakdar, Emission spectrum of an electron in a double quantum well driven by ultrashort half-cycle pulses (to appear in Phys. Scripta).

5. A. Matos-Abiague and J. Berakdar, Femtosecond control of electronic motion in semiconductor double quantum wells, Phys. Rev. B **69**, 155304 (2004).

6. A. Matos-Abiague and J. Berakdar, Emission spectrum of a mesoscopic ring driven by fast unipolar pulses, Phys. Lett. A, **330**, 113 (2004).

7. A. Matos-Abiague and J. Berakdar, Field-free charge polarization of mesoscopic rings, Phys. Rev. B **70**, 195338 (2004).

8. A. Matos-Abiague and J. Berakdar, Ultrafast build-up of polarization in mesoscopic rings, Europhys. Lett. **69**, 277 (2005).

9. A. Matos-Abiague and J. Berakdar, Photo-induced charge currents in mesoscopic rings (accepted in Phys. Rev. Lett.).

10. A. Matos-Abiague and J. Berakdar, Aharonov-Anandan phase and the quasistationarity of driven quantum systems (submitted).

Table of Contents

Table of Contents **i**

Acknowledgements **iii**

Abstract **iv**

1 Introduction **1**

2 Half-Cycle Pulses (HCPs) **3**
- 2.1 General overview 3
- 2.2 Experimental generation of HCPs 3
- 2.3 HCPs and *kicked* quantum systems 5

3 Dynamics of driven quantum systems **8**
- 3.1 Generalized Bloch vector approach (GBVA) 8
- 3.2 Floquet approach (FA) 14
- 3.3 Splitting operator approach 17

4 Quasistationarity of a time-dependent quantum state **22**
- 4.1 General definitions 22
- 4.2 Quasistationarity within the GBVA 27
- 4.3 Quasistationarity within the FA 30

5 Sustainable orientation of polar molecules **34**
- 5.1 General formulation 36
  - 5.1.1 Analytical approach 39
  - 5.1.2 Numerical approach 42
- 5.2 Orienting NaI molecules 43

6 Control of electronic motion in double quantum wells **48**
- 6.1 General formulation 49
  - 6.1.1 Numerical approach 50
  - 6.1.2 Analytical approach 50

6.2 Coherent control of the electron dynamics 52
    6.2.1 Tunnelling initial condition 52
    6.2.2 Optical initial condition 60

7 HCPs induced currents in ballistic mesoscopic rings 63
7.1 Postpulse polarization of mesoscopic rings 64
7.2 Field-free currents in mesoscopic rings 73

8 Conclusions 84

Zusammenfassung 86

A Products: Definitions and properties. 88

B Solving the TDSE for kicked systems 90

C Floquet analysis of a kicked two-level system 93

D Sums involving Bessel functions 95

Bibliography 96

Acknowledgements

I would like to express my gratitude to my supervisor PD Dr. Jamal Berakdar for his support, attention, and precious suggestions during the accomplishment of this research.

I appreciate the discussions with my colleagues during our seminars at the Theory Department of the Max Planck Institute of Microstructure Physics, where many of the ideas and results here reported were debated. In particular Prof. Patrick Bruno, Dr. Vitalii Dugaev, and PD Dr. Leonid Sandratskii are specially acknowledged for asking the right questions that guided me to improve several definitions and ideas exposed throughout this work.

I am grateful to Dr. Konstantin A. Kouzakov, Dr. Tribhuvan P. Pareek, and Dr. Georges Bouzerar for our *very informal* but fruitful scientific discussions.

I thank Prof. Melquiades de Dios Leyva and Prof. Luis E. Oliveira for their guidance during my first research experiences at the University of Havana.

Many thanks to my Cuban and Bulgarian friends and to the friends I found in the MPI for their warm friendship and to all the people at the MPI who helped me in one way or another.

Last but not least, I wish to thank the unconditional support, help, encourage, and love of my families (both that near the Black Sea and the one near the Caribbean Sea).

Alex Matos Abiague
Halle (Saale), Germany
March 16, 2004

Abstract

A variety of phenomena that are not accessible within the ordinary stationary quantum mechanics emerges when subjecting a quantum system to a time-dependent external field. The possibility of controlling the dynamics of quantum systems becomes then an issue of great importance from both the fundamental and the practical points of view. The designing of efficient electro-optical devices, the control of chemical reactions, the creation of entangled states, and the realization of quantum computation are just few examples of the potential applications that could result from an efficient dynamical control process.

When a quantum system is subject to the action of half-cycle pulses (HCPs), because of their highly asymmetric nature, some effects, qualitatively different to those resulting when employing continuous wave lasers or nearly symmetric laser pulses as the driving fields can occur. In the present work we investigate the possibility of controlling the dynamics of quantum systems driven by HCPs and under which conditions can the control process be sustainable in time. The dynamics of three specific physical systems is studied.

The first quantum system considered here consists of a polar diatomic molecule driven by a train of HCPs. Based on a simple analytical model we were able to estimate the characteristics and parameters of the train of HCPs that is capable of inducing a strong and sustainable molecular orientation in the non-adiabatic regime. In addition, the optimization of the control process was performed for the NaI molecule through full numerical calculations. The obtained results show that the molecular orientation obtained within our scheme is stronger than that obtained within previous methods and that it is robust to thermal average up to temperatures of about 10 K.

An electron confined in a symmetric double quantum well driven by HCPs is the second specific system investigated in the present work. It is shown that when subjecting such a system to an appropriately designed train of HCPs both the motion and the emission spectrum of the electron can be engineered on a subpicosecond time scale. Some interesting phenomena such as low-frequency and half-harmonic generations as well as the coherent suppression of tunnelling in the absence of quasienergy degeneracy are predicted to occur.

Finally, we investigate the dynamical properties of a ballistic thin mesoscopic ring (MR) subject to the action of HCPs. We show that the application of a single HCP on a ballistic thin MR can result in a postpulse, ultrafast build-up of the polarization of the ring. We also show that when a ballistic thin MR is exposed to the action of two orthogonal, linearly polarized HCPs, a non-equilibrium current can be induced in the ring. The induced non-equilibrium current lasts as long as the coherence of the wave function of the carriers is preserved and its peak value can be more than one order of magnitude greater than the persistent currents measured in ballistic MRs. Some potential applications and the possibility of experimentally detecting the postpulses non-equilibrium current are also discussed.

Chapter 1

Introduction

The study of both fundamental and experimental aspects concerning the dynamics of quantum systems constitutes a major area of investigation. Much progress in the creation of new principle and techniques towards achieving the long-standing dream of controlling the quantum dynamics of physical systems has been made in the last few decades. From the fundamental point of view the study of explicitly time-dependent quantum systems results a topic of great interest because it gives the possibility of revealing novel phenomena that are not accessible within ordinary stationary quantum mechanics. From the practical viewpoint, the control of the dynamics of quantum systems can result in a wide variety of applications, e.g., the control of chemical reactions, the stabilization of a given configuration of an atom or molecule, and the creation of entangled states. The coherent control of the quantum dynamics of physical systems is also highly desirable for potential applications in designing electro-optical devices and is essential for the realization of quantum computation.

The control of the dynamics of a quantum system requires the appropriate design of the driving external fields capable to induce a desired time evolution to the system under investigation. Thus, a considerable amount of investigations has been devoted to the development of new principles and techniques for generating more sophisticated sources of electromagnetic fields. In particular it has recently been possible the generation of highly asymmetric mono-cycle pulses composed of a short and strong tail [called a half-cycle pulse (HCP)] followed by a long and weak tail of opposite polarity. Experiments realized by exposing Rydberg atoms to trains of HCPs have shown that the effects induced by the HCPs can be qualitatively different to those resulting when the atoms are subject to continuous wave lasers or nearly symmetric laser pulses. The experimental and theoretical investigations of the dynamics of quantum systems driven by HCPs have been limited, until now, to the study of the ionization and dynamical stabilization of Rydberg atoms subject to trains of HCPs. In the present work we explore the possibility of controlling the dynamics of different quantum systems [such as polar diatomic molecules, double quantum wells, and ballistic mesoscopic rings (MRs)] exposed to the action of HCPs. We show that a conveniently designed train of HCPs can lead to a fast and efficient control of the time evolution of quantum systems. Phenomena such as non-adiabatic, sustainable molecular orientation of a polar diatomic molecule and half-harmonic generation together with the coherent suppression of tunnelling in the absence of quasienergy degeneracy in a double quantum well are shown to occur as a consequence of the peculiar nature of the HCPs. The possibility of inducing field-free currents in a ballistic thin MR subject to two linearly polarized, orthogonal HCPs is another interesting effect that is addressed in the present work.

In Chap. 2 we present an overview of the properties, characteristics, and experimental generation of HCPs.

General methods such as the generalized Bloch vector approach, the Floquet formalism, and a numerical algorithm based on the splitting operator approach are discussed in Chap. 3 and are used throughout our study of the dynamics of driven quantum systems.

The definition of quasistationarity of a time-dependent quantum state is introduced in Chap. 4, where the necessary and sufficient conditions for inducing quasiperiodic quasistationarity to a quantum system driven by an external time-dependent field are discussed within the generalized Bloch vector approach and the Floquet formalism.

The sustainable orientation of a polar diatomic molecule induced by a conveniently designed train of HCPs is investigated in Chap. 5 by means of a simplified analytical model and full numerical calculations.

An study of the dynamics and emission properties of an electron in a double quantum well driven by a train of HCPs is given in Chap. 6.

The dynamical properties of electrons confined in a ballistic thin MR and subject to linearly polarized HCPs are investigated in Chap. 7, where the possibility of generating a postpulses current in the ring is discussed.

Finally, conclusions are summarized in Chap. 8 and some appendices are introduced as an additional complement to the chapters.

Chapter 2

Half-Cycle Pulses (HCPs)

2.1 General overview

The control of the dynamics of a quantum system requires the appropriate design of external fields capable of driving the system under investigation to a desired time evolution. Various difficulties (imposed by technical limitations or by the *quantum nature* itself) can then originate in the control process. In particular, the full control in designing electromagnetic fields still constitutes a challenge for experimentalists. Nevertheless, an enormous progress in the development of new principles and techniques for creating more powerful, efficient, and sophisticated sources of electromagnetic fields has been achieved in the last decades. Laser techniques available nowadays allow for the generation of electromagnetic pulses as intense as $\sim 10^{20}$ W/cm^2 (the so-called petawatt laser pulses [1]) and ultrashort pulses with durations in the femtosecond [2, 3] and even in the attosecond [4, 5] regimes. In these pulses the electric field oscillates in time between the opposite polarities in a nearly symmetric way. However, in the last years, it has also been possible to produce highly asymmetric pulses. Of particular interest are the asymmetric pulses composed by a single optical cycle. Such highly asymmetric mono-cycle pulses are composed by a sharp tail with a given polarity followed by a smooth tail of opposite polarity. As the amplitude (duration) of the sharp tail is usually much larger (shorter) than the amplitude (duration) of the smooth one, the dynamics of a system driven by such a pulse is, in general, determined by the sharp tail. For this reason the sharp tail is called a half-cycle pulse (HCP). In what follows we will refer to the entire mono-cycle pulse and its sharp tail as the full pulse and the HCP, respectively, while the smooth tail will be referred just as the tail.

2.2 Experimental generation of HCPs

HCPs are usually generated by illuminating a wafer of biased gallium-arsenide (GaAs) semiconductor with a short pulse from a Ti:Sapphire chirped-pulse amplifier [6, 7]. The GaAs wafer is photoconductive with a band gap of approximately 1.4 eV. The bias electric field is then shorted across the semiconductor surface when one side of the wafer is illuminated with the $\sim$ 770 nm laser pulse, which drives the GaAs into conduction. Due to the bias

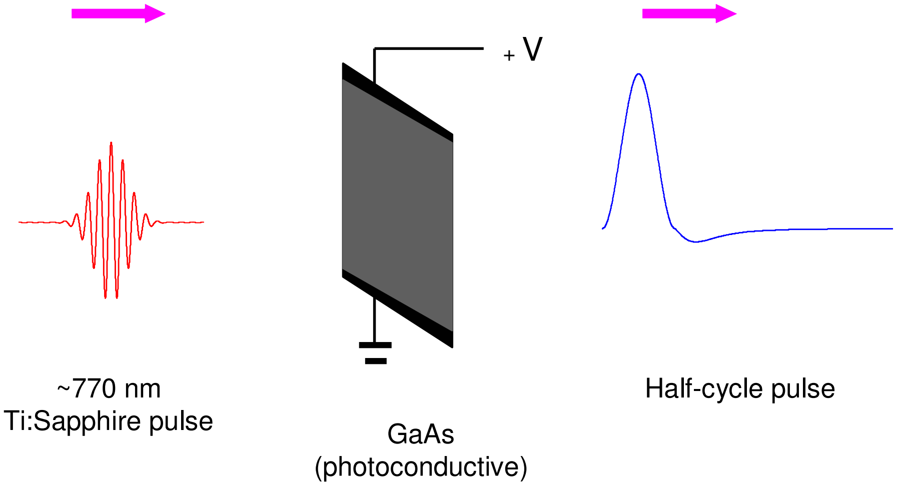

Figure 2.1: Schematics of the experimental procedure for generation of a HCP [6, 7, 8].

field, the electrons quickly accelerate when the Ti:Sapphire pulse hits the wafer and radiate a short (nearly unipolar) coherent electromagnetic pulse (i.e., the HCP) which propagates away from the wafer. The radiated HCP is polarized in the direction of the bias field and its strength depends linearly on the bias field strength. A schematic representation of the generation of a HCP is shown in Fig. 2.1.

Once the Ti:Sapphire laser pulse has past, the GaAs wafer returns to the insulating state. However, this transition is much slower than the conduction band transition and the electrons decelerate over a period of hundreds of picoseconds [8]. This deceleration produces the subsequent tail with opposite polarity to that of the HCP (see Fig. 2.2). The peak field of the tail is usually much smaller than the peak amplitude of the HCP. An amplitude asymmetry ratio of $\sim 10:1$ can be appreciated in Fig. 2.2, where the temporal profile of an experimentally obtained HCP [6] is displayed. HCPs with amplitude asymmetry ratio of $\sim 13:1$ have also been experimentally obtained [6, 7, 9]. It is also notable that the amplitude of the tail is significantly different from zero only during a time interval few times longer than the HCP duration (see Fig. 2.2). We will refer to this part of the pulse as the effective part of the tail. In Fig. 2.3 we summarize all the components of a highly asymmetric mono-cycle pulse.

Within the above discussed procedure, HCPs with peak field of up to several hundreds of kV/cm and duration in the picosecond and subpicosecond regimes can be experimentally generated nowadays [6, 7, 9]. Furthermore, new theoretical alternatives for generating shorter and stronger unipolar pulses have recently been proposed [10, 11, 12, 13]. Based on these novel principles unipolar pulses as short as 0.1 fs and with intensities up to 10^{16} W/cm^2 could be generated in the near future [10, 11].

Other aspect that deserves to be commented is the possibility of experimentally combining two or more HCPs. The Fig. 2.4 shows a diagram of an apparatus utilized for combining two orthogonal, linearly polarized HCPs with a relative delay between them that can be experimentally controlled [9]. Two biased GaAs wafers oriented at right angles with respect

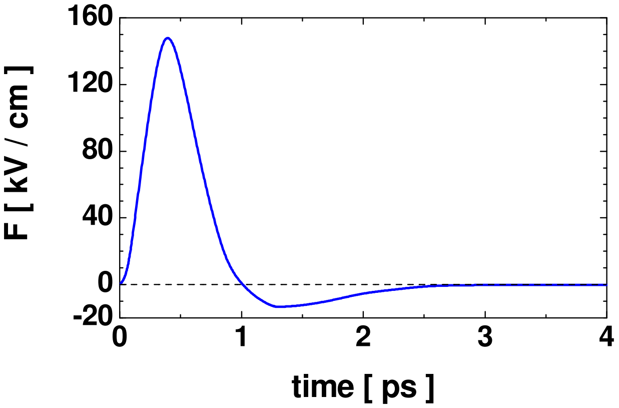

Figure 2.2: Typical pulse shape of an experimentally obtained HCP [6]. The HCP is approximately 1 ps in duration, while the negative tail persists for hundreds of picoseconds.

to each other produce two counterpropagating HCPs with orthogonal linear polarization (see Fig. 2.4). The peak field is varied by changing the bias voltage on both GaAs switches simultaneously, while the polarization of the resultant field is varied continuously by increasing the relative delay between the two Ti:Sapphire laser pulses used to illuminate the GaAs wafers. In the particular case the time delay between the two counterpropagating HCPs equals one-half of the HCP duration, a quarter-cycle analog of a circularly polarized pulse is produced. Such subpicosecond quarter-cycle circularly polarized pulses have been employed in the experimental investigation of the ionization of Na Rydberg atoms [9]. Similar methods for combining linearly polarized HCPs with polarizations in the same direction and used for designing trains of HCPs are also experimentally available [14, 15, 16, 17, 18, 19]. Note however, that in the case of combining linearly polarized HCPs with the same polarization it is convenient to choose an appropriate value of the time delay in order to avoid the overlapping between the effective tail of each mono-cycle pulse and the HCP of the subsequent one.

2.3 HCPs and *kicked* quantum systems

Because of their high asymmetry, the nature of HCPs and symmetric (or nearly symmetric) fields [e. g., continuous wave (CW) lasers and laser pulses] is qualitatively different. A key difference is that unlike CW lasers or laser pulses a HCP can deliver a non-zero momentum transfer to the system over a large number of optical half-cycles (for the case of a highly asymmetric mono-cycle pulse an optical half-cycle refers to the duration of the HCP). The impulse $\mathbf{\Delta p}$ transferred to a system by an electromagnetic field is, in general, determined by the time integral of the field, i.e., [14, 15, 16, 17, 18, 19]

$$\mathbf{\Delta p} = \int \mathbf{F}(t)dt \ , \tag{2.3.1}$$

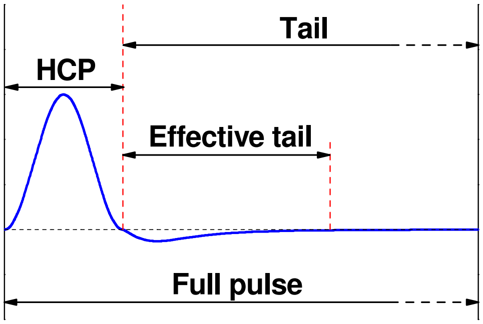

Figure 2.3: Parts of a highly asymmetric mono-cycle pulse

where $\mathbf{F}(t)$ is the time-dependent electric field. In the cases of CW lasers and laser pulses, the electric field oscillates between opposite polarities and, as different polarities deliver opposite momenta, the net transfer of momentum over an optical cycle is nearly zero (exactly zero for CW lasers). This situation drastically changes when HCPs are considered because of their nearly unipolarity. A HCP delivers a non-zero momentum transfer that is slightly decreased (remember the asymmetry ratio can be 13:1) by the subsequent effective part of the tail (see Fig. 2.3). The net momentum the field transfers to the system continuously decreases in time and vanishes over a period corresponding to the duration of the full pulse. However, the duration of the full pulse is, usually, several hundreds of times greater than the HCP duration and the net momentum transferred by the HCP goes to zero very slowly [note that after the effective part of the tail the field is extremely weak compared to the HCP peak field (see Figs. 2.2 and 2.3)]. Therefore, a net non-zero transfer of momentum, essentially determined by the HCP, becomes sustainable over a time period much shorter than the duration of the full pulse (note that such a period can still be quite large as compared to the HCP duration). This peculiarity of the HCPs has opened new possibilities for the experimental realization of *kicked* quantum systems [14, 15, 16, 17, 18, 19]. If the characteristic time corresponding to the system under investigation is much longer than the duration of the HCP (but still shorter than the duration of the full pulse) the interaction of the system with the HCP can be interpreted, in good approximation, as an instantaneous momentum transfer or impulsive *kick* received by the system from the HCP. Within this approximation, usually called impulsive approximation (IA) [20, 21], the interaction of the system under investigation with a train of HCPs is given by [17, 18, 19]

$$V(r,t) \sim \mathbf{r}.\sum_{k=1}^{N} \mathbf{\Delta p}_k \delta(t-t_k) \quad , \tag{2.3.2}$$

where $\mathbf{\Delta p}_k = \int \mathbf{F}_{HCP}(t)dt$ is the momentum transferred to the system by the kth HCP [14, 15, 16, 20] , N is the number of applied HCPs (or kicks), $\delta(x)$ is the Dirac delta function and t_k corresponds to the time of application of the kth kick.

Kicked quantum systems have been experimentally realized by exposing highly exited Rydberg atoms to trains of HCPs [7, 9, 14, 16, 17, 18, 19]. The classical orbital period associated to the highly exited Rydberg atom is much longer than the duration of the

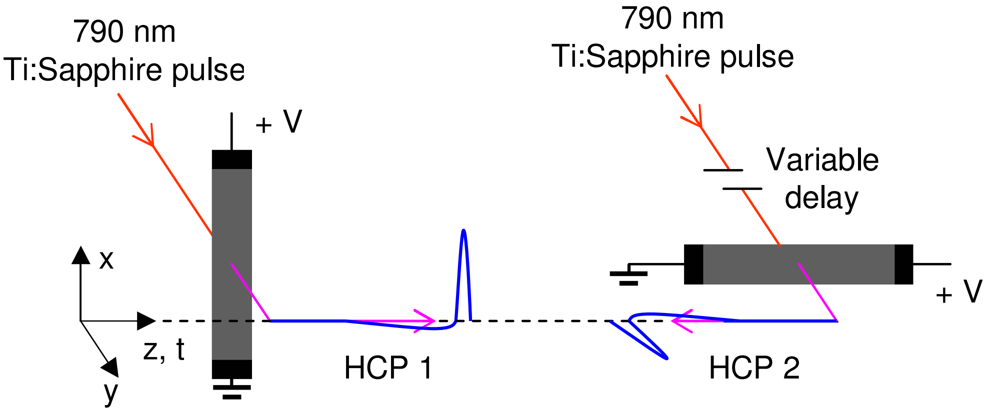

Figure 2.4: Diagram of the apparatus utilized for creating two counterpropagating orthogonal, linearly polarized HCPs [9].

HCPs and, consequently, the train of HCPs can be modelled as a series of impulsive kicks [16, 17, 18, 19]. On the basis of this considerations the ionization and dynamical stabilization of Rydberg atoms subject to trains of HCPs have been extensively investigated from both experimental and theoretical points of view [7, 14, 16, 17, 18, 19, 22, 23]. The possibility of creating, designing, and probing electronic wave packets by using HCPs has also been explored [14, 19, 24]. Furthermore recent theoretical investigations [21, 25] have suggested that HCPs could also be useful for orienting polar molecules.

From all the above mentioned studies (both experimental and theoretical) we can conclude that for HCPs with duration much shorter than the characteristic time of the system under investigation the impulsive approximation gives rather good results and that for an asymmetry ratio between the HCP and the tail greater than 10:1 the effects of the effective tail hardly affect the dynamics of the system, i.e., in this limit the system dynamics is determined by the HCP only.

Chapter 3

Dynamics of driven quantum systems

The dynamics of a non-relativistic quantum system subject to an external time-dependent field is described by the Schrödinger equation

$$i\hbar \frac{\partial \Psi}{\partial t} = H\Psi \quad , \tag{3.0.1}$$

where the Hamiltonian of the system can be written as

$$H = H_0 + V(r,t) \tag{3.0.2}$$

being H_0 the Hamiltonian of the field-free system and $V(r,t)$ represents the interaction of the system with the external time-dependent field.

In the present chapter we describe three different approximations for solving the time-dependent Schrödinger equation (3.0.1). We firstly present, in Sec. 3.1 a generalization of the Bloch vector approach to the case of an arbitrary N-level quantum system. A second approach (the so-called Floquet theory), particularly useful for the case of time-periodic external fields, is briefly reviewed in Sec. 3.2. Finally, in Sec. 3.3 we describe a numerical scheme based in the splitting operator approximation for propagating the wave function of the system through time.

3.1 Generalized Bloch vector approach (GBVA)

The main idea of the Bloch vector approach consists in performing a transition from the complex spinor space of the wave function to the real space of a coherence vector called the Bloch vector. The dynamics of the system then reduces to rotations of the (real) Bloch vector, giving, at qualitative level, a clear and comprehensive picture of the system evolution. The approach was originally formulated for the description of magnetic phenomena and is based on the equation (see, for example, Ref. [26, 27])

$$\frac{\partial \mathbf{S}}{\partial t} = \gamma \mathcal{B} \times \mathbf{S} \tag{3.1.1}$$

that describes the spin dynamics (characterized by the Bloch vector $\mathbf{S}$) of a spin system subject to an external magnetic field $\mathcal{B}$. In Eq. (3.1.1) γ represents the gyromagnetic ratio.

Although the Bloch vector approach was in principle formulated for the description of spin systems, R. P. Feynman and coworkers [28] demonstrated that the Bloch vector can also be used for describing nonspin systems. The standard treatment is valid only for spins or other physical systems whose energy levels are equally spaced [27, 28, 29]. However, a generalization (and that is why we call it the GBVA) of the standard Bloch vector approach that is valid for any N-level non-relativistic quantum system interacting with external forces of arbitrary strength and time dependence can be formulated, as shown in Refs. [30, 31, 32].

For an N-level system the solutions of (3.0.1) can be expanded on the eigenvectors of the stationary states $|k\rangle$ of the unperturbed system (that we assume are known) as follows

$$|\Psi(t)\rangle = \sum_{k=1}^{N} C_k(t)|k\rangle \quad , \tag{3.1.2}$$

where the stationary states $|k\rangle$ obey

$$H_0|k\rangle = E_k^{(0)}|k\rangle \quad , \tag{3.1.3}$$

with $E_k^{(0)}$ the energy corresponding to the kth unperturbed level. The Hamiltonian (3.0.2) can then be rewritten as

$$H(t) = \sum_{k=1}^{N} E_k^{(0)} P_{kk} + \sum_{k,l=1}^{N} V_{kl}(t) P_{kl} \quad , \tag{3.1.4}$$

where $P_{kl} = |k\rangle\langle l|$ are projection operators and $V_{kl}(t) = \langle k|V(r,t)|l\rangle$.

The N^2 projection operators P_{kl} are the generators of the U(N) group . However, for our purposes it is convenient to perform a transition from these operators to operators of SU(N). This transition can be done by introducing the following SU(N) operators [33]

$$Q_{kl} = P_{kl} - \delta_{kl}\left(\frac{\mathcal{I}_N}{N}\right) \quad , \tag{3.1.5}$$

where δ_{kl} and $\mathcal{I}_N$ are the Kronecker delta function and the $(N\times N)$ unit matrix, respectively. In terms of the new operators Q_{kl}, the Hamiltonian (3.1.4) can be rewritten as

$$H(t) = \frac{1}{N}\left(\sum_{k=1}^{N} V_{kk}(t)\right)\mathcal{I}_N + \mathcal{H}(t) \quad , \tag{3.1.6}$$

where

$$\mathcal{H}(t) = \sum_{k=1}^{N} E_k Q_{kk} + \sum_{k,l=1}^{N} V_{k,l}(t) Q_{kl} \quad , \tag{3.1.7}$$

and

$$E_k = E_k^{(0)} - \frac{1}{N}\sum_{k=1}^{N} E_k^{(0)} \quad . \tag{3.1.8}$$

The operator $\mathcal{H}(t)$ belongs to the SU(N) group and can therefore be expanded in the generators of SU(N), i.e.,

$$\mathcal{H}(t) = \sum_{i=1}^{N_D} a_i(t)\mathcal{F}_i = \mathbf{A}(t) \cdot \hat{\mathcal{F}} \quad , \tag{3.1.9}$$

where

$$\mathbf{A}(t) = \Big(a_1(t), a_2(t), ..., a_{N_D}(t)\Big) \quad , \tag{3.1.10}$$

and

$$\hat{\mathcal{F}} = \Big(\mathcal{F}_1, \mathcal{F}_2, ..., \mathcal{F}_{N_D}\Big) \quad . \tag{3.1.11}$$

In the equations above $N_D = \dim[\mathrm{SU}(N)] = N^2 - 1$, $\mathcal{F}_i$ are the N_D generators of the SU(N) group, and the expansion coefficients a_i can be found by solving the corresponding N_D-dimensional system of linear equations. We note that the expansion (3.1.9) is more convenient than (3.1.7) because, unlike the operators Q_{kl}, the generators $\mathcal{F}_i$ are linearly independent.

If the generators $\mathcal{F}_i$ are chosen in such a way to satisfy

$$\mathrm{Tr}[\mathcal{F}_i, \mathcal{F}_j] = 2\delta_{ij} \quad , \tag{3.1.12}$$

then the expansion coefficients can be expressed as

$$a_i(t) = \mathrm{Tr}[\mathcal{H}(t)\mathcal{F}_i] \quad . \tag{3.1.13}$$

Note that the generators are defined as in [30, 32, 33] and are one half of the Gell-Mann F-spin operators [33].

The wave function of the system is completely determined by the vector $\mathbf{C}(t)$ whose components are the expansion coefficients $C_k(t)$ ($k = 1, 2, ..., N$) in Eq. (3.1.2). According to Eqs. (3.1.2), (3.1.6), and (3.1.9) the vector $\mathbf{C}(t)$ satisfies

$$i\hbar\frac{\partial \mathbf{C}(t)}{\partial t} = \left[\frac{1}{N}\left(\sum_{k=1}^{N} V_{kk}(t)\right)\mathcal{I}_N + \frac{1}{2}\mathbf{A}(t) \cdot \hat{\mathcal{F}}\right]\mathbf{C}(t) \quad . \tag{3.1.14}$$

The vector $\mathbf{C}(t)$ is an N-dimensional complex vector. It is convenient, however, to perform a transition to a real space. Such a transition can be done through a transformation from U(N) [or SU(N) in the case $V_{kk} = 0$] to SO(N_D) by introducing the generalized (real) Bloch vector $\mathbf{B}(t) = \Big(B_1(t), B_2(t), ..., B_{N_D}(t)\Big)$ through the following map Ξ,

$$\mathbf{C}(t) \in \mathbb{C}^N \ : \ \Xi\left(\mathbf{C}(t)\right) = \mathbf{B}(t) = \mathbf{C}^\dagger(t)\hat{\mathcal{F}}\mathbf{C}(t) \in \mathbb{R}^{N_D} \quad . \tag{3.1.15}$$

For the case of two-level systems the map Ξ resembles a Hopf map (see for example [34, 35, 36]). Note that we represented the standard Bloch vector by $\mathbf{S}$ in Eq. (3.1.1) and from now on we use $\mathbf{B}$ for denoting the generalized Bloch vector.

From Eq. (3.1.15) one can find the following relations [30]

$$\rho(t) = \frac{\mathcal{I}_N}{N} + \frac{1}{2}\sum_{i=1}^{N_D} B_i(t)\mathcal{F}_i = \frac{\mathcal{I}_N}{N} + \frac{1}{2}\mathbf{B}(t) \cdot \hat{\mathcal{F}} \quad , \tag{3.1.16}$$

and

$$B_i(t) = \mathrm{Tr}[\rho(t)\mathcal{F}_i] \ , \tag{3.1.17}$$

where $\rho(t)$ represents the density matrix.

In the particular case $V_{kk} = 0$ and $N = 2$, Eq. (3.1.14) reduces to

$$i\hbar\frac{\partial \mathbf{C}(t)}{\partial t} = \frac{1}{2}\left[\sum_{i=1}^{3} a_i(t)\sigma_i\right]\mathbf{C}(t) \ , \tag{3.1.18}$$

where σ_i are the Pauli matrices. In this special case, the Hamiltonian belongs to SU(2). Since SU(2) and SO(3) are isomorphic, one can write by homomorphism the corresponding equation for the 3-dimensional Bloch vector $\mathbf{B}(t)$, directly from Eq. (3.1.18), i.e.,

$$i\hbar\frac{\partial \mathbf{B}(t)}{\partial t} = \frac{1}{2}\left[\sum_{i=1}^{3} a_i(t)J_i\right]\mathbf{B}(t) \ , \tag{3.1.19}$$

where J_i are the angular momentum operators, generators of SO(3).

The above discussed procedure for obtaining the corresponding equation for $\mathbf{B}(t)$ is, however, quite restrictive. It requires not only that $V_{kk} = 0$ but also the isomorphism (more precisely the homomorphism) between the groups SU(N) and SO($N^2 - 1$), something that is possible only if $N = 2$. Therefore, in the general case, the equation for $\mathbf{B}(t)$ has to be obtained from its definition (3.1.15). By introducing the antisymmetric structure constants [33],

$$f_{jkl} = -\frac{i}{4}\mathrm{Tr}\left([\mathcal{F}_j, \mathcal{F}_k]\mathcal{F}_l\right) \ , \tag{3.1.20}$$

and the symmetric coefficients [33],

$$d_{jkl} = \frac{1}{4}\mathrm{Tr}\left(\{\mathcal{F}_j, \mathcal{F}_k\}\mathcal{F}_l\right) \tag{3.1.21}$$

of the Lie algebra of SU(N), it is possible to define the following inner products [37, 38] for any two N_D-dimensional real vectors $\mathbf{X}$ and $\mathbf{Y}$ (for a detailed discussion of the different products and their properties see Appendix A),

$$(\mathbf{X} \wedge \mathbf{Y})_j = f_{jkl}X_kY_l \ , \tag{3.1.22}$$

$$(\mathbf{X} \star \mathbf{Y})_j = d_{jkl}X_kY_l \ , \tag{3.1.23}$$

where the Einstein's summation convention has been assumed. Then, after some mathematical manipulations, one can obtain from Eqs. (3.1.14), (3.1.15), (3.1.22), and (3.1.23) that the N_D-dimensional generalized Bloch vector satisfies the equation

$$\frac{\partial \mathbf{B}(t)}{\partial t} = \frac{1}{\hbar}\left(\mathbf{A}(t) \wedge \mathbf{B}(t)\right) \ , \tag{3.1.24}$$

with $\mathbf{A}(t)$ given by (3.1.10).

Taking into account that the structure constants f_{jkl} are totally antisymmetric under exchange of any two indices, we can rewrite (3.1.24) in matrix form as

$$\frac{\partial \mathbf{B}(t)}{\partial t} = \mathcal{A}(t)\mathbf{B}(t) \ , \tag{3.1.25}$$

where $\mathcal{A}(t)$ is an $(N_D \times N_D)$ real matrix whose elements $\tilde{a}_{kl}(t)$ are given by

$$\tilde{a}_{kl}(t) = \frac{i}{2\hbar}\mathrm{Tr}\left([\mathcal{F}_k, \mathcal{F}_l]\mathcal{H}(t)\right) \ . \tag{3.1.26}$$

The formal solution of Eq. (3.1.25) can be expressed as

$$\mathbf{B}(t) = U(t, t_0)\mathbf{B}(t_0) \ , \tag{3.1.27}$$

where the evolution operator from t_0 to t is given by

$$U(t, t_0) = T_t \exp\left[\int_{t_0}^{t} \mathcal{A}(t)dt\right] \ , \tag{3.1.28}$$

with T_t representing the time ordering operator. The evolution operator in (3.1.28) belongs to SO(N_D), i.e., it represents a rotation of the vector $\mathbf{B}(t_0)$ in the Euclidean generalized Bloch space. Therefore the action of $U(t, t_0)$ preserves the scalar product and the length of the generalized Bloch vector is a constant of motion ($|\mathbf{B}(t)| = \text{const.}$).

The length of the generalized Bloch vector $\mathbf{B}(t)$ can easily be calculated by taking $\mathbf{C} = \frac{1}{\sqrt{N}}(1, 1, ..., 1)^T$ in Eq. (3.1.15). One then obtains $B_i = \xi_i/N$, where ξ_i represents the sum over all the elements of the generator $\mathcal{F}_i$. Non-vanishing values of ξ_i are found only for the $N(N-1)/2$ non-diagonal symmetric generators, for which $\xi_i = 2$ [33]. Consequently, the length of $\mathbf{B}(t)$ is given by

$$|\mathbf{B}(t)| = \sqrt{\sum_{i=1}^{N_D} B_i^2} = \sqrt{\frac{2(N-1)}{N}} \quad ; \quad \forall\, t \ . \tag{3.1.29}$$

It is well known that for the case $N = 2$ the evolution of the system in the generalized Bloch space corresponds to the motion of a point in the two-dimensional unit sphere $\mathbb{S}^2$, embedded in the Euclidean three-dimensional space $\mathbb{R}^3$ [27, 28, 29, 37]. One could, naively, think that the domain $\mathbb{D}_N$ of evolution of an N-level system in the generalized Bloch space will correspond to a hypersphere $\mathbb{S}^{N_D - 1}$ of radius $|\mathbf{B}(t)|$ embedded in $\mathbb{R}^{N_D}$. This, however, is not strictly correct and for $N \geq 3$ (for the case $N = 3$, see for example, Ref. [37]) we will show that $\mathbb{D}_N \neq \mathbb{S}^{N_D - 1}$. The space of pure states (in the quantum mechanical sense, i.e., $\rho = |\Psi\rangle\langle\Psi|$) corresponds to a complex projective space $\mathbb{CP}^{N-1}$ in the Hilbert space $\mathbb{H}^N \simeq \mathbb{C}^N$. It is known that the real dimension of $\mathbb{CP}^{N-1}$ is equal to $2(N-1)$ [38, 39]. Therefore, the domain of evolution of an N-level system can be identified with a $2(N-1)$-dimensional submanifold of $\mathbb{R}^{N_D}$ and $\mathbb{D}_N$ is, in general, only a part of the hypersphere $\mathbb{S}^{N_D - 1}$ with radius $\sqrt{\frac{2(N-1)}{N}}$, i.e., $\mathbb{D}_N \subset \mathbb{S}^{N_D - 1} \subset \mathbb{R}^{N_D}$. It is clear now that $\mathbb{D}_N = \mathbb{S}^{N_D - 1}$ if, and only if, N satisfies $2(N-1) = N_D - 1$, a condition that holds only for $N = 2$.

It is worth noting note that Eq. (3.1.29) is, actually, equivalent to the condition $\mathrm{Tr}(\rho) = 1$. This condition, however, is not sufficient, in general, for guaranteeing the positivity of the density matrix ($\rho \geq 0$), i.e., a vector satisfying (3.1.29) does not necessarily imply the existence of a positive density matrix. We then search for further constraints on the generalized Bloch vector that guarantee the positivity of ρ.

In order to determine the domain $\mathbb{D}_N$ of evolution of an N-level system in the generalized Bloch vector space, we firstly note the following identity,

$$\begin{aligned}&\Big(\mathbf{B}(t) \star \mathbf{B}(t') + i\mathbf{B}(t) \wedge \mathbf{B}(t')\Big) \cdot \hat{\mathcal{F}} = \\ &\Big(\mathbf{B}(t) \cdot \hat{\mathcal{F}}\Big)\Big(\mathbf{B}(t') \cdot \hat{\mathcal{F}}\Big) - \frac{2}{N}\Big(\mathbf{B}(t) \cdot \mathbf{B}(t')\Big)\mathcal{I}_N \quad ; \quad \forall\, t, t' \ , \end{aligned} \tag{3.1.30}$$

that can be obtained from Eqs. (3.1.20) - (3.1.23) (for the details see Appendix A). By assuming $t = t'$ in the equation above and taking into account that for pure states ρ is a projector ($\rho^2 = \rho$) [note that this condition guarantees the positivity of the density matrix], we obtain from Eqs. (3.1.16) and (3.1.30) the relation

$$\frac{|\mathbf{B}(t)|^2}{N}\mathcal{I}_N + \frac{1}{2}\Big(\mathbf{B}(t) \star \mathbf{B}(t)\Big) \cdot \hat{\mathcal{F}} = \frac{2(N-1)}{N^2}\mathcal{I}_N + \frac{(N-2)}{N}\,\mathbf{B}(t) \cdot \hat{\mathcal{F}} \quad ; \quad \forall\, t \ . \tag{3.1.31}$$

From (3.1.31) one again obtains the condition (3.1.29) and a new constraint for $\mathbf{B}(t)$ is also obtained [38],

$$\Big(\mathbf{B}(t) \star \mathbf{B}(t)\Big) = \frac{2(N-2)}{N}\,\mathbf{B}(t) \quad ; \quad \forall\, t \ . \tag{3.1.32}$$

The domain of the N-level system in the generalized Bloch space is then determined by the points on the hypersphere $\mathbb{S}^{N_D-1}$ for which the corresponding generalized Bloch vectors satisfy Eq. (3.1.32), i.e.,

$$\mathbb{D}_N = \left\{\mathbf{B} \in \mathbb{R}^{N_D} \ \Big| \ \mathbf{B} \cdot \mathbf{B} = \frac{2(N-1)}{N}, \ \ \mathbf{B} \star \mathbf{B} = \frac{2(N-2)}{N}\,\mathbf{B}\right\} \subset \mathbb{S}^{N_D-1} \subset \mathbb{R}^{N_D} \quad . \tag{3.1.33}$$

For two-level systems mutually orthogonal vectors in the two-dimensional Hilbert space correspond to diametrically opposite points on $\mathbb{D}_2$ [37]. However, as a direct consequence of the asymmetry of $\mathbb{D}_N$, mutually orthogonal vectors in the N-dimensional Hilbert space $\mathbb{H}^N$ do not lead to antipodal points on $\mathbb{D}_N$ when $N \neq 2$ [note from Eq. (3.1.33) that if $\mathbf{B}(t) \in \mathbb{D}_N$ with $N \neq 2$, then $-\mathbf{B}(t) \notin \mathbb{D}_N$]. In fact, it results from (3.1.16) that

$$\mathrm{Tr}[\rho(t)\rho(t')] = \frac{1}{N} + \frac{1}{2}\,\mathbf{B}(t) \cdot \mathbf{B}(t') \ . \tag{3.1.34}$$

Therefore, as for pure states $0 \leq \mathrm{Tr}[\rho(t)\rho(t')] \leq 1$, one then obtain the following inequality relations [38],

$$-\frac{2}{N} \leq \mathbf{B}(t) \cdot \mathbf{B}(t') \leq \frac{2(N-1)}{N} \quad ; \quad \forall\, t, t' \ , \tag{3.1.35}$$

or, equivalently,

$$-\frac{1}{N-1} \leq \cos\vartheta \leq 1 \quad ; \quad \vartheta = \angle(\mathbf{B}(t), \mathbf{B}(t')) \ . \tag{3.1.36}$$

Consequently, mutually orthogonal states in $\mathbb{H}^N$ correspond, actually, to points with a maximum opening angle $\vartheta = \arccos\left(\frac{-1}{N-1}\right)$.

The representation of a given observable O (corresponding to the operator o) in the basis of the N stationary levels of the unperturbed system is given by

$$O = \sum_{k,l=1}^{N} O_{kl} P_{kl} \ , \tag{3.1.37}$$

where $O_{kl} = \langle k|o|l\rangle$.

Following the same procedure used for obtaining (3.1.6), one can rewrite (3.1.37) as [40]

$$O = \frac{1}{N}\left(\sum_{k=1}^{N} O_{kk}\right) I + \mathbf{W}\cdot\hat{\mathcal{F}} \ , \tag{3.1.38}$$

where $\mathbf{W}$ represents a vector whose components are the corresponding expansion coefficients.

In terms of the generalized Bloch vector, the expectation value $\langle O\rangle(t) = \langle\Psi|O|\Psi\rangle$ of the observable O can be calculated from the following relation

$$\langle O\rangle(t) = \mathbf{C}^{\dagger}(t) O \mathbf{C}(t) \ , \tag{3.1.39}$$

that leads to [40]

$$\langle O\rangle(t) = \frac{1}{N}\sum_{k=1}^{N} O_{kk} + \mathbf{W}\cdot\mathbf{B}(t) \ . \tag{3.1.40}$$

As previously commented, the motion of the system in the generalized Bloch space is restricted to the domain $\mathbb{D}_N$ specified in (3.1.33). Therefore, the possible values the observable $\langle O\rangle(t)$ can take are only those values corresponding to a point in $\mathbb{D}_N$. One can then calculate upper and lower bounds for the quantity $\langle O\rangle(t)$ through the optimization of (3.1.40) under the constraint that every point compatible with the evolution of the system must belong to $\mathbb{D}_N$ [40].

Two important aspects regarding the GBVA deserve to be remarked. The first one is that the GBVA is valid for every kind of time-dependent external perturbation, no matter their form or strength. The second one refers to the *price* that has to be paid for the elegance of the geometrical interpretation of the GBVA. This *price* is given by the fact that the dimension $N_D = N^2 - 1$ of the generalized Bloch space rapidly increases with N. Hence, quantitative calculations within the GBVA can become rather complicated for systems in which the number of levels involved in the system evolution is not small.

3.2 Floquet approach (FA)

In this section we consider the important case corresponding to a time periodic external field with period T, i.e., $V(r,t) = V(r, t+T)$. In such a case the Hamiltonian of the system [Eq. (3.0.2)] is invariant under discrete time translations, $t \to t + T$. Hence, one can study the system dynamics within the Floquet formalism [41, 42, 43, 44, 45]. The Floquet theorem states that for time periodic Hamiltonians there exist *particular* solutions (the so-called Floquet states) to Eq. (3.0.1) that have the form [41, 45]

$$|\Psi_\lambda(t)\rangle = e^{-i\varepsilon_\lambda t/\hbar}|\Phi_\lambda(t)\rangle \quad , \tag{3.2.1}$$

where ε_λ is a real-valued function of the system parameters and the function $|\Phi_\lambda(t)\rangle$, called a Floquet mode, is periodic in time with the same period of the external field, i.e.,

$$|\Phi_\lambda(t)\rangle = |\Phi_\lambda(t+T)\rangle \quad . \tag{3.2.2}$$

The substitution of Eq. (3.2.1) in the time dependent Scrödinger equation leads to the following eigenvalue problem

$$\mathcal{S}(t)|\Phi_\lambda(t)\rangle = \varepsilon_\lambda|\Phi_\lambda(t)\rangle \quad , \tag{3.2.3}$$

where

$$\mathcal{S}(t) = H(t) - i\hbar\frac{\partial}{\partial t} \quad ; \quad \mathcal{S}(t) = \mathcal{S}(t+T) \tag{3.2.4}$$

represents the Schrödinger operator [46]. Because of their analogy with the energies of the stationary states of the undriven system the eigenvalues ε_λ of (3.2.3) are termed *quasienergies* and in the limit of an external field switched off adiabatically, they become truly energies [45]. One can note from Eq. (3.2.3) that the Floquet modes

$$|\Phi_{\lambda'}(t)\rangle = e^{in\omega_0 t}|\Phi_\lambda(t)\rangle \quad ; \quad \omega_0 = \frac{2\pi}{T} \tag{3.2.5}$$

with n being an integer number ($n = 0, \pm1, \pm2, ...$) leads to a solution identical to that in (3.2.1), but with shifted quasienergy $\varepsilon_\lambda \to \varepsilon_{\lambda'} = \varepsilon_\lambda + n\hbar\omega_0$. The quasienergies are then unique up to multiples of $\hbar\omega_0$ and there is a whole class of solutions indexed by $\lambda' = (\lambda, n)$. Therefore, the quasienergies can be mapped into a first Brillouin zone, defined as $-\frac{\hbar\omega_0}{2} \leq \varepsilon \leq \frac{\hbar\omega_0}{2}$, and any solution from the equivalence class $\{\varepsilon_{\lambda'}, |\Phi_{\lambda'}(t)\rangle\}$ may be chosen to represent the Floquet state $|\Psi_\lambda(t)\rangle$.

The eigenvectors of the Schrödinger operator $\mathcal{S}(t)$ belong to the composite Hilbert space $\mathbb{H} = \mathbb{L} \otimes \mathbb{T}$ ($\mathbb{L}$ and $\mathbb{T}$ are the spaces of square integrable functions in the configuration space and of time periodic functions with period T, respectively) with the inner product [44, 45],

$$\langle\langle f|g\rangle\rangle = \frac{1}{T}\int_{t_0}^{t_0+T} \langle f|g\rangle dt \quad ; \quad f, g \in \mathbb{H} \quad . \tag{3.2.6}$$

Thus, the eigenvectors of $S(t)$ (i.e., the Floquet modes) obey the following orthonormality condition in the composite Hilbert space $\mathbb{H}$,

$$\langle\langle\Phi_{\lambda'}(t)|\Phi_{\nu'}(t)\rangle\rangle = \delta_{\lambda'\nu'} = \delta_{\lambda\nu}\delta_{nm} \quad , \tag{3.2.7}$$

and form a complete set in $\mathbb{H}$,

$$\sum_{\lambda'} |\Phi_{\lambda'}(t)\rangle\langle\Phi_{\lambda'}(t)| = \mathcal{I} \quad . \tag{3.2.8}$$

From the completeness of the Floquet modes in $\mathbb{H}$ [Eq. (3.2.8)] follows the completeness of the Floquet states $\Psi_\lambda(t)$ in $\mathbb{L}$ [45]. Therefore, the general solution of the time-dependent Schrödinger equation in the case of a time periodic external field can be expanded in the Floquet states, i.e.,

$$|\Psi(t)\rangle = \sum_\lambda A_\lambda |\Psi_\lambda\rangle = \sum_\lambda A_\lambda e^{-i\varepsilon_\lambda t/\hbar} |\Phi_\lambda(t)\rangle \ , \tag{3.2.9}$$

with the time-independent expansion coefficients given by

$$A_\lambda = e^{i\varepsilon_\lambda t_0/\hbar} \langle \Phi_\lambda(t_0)|\Psi(t_0)\rangle \ . \tag{3.2.10}$$

The evolution of the state vector from $t = t_0$ to $t = t'$ is given by

$$|\Psi(t')\rangle = U(t', t_0)|\Psi(t_0)\rangle \ , \tag{3.2.11}$$

where $U(t', t_0)$ represents the evolution operator. One can then find from Eqs. (3.2.2), and (3.2.9) the following eigenvalue problem

$$U(t_0 + T, t_0)|\Phi_\lambda(t_0)\rangle = \chi_\lambda |\Phi_\lambda(t_0)\rangle \quad ; \quad \chi_\lambda = e^{-i\varepsilon_\lambda T/\hbar} \tag{3.2.12}$$

for determining the quasienergies and the Floquet modes $|\Phi_\lambda(t_0 + kT)\rangle$ at stroboscopic times ($t = t_0 + kT$; $k = 0, 1, 2, ...$). Note also that, because of the time periodicity of the Floquet modes, at stroboscopic times Eq. (3.2.11) can be rewritten as [45]

$$|\Psi(t_0 + kT)\rangle = [U(t_0 + T, t_0)]^k |\Psi(t_0)\rangle \quad ; \quad k = 0, 1, 2, ... \ . \tag{3.2.13}$$

The stroboscopical description of the system evolution [see Eq. (3.2.13)] can be particularly useful when studying the long-time dynamics of a periodically driven quantum system, since the evolution operator need to be calculated only within one period [17, 18, 22, 45].

Taking into account Eqs. (3.2.1), (3.2.3), and (3.2.4), the averaged energy $\bar{E}_\lambda$ corresponding to a Floquet state (note that as the Hamiltonian of the system is time-dependent, the energy is no longer a constant of motion) is found to be given by

$$\bar{E}_\lambda = \langle\langle \Psi_\lambda(t)|H(t)|\Psi_\lambda(t)\rangle\rangle = \varepsilon_\lambda + \left\langle\left\langle \Phi_\lambda(t) \left| i\hbar \frac{\partial}{\partial t} \right| \Phi_\lambda(t) \right\rangle\right\rangle \ . \tag{3.2.14}$$

The total phase change ϕ_λ experimented by the Floquet state $|\Psi_\lambda(t)\rangle$ during a period is related to the corresponding quasienergy as [see Eq. (3.2.1)],

$$\phi_\lambda = -\frac{\varepsilon_\lambda T}{\hbar} \ . \tag{3.2.15}$$

Therefore, from (3.2.14) follows that the phase change ϕ_λ can be written as

$$\phi_\lambda = \phi_D^{(\lambda)} + \phi_G^{(\lambda)} \ , \tag{3.2.16}$$

where $\phi_D^{(\lambda)}$ is the dynamical phase of the Floquet state $|\Psi_\lambda(t)\rangle$ and is related to the averaged energy as,

$$\phi_D^{(\lambda)} = -\frac{\bar{E}_\lambda T}{\hbar} \ , \tag{3.2.17}$$

while the phase

$$\phi_G^{(\lambda)} = iT \left\langle\left\langle \Phi_\lambda(t) \left| \frac{\partial}{\partial t} \right| \Phi_\lambda(t) \right\rangle\right\rangle \tag{3.2.18}$$

is a *geometrical* phase, the so called Aharonov-Anandan geometric phase [45, 47] (also called nonadiabatic generalized Berry phase).

For an external field that if switched off (the field strength $F \to 0$) adiabatically, the Floquet modes and the quasienergies satisfy [45],

$$\lim_{F\to 0} |\Phi_\lambda(t)\rangle = e^{in\omega_0 t}|k\rangle \quad ; \quad \lambda = (k, n) \ , \tag{3.2.19}$$

and

$$\lim_{F\to 0} \varepsilon_\lambda = \varepsilon_\lambda^{(0)} = E_k^{(0)} + n\hbar\omega_0 \quad ; \quad \lambda = (k, n) \ , \tag{3.2.20}$$

where E_k^0 and $|k\rangle$ are the eigenenergies and eigenvectors of the unperturbed system. One can see from (3.2.20) that when $F \to 0$, the quasienergies depend linearly on ω_0, therefore there exist frequency values at which different levels $\varepsilon_\lambda^{(0)}$ intersect. A non-vanishing external field (with $F \neq 0$) mixes these levels, depending on the symmetry properties of the Hamiltonian. If the Hamiltonian has a well defined symmetry, the quasienergies can be separated into symmetry classes. According to the von-Neumann-Wigner theorem [48], levels of the same symmetry class will no longer intersect for a finite time-dependent external field (i.e., the levels of the same class develop into avoided crossings) while levels belonging to different classes exhibit exact crossings at finite strength of the external field. If, on the contrary, the system does not have any symmetry, the quasienergies exhibit typically avoided crossings at $F \neq 0$. The competition between avoided and exact crossings of the quasienergies can determine interesting phenomena (e.g., the coherent suppression of tunnelling [45]) in driven quantum systems.

It is worth noting that although the Floquet theory is, in principle, a formalism conceived for the case of time periodic external fields, a generalization of the Floquet approach to the case of nonperiodic driven quantum systems is also possible [45].

3.3 Splitting operator approach

In the present section we describe a computational procedure for the numerical propagation of the wave function through time. The method is particularly efficient when the wave function of the system is localized throughout its time evolution. It was proposed by Heather and Metiu [49] and is based on the combination of a splitting operator approximation [50, 51, 52] and a fast Fourier transform (FFT) scheme [53].

The basic idea is to exploit the fact that if the wave function is spatially localized one can use very efficiently a set of coordinate eigenfunctions to compute expressions involving the potential energy operator and a set of eigenfunctions of the conjugate momentum for computing functions of the kinetic operator. Since the transformation matrix elements between the coordinate and momentum representations are plane waves, all the matrix operations required for the propagation of the wave function become Fourier transforms and can be performed efficiently by using a FFT algorithm [53].

For our purpose it is convenient to separate the kinetic energy operator from the potential energy terms by rewriting (3.0.2) as

$$H = K + V_0(r) + V(r,t) \quad , \tag{3.3.1}$$

where K represents the kinetic energy operator, $V_0(r)$ is a time-independent potential (e. g., a confinement potential) and $V(r,t)$ represents the interaction of the system with the external time-dependent field.

The state vector $|\Psi(t_f)\rangle$ at the final time t_f is related to the initial state $|\Psi(t_i)\rangle$ as follows

$$|\Psi(t_f)\rangle = U(t_f,t_i)|\Psi(t_i)\rangle \quad , \tag{3.3.2}$$

where $U(t_f,t_i)$ represents the evolution operator (or propagator) from the initial time t_i to $t = t_f$. The propagator satisfies the property,

$$U(t_f,t_i) = \prod_{l}^{l_{max}} U(t_{l+1},t_l) \quad ; \quad t_l = (l-1)\Delta t + t_i \quad , \tag{3.3.3}$$

where $t_1 = t_i$, $t_{l_{max}+1} = t_f$, and

$$\Delta t = \frac{(t_f - t_i)}{l_{max}} \quad . \tag{3.3.4}$$

If we take a value for Δt such that

$$\Delta t \frac{\partial V(r,t)}{\partial t}\bigg|_{t=t_l} \ll V(r,t_l) \quad ; \quad t_l \leq t \leq t_{l+1} \quad , \tag{3.3.5}$$

the change of the potential $V(r,t)$ in the time interval $t \in [t_l, t_{l+1}]$ is very small. Hence $V(r,t)$ can be considered as constant for $t \in [t_l, t_{l+1}]$. The propagator in (3.3.3) can then be approximated by

$$U(t_{l+1},t_l) = \exp\left[-i\frac{\Delta t}{\hbar}\left(K + V_0(r) + V(r,t_l)\right)\right] \quad . \tag{3.3.6}$$

By using the symmetric splitting operator approach [50, 51, 52], one can rewrite (3.3.6) as follows,

$$U(t_{l+1},t_l) = \exp\left(-i\frac{\Delta t}{2\hbar}K\right)\exp\left[-i\frac{\Delta t}{\hbar}(V_0(r) + V(r,t_l))\right]\exp\left(-i\frac{\Delta t}{2\hbar}\right) + \mathcal{O}[(\Delta t)^3] \quad . \tag{3.3.7}$$

Note that the equation above is accurate to order $\mathcal{O}[(\Delta t)^3]$. The substitution of (3.3.7) into (3.3.3) leads to

$$U(t_f,t_i) = \exp\left(-i\frac{\Delta t}{2\hbar}K\right)\left[\prod_{l=1}^{l_{max}} U_l(\Delta t)\right]\exp\left(i\frac{\Delta t}{2\hbar}K\right) \quad , \tag{3.3.8}$$

where

$$U_l(\Delta t) = \exp\left[-i\frac{\Delta t}{\hbar}\left(V_0(r) + V(r,t_l)\right)\right]\exp\left(-i\frac{\Delta t}{\hbar}K\right) \quad . \tag{3.3.9}$$

Consequently, the wave function at time t_f is given by

$$|\Psi(t_f)\rangle = \exp\left(-i\frac{\Delta t}{2\hbar}K\right)\left[\prod_{l=1}^{l_{max}} U_l(\Delta t)\right]\exp\left(i\frac{\Delta t}{2\hbar}K\right)|\Psi(t_i)\rangle \ \ . \tag{3.3.10}$$

Now, if we denote

$$|\zeta_{l+1}\rangle = U_l(\Delta t)|\zeta_l\rangle \ \ , \tag{3.3.11}$$

with

$$|\zeta_1\rangle = \exp\left(i\frac{\Delta t}{2\hbar}K\right)|\Psi(t_i)\rangle \ \ , \tag{3.3.12}$$

then the wave function at $t = t_f$ can be expressed as

$$|\Psi(t_f)\rangle = \exp\left(-i\frac{\Delta t}{2\hbar}K\right)|\zeta_{l_{max}}\rangle \ \ , \tag{3.3.13}$$

where, from (3.3.11) and (3.3.12), we have

$$|\zeta_{l_{max}}\rangle = \prod_{l=1}^{l_{max}-1} |\zeta_l\rangle \ \ . \tag{3.3.14}$$

The set of equations (3.3.11) - (3.3.14) can be used for the computation of $|\Psi(t_f)\rangle$. By inserting (3.3.11) with the initial condition (3.3.12), one can calculate the function $|\zeta_l\rangle$ at each $t = t_l$. After $(l_{max} - 1)$ iterations $|\zeta_{l_{max}}\rangle$ is obtained and $|\Psi(t_f)\rangle$ can be computed from (3.3.13).

In order to efficiently compute the functions $|\zeta_l\rangle$ it is convenient to introduce discrete coordinate and momentum representations. For the sake of simplicity we restrict our discussion to the case of systems with a single spatial degree of freedom (the generalization to systems with multiple spatial degrees of freedom is straightforward).

If the spatial region of the evolution of the wave function has a length L on the x-axis, one can introduce a coordinate grid $\{x_n\}$ by dividing the segment of length L into n_{max} segments of equal length $\Delta x = \frac{L}{n_{max}}$. Then we can define a basis set $|x_n\rangle$ $(n = 1, 1, ..., n_{max})$ corresponding to a state in which the particle position is at the point $x_n = (n-1)\Delta x$ of the spatial grid $\{x_n\}$. If the spatial grid has enough points then the completeness relation

$$\sum_{n=1}^{n_{max}} |x_n\rangle\langle x_n| = 1 \tag{3.3.15}$$

can be reached and the properties of the wave function at each $t = t_l$, $\Psi(x, t_l) = \langle x|\Psi(t_l)\rangle$ are well described by its values $\Psi(x_n, t_l) = \langle x_n|\Psi(t_l)\rangle$ at the grid points x_n.

In a similar way one can introduce a set of discrete momentum eigenstates $|q_j\rangle$ corresponding to the momentum grid $\{q_j\}$, with $q_j = \left(j - \frac{n_{max}}{2} - 1\right)\frac{2\pi}{L}$, $(j = 1, 2, ..., n_{max})$. If the grid $\{q_j\}$ is well defined, the momentum states satisfy

$$\sum_{j=1}^{n_{max}} |q_j\rangle\langle q_j| = 1 \ \ , \tag{3.3.16}$$

and the wave function can be written in the momentum representation as $\Psi(q_j, t_l) = \langle q_j|\Psi(t_l)\rangle$.

Taking into account the completeness relations (3.3.15) and (3.3.16), the wave function can be transformed from one representation to the other by means of the following relations

$$\Psi(q_j, t_l) = \langle q_j|\Psi(t_l)\rangle = \sum_{n=1}^{n_{max}} \langle q_j|x_n\rangle\langle x_n|\Psi(t_l)\rangle \tag{3.3.17}$$

and

$$\Psi(x_n, t_l) = \langle x_n|\Psi(t_l)\rangle = \sum_{j=1}^{n_{max}} \langle x_n|q_j\rangle\langle q_j|\Psi(t_l)\rangle \ , \tag{3.3.18}$$

where

$$\langle q_j|x_n\rangle = \frac{e^{-ix_nq_j}}{\sqrt{n_{max}}} \quad ; \quad \langle x_n|q_j\rangle = \frac{e^{ix_nq_j}}{\sqrt{n_{max}}} \ , \tag{3.3.19}$$

i.e., the transformation from the coordinate to the momentum representation (or viceversa) can be carried out by performing the corresponding Fourier transform.

In the momentum representation the kinetic energy operator K is diagonal with eigenvalues $\frac{\hbar^2 q^2}{2m}$ (with m, the mass of the particle) and the exponential operators involving K in (3.3.8) can be written as

$$\exp\left(-i\frac{\Delta t}{\hbar}K\right) = \sum_{j=1}^{n_{max}} |q_j\rangle Q_j\langle q_j| \ , \tag{3.3.20}$$

where

$$Q_j = \exp\left(-i\frac{\Delta t}{2m}\hbar q_j^2\right) \ . \tag{3.3.21}$$

On the other hand, the exponential operators involving potential energies in (3.3.8) can be expanded in the coordinate basis as follows

$$\exp\left[-i\frac{\Delta t}{\hbar}\left(V_0(x) + V(x, t_l)\right)\right] = \sum_{n=1}^{n_{max}} |x_n\rangle X_{ln}\langle x_n| \ , \tag{3.3.22}$$

with

$$X_{ln} = \exp\left[-i\frac{\Delta t}{\hbar}\left(V_0(x_n) + V(x_n, t_l)\right)\right] \ . \tag{3.3.23}$$

From (3.3.12), (3.3.20), and (3.3.21) one can easily find $|\zeta_1\rangle$ in the momentum representation,

$$\langle q_j|\zeta_1\rangle = (Q_j^*)^{1/2}\langle q_j|\Psi(t_i)\rangle \ . \tag{3.3.24}$$

Similarly, one can obtain from (3.3.9), (3.3.11), and (3.3.22) - (3.3.24) the function $|\zeta_2\rangle$ in the coordinate representation,

$$\langle x_n|\zeta_2\rangle = X_{1n}\langle x_n|\zeta_1'\rangle \ , \tag{3.3.25}$$

where

$$\langle x_n|\zeta_1^{'}\rangle = \sum_{j=1}^{n_{max}} \langle x_n|q_j\rangle Q_j \langle q_j|\zeta_1\rangle \tag{3.3.26}$$

is the Fourier transform of $Q_j\langle q_j|\zeta_1\rangle$. By Fourier inverting Eq. (3.3.25) the momentum representation of $|\zeta_2\rangle$ can be obtained and then used as an input in (3.3.11) for the computation of $|\zeta_3\rangle$ in the next time step (at $t = t_3$). This procedure is iterated until $|\zeta_{n_{max}}\rangle$ is obtained. Once $|\zeta_{n_{max}}\rangle$ has been calculated, the wave function of the system $\langle q_j|\Psi(t_f)\rangle$ at $t = t_f$ can be found from (3.3.13), (3.3.20), and (3.3.21), as

$$\langle q_j|\Psi(t_f)\rangle = (Q_j)^{1/2}\langle q_j|\zeta_{n_{max}}\rangle \ . \tag{3.3.27}$$

The Fourier inversion of the equation above gives then the final wave function in the coordinate representation. We note that all the discrete Fourier transforms needed for propagating the wave function can be performed very efficiently by implementing a FFT algorithm [53].

It is worth remarking that the above discussed scheme is particularly efficient when the evolution of the wave function occurs in a localized spatial region. When the size of that region increases a greater number of grid points is required and the efficiency of the method decreases. In particular, a well pre-defined grid can lead to a good description of the system evolution at early times. It can happen, however, that at some time, the wave function approaches the edge of the pre-defined grid and, consequently, further propagation would cause reflection from the grid's edge and falsify the results. Of course, this problem can be eliminated by increasing the length of the grid. However, as mentioned above, the enlargement of the grid leads to a decreasing of the computational efficiency, and in some cases it could be necessary to optimize the way the grid is enlarged (for example by complementing the method here discussed with a wave function splitting algorithm [49]).

Chapter 4

Quasistationarity of a time-dependent quantum state

4.1 General definitions

The variation in time of the expectation value $\langle O\rangle(t)$ of an observable O, strongly depends on the time evolution of the quantum system under investigation. Therefore, by driving the system with an appropriately designed external field it is possible, in principle, to control the range of values of $\langle O\rangle(t)$ in a desired way.

Suppose the system is initially (at $t = 0$) in a known state for which the expectation value of O is known to be $\langle O\rangle_0 = \langle O\rangle(0)$. Here, and from now on, we consider the expectation values $\langle O\rangle(t)$ are measured at any time with respect to its value $\langle O\rangle^{(0)}$ corresponding to the ground state of the system. The main goal of the quantum dynamical control process is then to promote the system from its initial state to a *target* state giving the desired expectation value $\langle O\rangle_{target}$. A step further consists in maintaining the values of $\langle O\rangle(t)$ close to the target expectation value $\langle O\rangle_{target}$ for a desired time interval, i.e., to make the control process *sustainable* in time. The sustainability of the quantum dynamical control of the expectation value of a given observable can be important from the practical point of view, in order to avoid limitations imposed by the finite resolution of the experimental measurements.

We are particularly interested in non-stationary systems whose time dependent evolution can be well described by pure states composed by the coherent superposition of a finite number N of unperturbed states, i.e., we assume the wave function of the system can be expressed at any time as in (3.1.2) and the corresponding density matrix as $\rho(t) = |\Psi(t)\rangle\langle\Psi(t)|$. Therefore, from now on we restrict all our analysis to such kind of quantum systems.

We focus now on the problem of the sustainability of the expectation value $\langle O\rangle(t)$ of a given observable O through time. In what follows we consider that the desired value $\langle O\rangle_{target}$ of $\langle O\rangle(t)$ has been reached at $t = t_0$ [i.e., $\langle O\rangle_{target} = \langle O\rangle(t_0)$] and that $\langle O\rangle(t)$ is time-dependent even when for $t > t_0$ no external field is applied. Note that in the opposite case the problem of sustainability becomes trivial, since in such a situation the field-free evolution of the system guarantees that $\langle O\rangle(t) = \langle O\rangle_{target}$ at any time $t > t_0$, i.e., $\langle O\rangle(t)$ becomes sustainable by *nature* and no driving is required. We, therefore, exclude this case from our study. For brevity, the observables O whose expectation values $\langle O\rangle(t)$ are time-dependent will be referred to, from now on, as time-dependent observables (note, however, that the operator o corresponding to the observable O does not depend, in general, on time).

Taking as reference the field-free system, we introduce the *deviation* time $\tau_o = (t' - t_0)$ of the observable O, where t' denotes the time at which the expectation value $\langle O\rangle(t)$ reaches its maximum deviation from $\langle O\rangle(t_0)$, in the absence of the external field. Thus, the deviation time τ_o represents the time the difference $|\langle O\rangle(t) - \langle O\rangle(t_0)|$ lasts for evolving from its minimum value at $t = t_0$ to its maximum value at $t = t'$ in the case the system is in the absence of external time-dependent fields. Note that the existence of maximum and minimum of $|\langle O\rangle(t) - \langle O\rangle(t_0)|$ is guaranteed, since we are considering time-dependent observables [$\langle O\rangle(t) \neq$ const.] and $\langle O\rangle(t)$ has upper and lower bounds [40].

On the basis of the above considerations, it is convenient to introduce some general definitions.

Definition 4.1.1. A time-dependent observable [with $\langle O\rangle(t_0) \neq 0$] is called a *quasistationary* observable if for all $\eta > \eta_o$ ($\eta,\ \eta_o \in \mathbb{R}^+$) there exists $t_\eta > \tau_o$ ($t_\eta,\ \tau_o \in \mathbb{R}^+$) such that if $0 < |t - t_0| < t_\eta$ then $|\langle O\rangle(t) - \langle O\rangle(t_0)| < \eta_o$, with η_o [$\eta_o \ll |\langle O\rangle(t_0)|$] a parameter that characterizes the degree of quasistationarity of $\langle O\rangle(t)$.

From the above definition it results that the control process of the expectation value $\langle O\rangle(t)$ of an observable O is sustainable within the time interval $t_0 < t < \tau_o$ if the external time-dependent field is capable of inducing quasistationarity to that observable.

We now introduce other definitions regarding some special cases of quasistationarity.

Definition 4.1.2. A time-dependent observable is called a *cyclic quasistationary* observable if it is quasistationary and its expectation value satisfies $\langle O\rangle(t_0 + \mathcal{T}_k) = \langle O\rangle(t_0 + \mathcal{T}_{k-1})$ ($k = 1, 2, ..., n_c$), with $\mathcal{T}_0 = 0$, n_c the number of cycles, and $\mathcal{T}_k$ ($\mathcal{T}_k > 0$) the duration of the kth cycle.

Definition 4.1.3. A time-dependent observable is called *quasiperiodic quasistationary* if it is quasistationary and there exists $\mathcal{T} > 0$ such that $\langle O\rangle(t_0 + k\mathcal{T}) = \langle O\rangle(t_0)$ with $k = 1, 2, ..., n_{pc}$). The quantity $\mathcal{T}$ is then called the period of the observable and n_{pc} is the number of periodic cycles.

We note that the number of periodic cycles n_{pc} does not necessarily coincide with the total number of cycles n_c, since each periodic cycle can contain sub-cycles (see Fig. 4.1). Therefore, one has that $n_c \geq n_{pc}$.

The special case of quasistationarity given in the definition 4.1.3 is of particular interest,

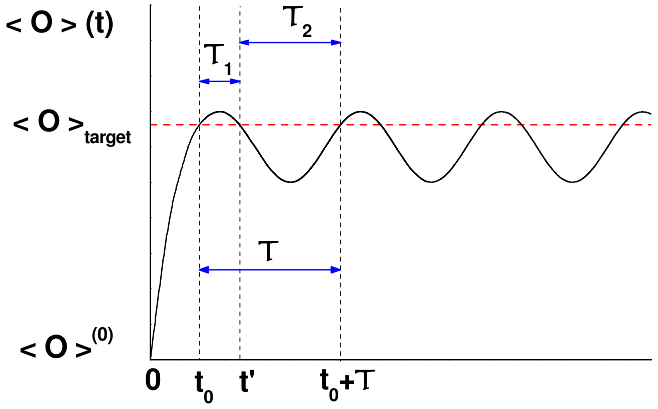

Figure 4.1: An example of a periodic cycle (of duration $\mathcal{T}$) composed of two sub-cycles of durations $\mathcal{T}_1$ and $\mathcal{T}_2$.

since it contains as particular cases phenomena such as the coherent suppression of tunnelling [45, 54, 55, 56], dynamical localization [45, 57, 58, 59], and sustainable molecular orientation [60, 61]. The coherent suppression of tunnelling, for example, occurs when a particle initially (at $t = t_0$) in one of the wells (say, the left well) of a symmetric double quantum well is subject to an external CW laser field. For certain parameters of the external time-dependent field the particle remains localized in the left well, i.e., the tunnelling is coherently suppressed [45, 54, 55, 56]. In this case the observable utilized for monitoring the system is the time-dependent probability $P_L(t)$ of finding the particle in the left well. Coherent suppression of tunnelling then occurs when [45, 54, 55, 56]

$$P_L(t_0 + kT) \approx P_L(t_0) \quad ; \quad k = 1, 2, 3, \dots \ , \tag{4.1.1}$$

under the condition that the escaping time of the particle is much longer than the period T of the applied CW laser field [this condition prevents the escape of the particle to the other well within a period, i.e., it guarantees that $P_L(t)$ remains close to the initial value $P_L(t_0)$ inclusive for $kT < t < (k+1)T$]. Therefore, the coherent suppression of tunnelling can be interpreted as a particular case of quasiperiodic quasistationarity in which the observable of interest is $P_L(t)$ and its period $\mathcal{T} = T$ coincides with the period of the driving CW laser. Because of its particular importance, we further focus on the study of the special case corresponding to quasiperiodic quasistationarity.

Having in mind Def. 4.1.3 one can also define quasiperiodic quasistationary states as follows.

Definition 4.1.4. A time-dependent quantum state $|\Psi(t)\rangle$ is called a quasiperiodic quasistationary state if the expectation values of any set of observables are quasiperiodic quasistationary, i.e., if

$$\langle O\rangle(t_0 + k\mathcal{T}) = \langle\Psi(t_0 + k\mathcal{T})|o|\Psi(t_0 + k\mathcal{T})\rangle = \langle\Psi(t_0)|o|\Psi(t_0)\rangle = \langle O\rangle(t_0) \ , \tag{4.1.2}$$

($k = 1, 2, ..., n_{pc}$) for any observable O.

From the above definition and taking into account that the wave function of a quantum state is defined (in a unique way) up to a phase, one can see that a *necessary* condition for a quantum state to be quasiperiodic quasistationary is the corresponding wave function to have a quasiperiodic cyclic evolution, i.e.,

$$|\Psi(t_0 + k\mathcal{T})\rangle = e^{i\phi_k}|\Psi(t_0)\rangle \quad ; \quad k = 1, 2, ..., n_{pc} \ , \tag{4.1.3}$$

where ϕ_k is a real number (the phase change within k periodic cycles) and $\mathcal{T}$ represents the duration of each periodic cycle. Note, however, that condition (4.1.3) is not *sufficient* for the quantum state to be quasiperiodic quasistationary, since it only guarantees the quasiperiodicity of the time-dependent observables but not their quasistationarity. The *sufficient* condition for a quasiperiodic cyclic quantum system to be quasistationary is related to the Aharonov-Anandan (AA) geometric phase (also called the nonadiabatic generalized Berry phase) [34, 35, 47] as will be shown in the following sections. For completeness we discuss now some general aspects regarding the AA geometric phase.

Let us consider, for simplicity that the wave function of the system performs a single cycle during the time interval $[t_0, t_0 + \mathcal{T}]$. It results from Eq. (4.1.3) that

$$|\Psi(t_0 + \mathcal{T})\rangle = e^{i\phi}|\Psi(t_0)\rangle \quad ; \quad \phi = \phi_1 \ . \tag{4.1.4}$$

The wave function of the N-level system is determined by the complex vector $\mathbf{C}(t) = (C_1(t), C_2(t), ..., C_N(t))^T$ [$\mathbf{C}(t) \neq 0,\ \mathbf{C}(t) \in \mathbb{C}^N$] whose components are the expansion coefficients in (3.1.2). Let assume, without lost of generality, that $C_1(t)$ is nonzero throughout the system evolution. Then the projective Hilbert space $\mathbb{CP}^{N-1}$ can be characterized by the complex coordinates

$$\tilde{C}_k(t) = \frac{C_k(t)}{C_1(t)} \quad ; \quad k = 2, 3, ..., N \ . \tag{4.1.5}$$

It is clear from (4.1.5) that all vectors $\mathbf{C}(t) \in \mathbb{C}^N$ that differ by only a multiplicative phase have the same image in the projective space $\mathbb{CP}^{N-1}$. Hence, the evolution of a cyclic state [$\mathbf{C}(t_0+\mathcal{T}) = e^{i\phi}\mathbf{C}(t_0)$, see also Eq. (4.1.4)] in $\mathbb{C}^N$ is characterized by a closed path $\mathcal{L}_{cp}$ in the projective Hilbert space $\mathbb{CP}^{N-1}$ [note that for cyclic states (4.1.5) gives $\tilde{C}_k(t_0+\mathcal{T}) = \tilde{C}_k(t_0)$ $\forall\ k = 2, 3, ..., N$]. One can then expect $\mathbb{C}^N$ to be related to the product of $\mathbb{CP}^{N-1}$ and the group $U(1)$ of phases. This relationship is not direct, as $\mathbb{C}^N = U(1) \otimes \mathbb{CP}^{N-1}$ does not hold in general [34, 35, 36]. However, it does hold locally, i.e., one can express the projective space as the union of subsets $\mathbb{CP}_i^{N-1}$ [$\mathbb{CP}^{N-1} = \bigcup \mathbb{CP}_i^{N-1}$] such that $\mathbb{C}^N$ can be expressed as $\mathbb{C}^N = \bigcup \left(U(1) \otimes \mathbb{CP}_i^{N-1}\right)$. Consequently $\mathbb{C}^N$ is a principal fiber bundle over $\mathbb{CP}^{N-1}$ [34, 35, 36, 47].

To specify some cyclic vector $\mathbf{C}(t_0 + \mathcal{T}) = e^{i\phi}\mathbf{C}(t_0)$ one has to specify a path $\mathcal{L}_c$ on $\mathbb{C}^N$ that projects onto $\mathcal{L}_{cp}$. Mathematically such paths are called *lifts* [34, 35, 36]. The initial and final points of an arbitrary lift corresponding to a closed curve in $\mathbb{CP}^{N-1}$ can differ by only a multiplicative phase. This difference is called the *holonomy* (some times also referred to as *anholonomy* [34, 35]) [34, 35, 36]. As it my depends on the choice of lift, in order to obtain the holonomy it is necessary a rule that enables one to chose a lift for each curve in the projective space. Such a rule is called a *connection* [34, 35, 36]. Therefore the holonomy depends also on the choice of connection and it is usually referred to as the holonomy of the connection. It appears that for each path in the projective space there exists exactly one natural lift that is orthogonal to its tangent vector [34, 35, 36, 62]. Hence this condition, usually called parallel transport, defines a natural connection.

The most general vector $\mathbf{G}(t) \in \mathbb{C}^N$ that is equal to $\mathbf{C}(t)$ modulo a multiplicative phase and obeys $\mathbf{G}(t_0) = \mathbf{C}(t_0)$ is given by [63]

$$\mathbf{G}(t) = e^{-i\phi_D(t)}\mathbf{C}(t) \ , \tag{4.1.6}$$

where

$$\phi_D(t) = -i\int_{t_0}^{t} \mathbf{C}^\dagger(t')\frac{d\mathbf{C}(t')}{dt'}dt' \ . \tag{4.1.7}$$

One can obtain from Eqs. (4.1.6) and (4.1.7) that

$$\mathbf{G}^\dagger(t)\frac{d\mathbf{G}(t)}{dt} = -i\frac{d\phi_D(t)}{dt} + \mathbf{C}^\dagger(t)\frac{d\mathbf{C}(t)}{dt} = 0 \ , \tag{4.1.8}$$

i.e., the vector $\mathbf{G}(t) \in \mathbb{C}^N$ is orthogonal to its tangent vector $\frac{d\mathbf{G}(t)}{dt}$ and (4.1.8) determines the connection. Consequently, the path in $\mathbb{C}^N$ corresponding to $\mathbf{G}(t)$ constitutes the natural lift. The AA geometric phase ϕ_G is defined as the holonomy of the natural connection [34, 35, 47, 62], i.e.,

$$e^{i\phi_G} = \mathbf{G}^\dagger(t_0)\mathbf{G}(t_0 + \mathcal{T}) \ . \tag{4.1.9}$$

In the vector state notation Eq. (4.1.9) can be rewritten as

$$e^{i\phi_G} = \langle\Lambda(t_0)|\Lambda(t_0 + \mathcal{T})\rangle \ , \tag{4.1.10}$$

where

$$|\Lambda(t)\rangle = e^{-i\phi_D(t)}|\Psi(t)\rangle \ , \tag{4.1.11}$$

satisfies [see Eq. (4.1.8)]

$$\left\langle \Lambda(t) \left| \frac{d}{dt} \right| \Lambda(t) \right\rangle = 0 \ , \tag{4.1.12}$$

and

$$\phi_D(t) = -i\int_{t_0}^{t} \left\langle \Psi(t') \left| \frac{d}{dt'} \right| \Psi(t') \right\rangle dt' \ . \tag{4.1.13}$$

Note that $\phi_D(t = t_0 + \mathcal{T}) = \phi_D$ is the dynamical phase acquired by the system within an evolution cycle. One then has from (4.1.4) and (4.1.10) - (4.1.13), that the total phase change ϕ within an evolution cycle is given by $\phi = \phi_D + \phi_G$.

The AA geometric phase is clearly a geometric quantity in the sense that it does not depend on the choice of the Hamiltonian as long as the Hamiltonians describe the same closed path $\mathcal{L}_{cp}$ in the projective Hilbert space, i.e., it depends only on the closed path $\mathcal{L}_{cp}$. Consequently, the AA phase constitutes a “geometric” property of $\mathcal{L}_{cp}$.

Before concluding this section, it is worth noting that although we have considered the AA geometric phase for quantum systems following a cyclic evolution, it is also possible to generalize the geometric phase to the case of non-adiabatic non-cyclic quantum evolution [34, 35, 37, 39, 64, 65, 66].

4.2 Quasistationarity within the GBVA

Within the GBVA one easily obtain from (3.1.40) that

$$\langle O\rangle(t)-\langle O\rangle(t_0)=|\mathbf{W}||\mathbf{B}(t)|\left(\cos\nu(t)-\cos\nu(t_0)\right)\quad;\quad \nu(t)=\angle\big(\mathbf{W},\mathbf{B}(t)\big)\ . \tag{4.2.1}$$

On the other hand, taking into account (3.1.40), (4.1.2) can be rewritten in terms of the generalized Bloch vector as follows:

$$\mathbf{B}(t_0+k\mathcal{T})=\mathbf{B}(t_0)\quad;\quad k=1,2,...,n_{pc}\ . \tag{4.2.2}$$

Then it results from Defs. 4.1.1 - 4.1.4 that the quantum state is quasiperiodic quasistationary if for all $\eta>\eta_o$ there exists $t_\eta>\tau_o$ such that

$$|\cos\nu(t)-\cos\nu(t_0)|<\frac{\eta_o}{|\mathbf{W}||\mathbf{B}(t)|}\ll\cos\nu(t_0)\ , \tag{4.2.3}$$

or, equivalently, if

$$\mathbf{B}(t)\approx\mathbf{B}(t_0)\ , \tag{4.2.4}$$

for all $t\in[t_0,t_\eta]$, and condition (4.2.2) holds. Note that in (4.2.3) $\nu(t_0)\neq\frac{\pi}{2}$, since by definition we have assumed that $\langle O\rangle(t_0)\neq 0$.

Let us investigate now under which conditions Eqs. (4.2.2) and (4.2.4) are fulfilled, i.e., which are the *necessary* and *sufficient* conditions for reaching quasiperiodic quasistationarity.

The substitution of Eq. (3.1.27) into (4.2.2) leads to

$$U(t_0+k\mathcal{T},t_0)\mathbf{B}(t_0)=\mathbf{B}(t_0)\quad;\quad k=1,2,...,n_{pc}\ , \tag{4.2.5}$$

with the evolution operator $U(t,t_0)$ given by (3.1.28). Therefore a necessary and sufficient condition for an N-level system to be quasiperiodic is its corresponding evolution operator to periodically perform cyclic rotations in the generalized Bloch space, i.e.,

$$U(t_0+k\mathcal{T})=\mathcal{I}_{N}\ . \tag{4.2.6}$$

In the particular case of a periodic external field with period T (note that T does not necessarily coincides with $\mathcal{T}$) one finds from (3.1.26) and (3.1.28) that the evolution operator satisfies $U(t_0+T,t_0)=U(t_0+kT,t_0+(k-1)T)$ for $k=1,2,...$ and, consequently, the generalized Bloch vector evolves as

$$\mathbf{B}(t_0+kT)=\left(U(t_0+T)\right)^k\mathbf{B}(t_0)\ . \tag{4.2.7}$$

If for some $\mathcal{T}=lT$ (with l a positive integer) the evolution operator obeys

$$U(t_0+\mathcal{T},t_0)=\mathcal{I}_{N}\ , \tag{4.2.8}$$

then the Bloch vector becomes quasiperiodic with period $\mathcal{T}$.

Within the GBVA the evolution operator of an N-level system consists of a $(N_D\times N_D)$ matrix whose elements are functions of the system parameters. Once $U(t,t_0)$ has been obtained, the relations (4.2.6) or (4.2.8) can be utilized for obtaining the field parameters that lead to the quasiperiodic evolution of the generalized Bloch vector. We note, however, that the existence or not of such specific values of the driving-field parameters will depend essentially on the initial value of $\mathbf{B}(t_0)$ and the form of the external field itself. Actually, the relations (4.2.6) and (4.2.8) look quite restrictive but, as will be shown in the following chapters, it is possible to achieve such conditions in actual physical systems.

We suppose now that we have already determined the appropriate field parameters that induce the quasiperiodic evolution of the generalized Bloch vector. This, although necessary, is still not sufficient for achieving quasiperiodic quasistationarity. The quasistationarity is determined by the deviation $|\mathbf{B}(t) - \mathbf{B}(t_0)|$ of the generalized Bloch vector $\mathbf{B}(t)$ from its initial value $\mathbf{B}(t_0)$ throughout the system evolution. The fact that $\mathbf{B}(t)$ is quasiperiodic means that it performs closed paths [containing the point $\mathbf{B}(t_0)$] in the generalized Bloch space. Consequently, the *area* enclosed by these paths constitutes a measure of the deviation $|\mathbf{B}(t) - \mathbf{B}(t_0)|$. On the other hand each closed path of $\mathbf{B}(t)$ in the generalized Bloch space is associated to an AA geometric phase. One can then expect the nonadiabatic geometric phase to be useful in describing the degree of quasistationarity of a quantum system.

In the preceding section we briefly discussed some aspects and concepts regarding the AA geometric phase in terms of complex vectors of the Hilbert space $\mathbb{H}^N \simeq \mathbb{C}^N$. It is now convenient to express the AA geometric phase in terms of the (real) generalized Bloch vectors. With this aim, we firstly introduce the map Π from the complex Hilbert space $\mathbb{H}^N$ whose vectors $|\Psi(t)\rangle$ define pure quantum states to the space $\mathbb{P}^{2N-1}$ of the pure state density matrix ρ, i.e.,

$$|\Psi(t)\rangle \in \mathbb{H}^N \ : \ \Pi(|\Psi(t)\rangle) = \rho(t) = |\Psi(t)\rangle\langle\Psi(t)| \in \mathbb{P}^{2N-1} \quad . \tag{4.2.9}$$

The space $\mathbb{P}^{2N-1}$ is usually called the *ray* space [37, 39].

The AA geometric phase in terms of the vector state $|\Lambda(t)\rangle$ corresponding to the natural lift in the complex Hilbert space was given in Eq. (4.1.10). We now try to find the AA geometric phase in terms of the elements of the ray space $\mathbb{P}^{2N-1}$ by noting that the map (4.2.9) together with (4.1.11) lead to

$$\rho(t) = |\Psi(t)\rangle\langle\Psi(t)| = |\Lambda(t)\rangle\langle\Lambda(t)| \ , \tag{4.2.10}$$

and therefore,

$$\frac{d\rho(t)}{dt} = \frac{d|\Lambda(t)\rangle}{dt}\langle\Lambda(t)| + |\Lambda(t)\rangle\frac{d\langle\Lambda(t)|}{dt} \quad . \tag{4.2.11}$$

Taking into account (4.1.12) and (4.2.11) one can easily obtain

$$\frac{d|\Lambda(t)\rangle}{dt} = \frac{d\rho(t)}{dt}|\Lambda(t)\rangle \quad . \tag{4.2.12}$$

We can formally solve Eq. (4.2.12) as a Dyson-like ordered series. As a result, the following expression is obtained,

$$|\Lambda(t)\rangle = T_t\left(\exp\left[\int_{t_0}^{t} dt' \frac{d\rho(t')}{dt'}\right]\right)|\Lambda(t_0)\rangle \quad . \tag{4.2.13}$$

By substituting (4.2.13) in (4.1.10) we arrive to the relation,

$$e^{i\phi_G} = \mathrm{Tr}\left\{\rho(t_0)T_t\left(\exp\left[\int_{t_0}^{t_0+\mathcal{T}} dt\frac{d\rho(t)}{dt}\right]\right)\right\} \quad . \tag{4.2.14}$$

From Eqs. (3.1.16) and (4.2.14) one then obtains,

$$e^{i\phi_G} = \mathrm{Tr}\left\{\left(\frac{\mathcal{I}_N}{N}+\frac{1}{2}\mathbf{B}(t_0)\cdot\hat{\mathcal{F}}\right)T_t\left(\exp\left[\frac{1}{2}\int_{t_0}^{t_0+\mathcal{T}} dt\frac{d\mathbf{B}(t)}{dt}\cdot\hat{\mathcal{F}}\right]\right)\right\} \quad . \tag{4.2.15}$$

By introducing the matrices $\mathcal{M}^{(n)}$ obeying the following iteration relation,

$$\mathcal{M}^{(n)}(t) = \frac{1}{2}\int_{t_0}^{t}\left(\frac{d\mathbf{B}(t')}{dt'}\cdot\hat{\mathcal{F}}\right)\mathcal{M}^{(n-1)}(t')dt' \quad ; \quad \mathcal{M}^{(0)} = \mathcal{I}_N \quad , \tag{4.2.16}$$

we can rewrite (4.2.15) as follows,

$$e^{i\phi_G} = \mathrm{Tr}\left[\left(\frac{\mathcal{I}_N}{N}+\frac{1}{2}\mathbf{B}(t_0)\cdot\hat{\mathcal{F}}\right)\left(\sum_{n=0}^{\infty}\mathcal{M}^{(n)}(t_0+\mathcal{T})\right)\right] \quad . \tag{4.2.17}$$

An identity that results useful in the calculation of $\mathcal{M}^{(n)}$ is (see Appendix A),

$$(\mathbf{X}\cdot\hat{\mathcal{F}})(\mathbf{Y}\cdot\hat{\mathcal{F}}) = \frac{2}{N}\mathcal{I}_N(\mathbf{X}\cdot\mathbf{Y}) + [(\mathbf{X}\star\mathbf{Y}) + i(\mathbf{X}\wedge\mathbf{Y})]\cdot\hat{\mathcal{F}} \quad , \tag{4.2.18}$$

where $\mathbf{X}$ and $\mathbf{Y}$ are any two vectors in $\mathbb{R}^{N_D}$.

The computation of the trace in (4.2.17) for the case of an N-level system is, in general, a complicated task. However, some qualitative information can be extracted by taking into account that all the relations (4.2.16) for $n > 1$ contain the matrix

$$\mathcal{M}^{(1)}(t) = (\mathbf{B}(t) - \mathbf{B}(t_0))\cdot\hat{\mathcal{F}} \tag{4.2.19}$$

as a factor in their integrands. Consequently if the system is in a quasiperiodic quasistationary state Eq. (4.2.4) holds and $\mathcal{M}^{(1)}(t) \approx 0$,$\forall\ t \in [t_0, t_0+\tau_o]$. In such a case if, in addition, $\tau_o > \mathcal{T}$ one has from (4.2.16) and (4.2.17) that

$$e^{i\phi_G} \approx 1 \quad , \tag{4.2.20}$$

i.e., $\phi_G \approx 0$ (modulo 2π). After some lengthy mathematical manipulations one can obtain from Eqs. (4.2.16) - (4.2.19) that $\phi_G \approx 0$ if $\mathbf{B}(t) \approx \mathbf{B}(t_0)$ $\forall\ t \in [t_0, t_0+\mathcal{T}]$ or if there exists $t' \in [t_0, t_0+\mathcal{T}]$ such that $\mathbf{B}(t)$ evolves from t_0 to t' and then from t' to $t_0+\mathcal{T}$ through closely the same path. The latter condition is quite restrictive and physically unlikely to occur in most of the physical systems of practical interest (e.g., for the systems here considered such a situation never occurs). Therefore, excluding this unlikely situation, the relation $\phi_G \approx 0$ (modulo 2π) can be regarded as a necessary and sufficient condition for the cyclic evolution of the system to be quasistationary (in the case of quasiperiodic cyclic evolution ϕ_G corresponds to the AA geometric phase acquired during each evolution cycle). We note that in the case $\phi_G = 0$, the system becomes truly stationary. The value of ϕ_G can then be

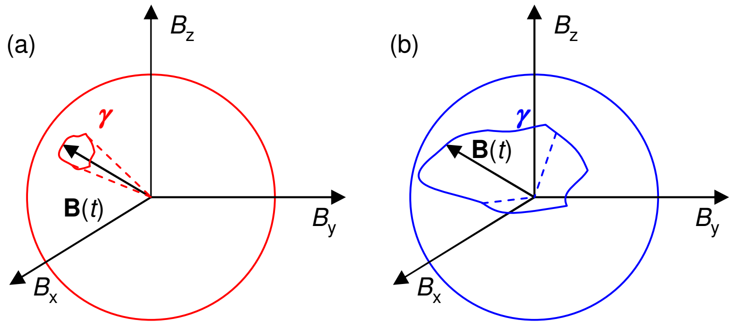

Figure 4.2: Closed path γ described by the Bloch vector $\mathbf{B}(t)$ on the sphere $\mathbb{S}^2$. a) Strong quasistationarity. b) Weak quasistationarity.

used for characterizing the degree of quasistationarity of a cyclic (in time) quantum system on the basis of the following criterium: closer to zero ϕ_G, strongest the quasistationarity of the system. This conclusion becomes somehow trivial for the case of a two-level system. In such a case the AA geometric phase is given by half of the solid angle Ω_γ subtended by the closed path γ (described by the Bloch vector on the two-dimensional sphere $\mathbb{S}^2$ of unit radius) at the center of $\mathbb{S}^2$ [34, 35, 37, 39, 62]. The analysis of the quasistationarity for a two-level system then becomes very simple since it is *visually* clear (see Fig. 4.2) that closer Ω_γ (and therefore ϕ_G) to zero, strongest the quasistationarity of the Bloch vector.

It is worth remarking that for achieving quasistationarity the relation $\phi_G \approx 0$ has to be fulfilled by the AA geometric phase acquired during each evolution cycle, i.e., during each periodic cycle and its corresponding sub-cycles (if any).

In summary, Eq. (4.2.6) [or (4.2.8)] together with (4.2.20) constitute a necessary and sufficient condition for inducing quasiperiodic quasistationarity to a quantum system.

For systems in which the number of levels involved in their evolution is not small, the formalism described in the present section can turn inefficient for quantitative calculations (remember that the dimension of the generalized Bloch space scales as $N^2 - 1$). As a complement to the qualitative results of the GBVA we present in the following section a study of the quasistationarity of quantum system driven by a time-periodic external field, within a formalism (the Floquet approach) that is, in the general case, more convenient for performing quantitative calculations.

4.3 Quasistationarity within the FA

As was shown in Sec. 3.2, if the time-dependent external field is periodic with period T (and $\omega_0 = 2\pi/T$), the state vector of the system can be written as

$$|\Psi(t)\rangle = \sum_\lambda A_\lambda e^{-i\varepsilon_\lambda t/\hbar}|\Phi_\lambda(t)\rangle \quad , \tag{4.3.1}$$

where the Floquet modes $|\Phi_\lambda(t)\rangle$ have the same periodicity as the external field [see Eq. (3.2.2)]. Let us concentrate in the analysis of the quasiperiodic cyclic evolution of a quantum system.

Without lost of generality, we can restrict our study to a single evolution cycle. Then it follows from (4.1.4) and (4.3.1) that the condition for the evolution of the system to be cyclic is given by

$$|\Psi(t_0+\mathcal{T})\rangle = e^{i\phi}\sum_{\lambda} A_\lambda e^{-i\varepsilon_\lambda t_0/\hbar}|\Phi_\lambda(t_0)\rangle \ . \tag{4.3.2}$$

We now investigate how the AA geometric phase of the system described by the state vector in (4.3.2) is related to the phases $\phi_D^{(\lambda)}$ and $\phi_G^{(\lambda)}$ corresponding to the Floquet modes $|\Phi_\lambda(t)\rangle$. We note that the dynamical phase ϕ_D of the system is given by [see (4.1.13) and further comments],

$$\phi_D = -i\int_{t_0}^{t_0+\mathcal{T}} \left\langle \Psi(t)\left|\frac{d}{dt}\right|\Psi(t)\right\rangle dt \ . \tag{4.3.3}$$

If the duration $\mathcal{T}$ of the evolution cycle is a multiple of the period T of the external field (i.e., $\mathcal{T} = lT$, with l a positive integer) then one can obtain from Eqs. (3.2.3), (3.2.7), (4.3.2), and (4.3.3) the following relation

$$\phi_D = \frac{\mathcal{T}}{T}\sum_{\lambda} |A_\lambda|^2\,\phi_D^{(\lambda)} + \sum_{\lambda,\nu\ (\lambda\neq\nu)} A^*_\lambda A_\nu \int_{t_0}^{t_0+\mathcal{T}} e^{\frac{i}{\hbar}(\varepsilon_\lambda-\varepsilon_\nu)t}\left\langle \Phi_\lambda(t)\left|\frac{d}{dt}\right|\Phi_\nu(t)\right\rangle dt \ , \tag{4.3.4}$$

with $\phi_D^{(\lambda)}$ determined by (3.2.17). The AA geometric phase acquired by the system within an evolution cycle is then given by

$$\phi_G = \phi - \phi_D \tag{4.3.5}$$

For the sake of simplicity we consider at first the case of a two-level system. In such a case the state vector at stroboscopic times can be written as,

$$|\Psi(t_0+kT)\rangle = e^{-i\frac{\epsilon_2 kT}{\hbar}}\left(e^{-i\frac{(\epsilon_1-\epsilon_2)kT}{\hbar}}A_1 e^{-i\frac{\epsilon_1 t_0}{\hbar}}\Phi_1(t_0) + A_2 e^{-i\frac{\epsilon_2 t_0}{\hbar}}\Phi_2(t_0)\right) \ . \tag{4.3.6}$$

In the equation above we have denoted by ϵ_1 and ϵ_2 the quasienergies ε_λ corresponding to $\lambda = (1,0)$ and $\lambda = (2,0)$, respectively (i.e., ϵ_1 and ϵ_2 are the representatives of the two quasienergy classes in the first Brillouin zone). One can see from (4.3.6) that the state vector becomes quasiperiodic cyclic [see condition (4.1.3)] if all the relevant Floquet states have the same phase (up to a multiple of 2π) at $t = t_0 + \mathcal{T}$, i.e., if one of the following conditions is fulfilled [67]:

a) If $\epsilon_1 - \epsilon_2 = n\hbar\omega_0$; $(n \in \mathbb{Z})$.

b) If $A_1 = 0$ or $A_2 = 0$.

c) If $(\epsilon_1 - \epsilon_2)l = m\hbar\omega_0$; $(l, m \in \mathbb{Z},\ m/l \notin \mathbb{Z})$.

The condition a) corresponds to the degeneracy of the quasienergies and leads to $\mathcal{T} = T$. The condition b) leads also to $\mathcal{T} = T$ and corresponds to the case in which the wave function of the system collapses into a Floquet state. The condition c) leads to a quasiperiodic cyclic evolution with the duration of each cycle being a multiple of the period of the external field, i.e., $\mathcal{T} = |l|T$. It is worth noting that conditions b) and c) do not require crossing of quasienergies. The conditions a), b), and c) can be regarded as necessary and sufficient conditions for the quasiperiodicity of the system. If these conditions are complemented with the requirement that the corresponding AA geometric phase acquired during each evolution cycle approaches zero, then the quasiperiodic quasistationarity of the system is guaranteed.

In addition to the general equation (3.2.18), one can also obtain in the case of absence of quasienergy degeneracy, an expression that relates the geometric phases $\phi_G^{(\lambda)}$ to the corresponding quasienergies. The basic idea is to transform the composite Hilbert space $\mathbb{H}$ associated to the Schrödinger operator $\mathcal{S}(t)$ [see (3.2.3) and (3.2.4)] into a space $\mathbb{H}'$ independent of the parameter T by changing the timescale through the introduction of the new variable $\mathsf{t} = \omega_0 t$ [45, 46]. The Schrödinger operator $\mathcal{S}'(t)$ in $\mathbb{H}'$ is then given by

$$\mathcal{S}'(\mathsf{t}, \omega_0) = H'(\mathsf{t}) - i\hbar\omega_0 \frac{\partial}{\partial \mathsf{t}} \quad ; \quad H'(\mathsf{t}) = H(\mathsf{t}/\omega_0) \ . \tag{4.3.7}$$

The partial derivative of (4.3.7) with respect to ω_0 gives,

$$i\hbar \frac{\partial}{\partial \mathsf{t}} = -\frac{\mathcal{S}'(\mathsf{t}, \omega_0)}{\partial \omega_0} \ . \tag{4.3.8}$$

The substitution of (4.3.8) in (3.2.18) leads to the following relation,

$$\phi_G^{(\lambda)} = -\frac{2\pi}{\hbar} \left\langle\!\!\left\langle \Phi'_\lambda(\mathsf{t}) \left| \frac{\mathcal{S}'(\mathsf{t}, \omega_0)}{\partial \omega_0} \right| \Phi'_\lambda(\mathsf{t}) \right\rangle\!\!\right\rangle \quad ; \quad \Phi'_\lambda(\mathsf{t}) = \Phi_\lambda(t) \ . \tag{4.3.9}$$

If the Floquet mode $\Phi_\lambda(t)$ of the discrete spectrum of $\mathcal{S}(t)$ is a single-valued function of ω_0 in some interval $\Delta\omega$, and the associated quasienergy ε_λ is a differentiable function of ω_0 in this interval, one can apply the Hellman-Feynman theorem [68] and Eq. (3.2.3) to obtain

$$\left\langle\!\!\left\langle \Phi'_\lambda(\mathsf{t}) \left| \frac{\mathcal{S}'(\mathsf{t}, \omega_0)}{\partial \omega_0} \right| \Phi'_\lambda(\mathsf{t}) \right\rangle\!\!\right\rangle = \frac{\partial}{\partial \omega_0} \langle\langle \Phi_\lambda(t) \left| \mathcal{S}(t, \omega_0) \right| \Phi_\lambda(t) \rangle\rangle = \frac{\partial \varepsilon_\lambda}{\partial \omega_0} \ . \tag{4.3.10}$$

Note that for (4.3.10) to holds it is also necessary the time-dependent Hamiltonian of the system to be a continuous function of time.

From the equation above and the relation (4.3.9) it follows that

$$\phi_G^{(\lambda)} = -\frac{2\pi}{\hbar} \frac{\partial \varepsilon_\lambda}{\partial \omega_0} \tag{4.3.11}$$

[we remark that (4.3.11) is valid only for the case of non-degenerate quasienergies and Hamiltonians that are continuous in time].

Taking into account the periodicity of the Floquet mode $\Phi_\lambda(t)$ one can expand it in a Fourier series and for an N-level system (4.3.1) can be rewritten as

$$|\Psi(t)\rangle = \sum_{\lambda=1}^{N} \sum_{n=-\infty}^{\infty} A_\lambda A'_{\lambda n} \exp\left[-i \frac{(\varepsilon_\lambda - n\hbar\omega_0)}{\hbar} t\right] \ , \tag{4.3.12}$$

where $A'_{\lambda n}$ is the nth Fourier coefficient in the expansion of $\Phi_\lambda(t)$. Following the same procedure as for the case of a two-level-system, one can obtain from (4.3.12) that for the cyclic evolution of an N-level system the conditions a), b), and c) or their combination have to occur repeatedly. Thus, in the general case the necessary conditions for quasiperiodic cyclic evolution corresponding to the cases a), b), and c) are given, respectively, by a') $\epsilon_i - \epsilon_j = n_{ij}\hbar\omega_0$ $(i, j = 1, 2, ..., N;\ n_{ij} \in \mathbb{Z})$.

b') All but one of the products $A_\lambda A'_{\lambda n}$ vanish.

c')$(\epsilon_i - \epsilon_j)l = m_{ij}\hbar\omega_0$ $(i, j = 1, 2, ..., N;\ l, m_{ij} \in \mathbb{Z};\ m_{ij}/l \notin \mathbb{Z})$.

It is worth noting that if a quantum system satisfies not one but a combination of the above conditions then its evolution becomes also quasiperiodic cyclic.

These conditions look quite restrictive but as will be shown in the following chapters, inducing cyclic evolution to an N-level system can be achieved in actual physical systems. Regarding the existence or not of cyclic states for a given system [i.e., whether or not conditions a), b) or c) or their combinations can be fulfilled for a given system], it depends essentially on the initial conditions as well as on the specific form of the Hamiltonian of the system. If the initial wave function $|\Psi(t_0)\rangle$ is an eigenfunction of the evolution operator $U(t_0 + \mathcal{T}, t_0)$ then cyclic evolution occurs independently of the concrete form of the Hamiltonian [69]. This situation is particular clear for the case of time-periodic Hamiltonians. In such a case the existence of the Floquet modes $|\Phi_\lambda\rangle$ is guaranteed since they are the eigenvectors of the evolution operator $U(t_0 + T, t_0)$ [see (3.2.12)] (note that the evolution operator is an $N \times N$ matrix that can always be diagonalized). Now, if the initial vector state $|\Psi(t_0)\rangle = A_{\lambda'} \exp[-i\varepsilon_{\lambda'} t_0/\hbar]|\Phi_{\lambda'}(t_0)\rangle$ for some specific $\lambda = \lambda'$, then the wave function of the system collapses into a pure Floquet mode, i.e., the condition b) is realized and the state vector becomes cyclic $|\Psi(t)\rangle = A_{\lambda'} \exp[-i\varepsilon_{\lambda'} t/\hbar]|\Phi_{\lambda'}(t)\rangle$. On the other hand, for the case of an arbitrary initial condition (different from the kind of initial wave functions considered above) the existence or not of cyclic states has to be inferred after performing explicitly the calculations by checking whether or not one of the conditions a'), b') or c') can be reached, since, to our knowledge, a complete characterization of which kind of Hamiltonians have a complete set of cyclic states is not known.

Chapter 5

Sustainable orientation of polar molecules

In the last few decades there has been an impressive progress in the creation of new techniques an methods towards achieving the long-standing dream of controlling chemical reactions. In particular, it has been shown both theoretically and experimentally [70, 71, 72, 73, 74, 75, 76, 77, 78, 79, 80] that the initial orientation of molecules (here orientation refers to that of the direction of the molecular axis with respect to an applied external field, see Fig. 5.1) can play an important role for the outcome of molecular collisions as well as in chemical reaction dynamics. The steric effects in atom-molecule reactions strongly depend on the reagent orientation. By controlling the mutual orientation of the reagents one then observes its influence on the reaction probability, i.e., the total reaction cross section, or, better yet, the angular distribution of products from the reaction of oriented reagents. For example, it has been found that in the reactions $\mathrm{K} + \mathrm{CH_3I} \rightarrow \mathrm{KI} + \mathrm{CH_3}$ and $\mathrm{Rb} + \mathrm{CH_3I} \rightarrow \mathrm{RbI} + \mathrm{CH_3}$ products are formed more likely if the atoms approach the iodine end of the molecule (*head*) than if they encounter the $\mathrm{CH_3}$-end (*tail*) [71, 72, 73]. Thus, molecular orientation should greatly expand its range of applications in stereodynamical studies of chemical reactions [77, 79]. Furthermore, it has been shown that molecules subject to a laser field exhibit an enhanced ionization along the direction of the laser electric field [81, 82]. Other applications for which the molecular orientation results relevant are the laser-induced isomerization [83], molecular trapping [84], catalysis [85], high-order harmonic generation [86], and nanoscale design by laser focusing of molecular beams [84, 87].

There exist several methods for orienting molecules. For example, it has been experimentally demonstrated that an hexapole electric field can be used for orienting polar symmetric top or symmetric top-like molecules [70, 71, 72]. Other methods based on the notion that molecular rotation can be transformed into pendular motion by the interaction of a permanent dipole moment with an external field, resulting in orientation of the molecular axis, have also been proposed [75, 76, 88]. The pendular states are created by a field-induced coherent superposition (hybridization) of the field-free rotor states. The hybridization occurs most easily for the lowest rotational states and therefore rotationally cold molecules and strong fields (*brute force*) are required.

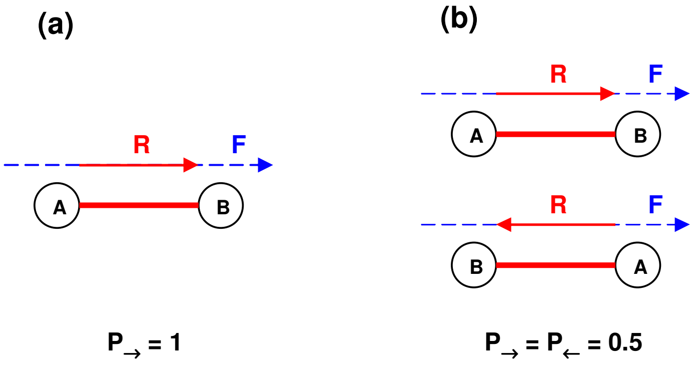

Figure 5.1: a) Perfect orientation: the molecular axis $\mathbf{R}$ is perfectly oriented in the direction of the external field $\mathbf{F}$ with probability $P_{\rightarrow} = 1$. b) Perfect alignment: the configurations corresponding to orientation and anti-orientation are equiprobable and $P_{\rightarrow} = P_{\leftarrow} = 0.5$.

A similar version of hybridization, applicable to nonpolar as well as polar molecules, exploits the induced dipole moment resulting from the interaction of an intense, nonresonant plane-polarized laser field with the anisotropic polarizability of the molecule [89, 90]. This procedure leads to the alignment of the molecule (here alignment refers to axial anisotropy but, unlike orientation that corresponds to a single-headed arrow, it corresponds to a double-headed arrow, see Fig. 5.1). However, no orientation is induced, since the electric field of the laser rapidly switches directions and its interaction with the permanent dipole averages out. To overcome such a problem, a procedure that combines a relatively weak electrostatic field and nonresonant induced dipole forces has been recently proposed for orienting molecules [91, 92].

It has been pointed out that Stark effects by electrostatic fields may not be desirable in some precise spectroscopic studies [93]. For such situations, general alternative schemes that exclude electrostatic fields and yield molecular orientation have recently been proposed [21, 25, 60, 61, 93]. For example, it is possible to orientate polar molecules by using the field interaction with the permanent dipole moment, the polarizability, and the hyperpolarizability of the molecule [93]. Within this scheme an adiabatic molecular orientation stronger than that obtained within the *brute force* methods (but weaker than the obtained with the scheme discussed in the following sections) is achieved. Note that in the adiabatic limit the molecular orientation can be maintained for several nanoseconds but the orientation process (i.e., the time needed for rising the orientation from zero to its maximum value) also lasts several nanoseconds [93]. Consequently, for some specific applications requiring a rapid orientation of the molecule, the adiabatic regime may not be appropriate.

In the nonadiabatic regime, it has been shown that the application of a short HCP can lead to a fast orientation of polar molecules [21, 25]. However, the resulting molecular orientation within such a procedure is not sustainable in time, since the effective duration of the HCP is much smaller than the rotational period of the molecule. Hence, once it has passed by the molecule evolves in a field-free manner, oscillating from oriented to nonoriented configurations. As a result, the time average of the orientation over the rotational period of the molecule vanishes [21, 25]. Although the postpulse (and therefore field-free) orientation of the molecule can be desirable in some specific situations it could also lead to limitations imposed by the time resolution of the phenomena under study and/or of the experimental capabilities. Therefore, it could be also desirable to have a method capable of inducing strong and sustainable molecular orientation in the nonadiabatic regime. In the following sections we focus on this problem and show that a conveniently designed train of HCPs can induce a strong and sustainable molecular orientation without disturbing the electronic and vibrational modes. The molecule evolves in a quasi-field-free manner in the sense that between consecutive pulses the electric field is practically zero. The molecular orientation obtained within our scheme is stronger than that obtained with previous methods and it is shown to be robust to thermal average up to temperatures of about 10 K [60, 61].

5.1 General formulation

We consider a diatomic molecule in its electronic ground state. The molecule, which is assumed to have a relatively large permanent dipole moment and a large moment of inertia is subject to a conveniently designed train of short HCPs. The HCPs utilized throughout our study have the following properties:

i) they are weak enough so as to avoid any ionization damage of the molecule upon the action of the HCPs (for typical diatomic molecules such as LiCl, LiF, LiH, NaI, the peak amplitude of the HCPs can be of several hundreds of kV/cm [21, 25, 94, 95]).

ii) they are very short with respect to the rotational period of the molecule.

We note that the property ii) can be achieved in actual physical situations, since the duration of experimentally generated HCPs can be of a few picoseconds or even of fractions of picoseconds (see Chap. 2), while the rotational period of typical diatomic molecules ranges from tents to hundreds of picoseconds. Under these circumstances, the use of the impulsive approximation (IA) (see Sec. 2.3) is well justified. Consequently, the IA is used throughout our calculations. In addition, it has been shown that HCPs satisfying the properties i) and ii) do not induce any vibrational excitation [21, 25, 94, 95]. One can therefore consider the molecule as a rigid rotor.

Within the IA and the rigid rotor approximation, the dynamics of the molecule subject to a train of short HCPs is determined by the following time-dependent Schrödinger equation:

$$i\hbar\frac{\partial\Psi(\theta,\phi,t)}{\partial t} = \left[\frac{L^2}{2I} - \mu_0 V(t)\cos(\theta)\right]\Psi(\theta,\phi,t) \quad , \tag{5.1.1}$$

where $I = mR_0^2$ is the moment of inertia at the internuclear equilibrium distance R_0 and m is the reduced mass of the nuclei. L stands for the angular momentum operator, μ_0 is the permanent dipole moment, θ represents the angle between the molecular axis and the applied field and ϕ specifies the corresponding azimuthal angle. The time-dependent shape $V(t)$ of the HCPs train is modelled, within the impulsive approximation, by a series of N consecutive *kicks*, i.e.,

$$V(t) = \sum_{k=1}^{N} \Delta p_k \delta(t - t_k). \tag{5.1.2}$$

Here t_k is the time at which the kth pulse is applied and Δp_k is the area beneath the kth pulse. Physically, Δp_k is the momentum transferred by the kth pulse to the molecule (see Sec. 2.3).

It is worth noting that as long as the duration of the HCPs remains shorter than the rotational period τ_{rot} of the molecule under study, the specific shape of the pulses is irrelevant and the dynamics is essentially determined by the amount of momentum transferred to the system by the pulses [21]. It has also been shown that the effective tail of the pulse (see Fig. 2.3) hardly influences the dynamics of the system [21]. For a pulse with amplitude asymmetry ratio $\sim 13:1$ (see Sec. 2.2), for example, the effect of the effective tail reduces to a very small correction to the amount of momentum transferred to the molecule by the pulse. Anyway, these effects can easily be incorporated by taking into account the effective tail when calculating the corresponding Δp_k.

If the applied HCPs are linearly polarized and in the absence of any other symmetry breaking fields the molecule retains the cylindrical symmetry around the molecular axis. As a consequence, the projection of the angular momentum M_J onto the field polarization axis is conserved. The time-dependent wave function that describes the quantum dynamics of the molecule under the action of the HCPs can be written as an expansion in terms of the stationary eigenstates, namely

$$\Psi_M(\theta,\phi,t) = \sum_{J=0}^{J_{max}} C_{J,M}(t) Y_{J,M}(\theta,\phi) \quad . \tag{5.1.3}$$

We assume that the initial value of M_J is M. $Y_{J,M}(\theta,\phi)$ are the spherical harmonics, and J_{max} corresponds to the highest eigenstate which is relevant for the time evolution of the system.

Substituting Eq. (5.1.3) into Eq. (5.1.1) we obtain the following system of differential equations for determining the expansion coefficients

$$i\hbar \frac{\partial \mathbf{C}_M(t)}{\partial t} = \mathbf{E}_M \mathbf{C}_M(t) - \mu_0 V(t) \mathbf{U}_M \mathbf{C}_M(t) \quad , \tag{5.1.4}$$

where $\mathbf{C}_M(t)$ is a vector of the form

$$\mathbf{C}_M(t) = (C_{0,M}(t), C_{1,M}(t), \ldots C_{J_{max},M}(t))^T \quad ,. \tag{5.1.5}$$

The matrix $\mathbf{U}_M$ is composed of the elements

$$U_{JM,J'M} = \langle Y_{J,M}(\theta,\phi)|\cos\theta|Y_{J',M}(\theta,\phi)\rangle \quad . \tag{5.1.6}$$

Analytical expressions for the scalar products appearing in the equation above can be obtained by taking into account that $\cos\theta \sim Y_{1,0}(\theta,\phi)$. Then after performing the integration of the corresponding product of three spherical harmonics [96] one obtains,

$$\langle Y_{J,M}(\theta,\phi)|\cos\theta|Y_{J+1,M}(\theta,\phi)\rangle = \sqrt{\frac{(J+M+1)(J-M+1)}{(2J+3)(2J+1)}} \quad , \tag{5.1.7}$$

$$\langle Y_{J,M}(\theta,\phi)|\cos\theta|Y_{J-1,M}(\theta,\phi)\rangle = \sqrt{\frac{(J+M)(J-M)}{(2J+1)(2J-1)}} \quad , \tag{5.1.8}$$

and

$$\langle Y_{J,M}(\theta,\phi)|\cos\theta|Y_{J',M}(\theta,\phi)\rangle = 0 \;\text{ for } J' \neq J \pm 1 \quad . \tag{5.1.9}$$

Furthermore, we define

$$\mathbf{E}_M = \mathrm{diag}(E_{0,M}, E_{1,M}, ...E_{J_{max},M}) \;\;, \tag{5.1.10}$$

where $E_{J,M}$ are the eigenenergies of the stationary states.

Integrating Eq. (5.1.4) over the time we obtain the following stroboscopic map from $t = t_k$ to $t = t_{k+1}$ (see Appendix B):

$$\mathbf{C}_M^{(k+1)} = e^{i\frac{\mu_0 \Delta p_k}{\hbar}\mathbf{U}_M} e^{-\frac{i}{\hbar}\mathbf{E}_M(t_{k+1}-t_k)} \mathbf{C}_M^{(k)} \quad . \tag{5.1.11}$$

In this relation we introduced the notation $\mathbf{C}_M^{(n)} = \mathbf{C}_M(t_n)$ and employed the initial condition $\mathbf{C}_M^{(0)} = \mathbf{C}_M(t = 0)$. In addition to the stroboscopic description [Eq. (5.1.11)] of the wave function evolution a (continuous) propagation between consecutive pulses is performed. This can be done by noting that between consecutive *kicks* the system evolves in a field-free fashion. Therefore, the system dynamics can be described in the time intervals $t_k \leq t < t_{k+1}$ by

$$\mathbf{C}_M(t) = e^{-\frac{i}{\hbar}\mathbf{E}_M(t-t_k)} \mathbf{C}_M^{(k)} \quad ; \quad t_k \leq t < t_{k+1} \quad . \tag{5.1.12}$$

Alternating Eqs. (5.1.11) and (5.1.12) the all-time evolution of the system is obtained.

The degree of the orientation of the molecule can be characterized by the expectation value

$$\langle\cos\theta\rangle_M(t) = \langle\Psi_M(\theta,\phi,t)|\cos\theta|\Psi_M(\theta,\phi,t)\rangle \quad . \tag{5.1.13}$$

The orientation parameter $\langle\cos\theta\rangle_M(t)$ varies in the interval $[-1, 1]$. Perfect orientation is achieved when $\langle\cos\theta\rangle_M(t)$ reaches its extremal values. A direct visual picture on the overall quantum dynamics of the system is offered by the angular resolved, time-dependent probability density

$$P_M(\theta,t) = \int_0^{2\pi} |\Psi_M(\theta,\phi,t)|^2 d\phi \;\; . \tag{5.1.14}$$

The quantities $\langle\cos\theta\rangle_M(t)$ and $P_M(\theta,t)$ are the central objects of the analytical and the numerical analysis presented in the following sections.

Due to the smallness of the rotational level spacing the rotational modes can be thermally excited. Therefore, a realistic treatment including the effects of finite temperatures (T) has to include the corresponding thermal average. For the orientation parameter the thermal average $\langle\langle\cos\theta\rangle\rangle(t)$ is obtained, at low temperatures, from the relation

$$\langle\langle\cos\theta\rangle\rangle(t) = Z^{-1} \sum_{J=0}^{J_{max}} P(J) \sum_{M_J=-J}^{J} \langle\cos\theta\rangle_{J,M_J}(t) \quad . \tag{5.1.15}$$

In the equation above $\langle\cos\theta\rangle_{J,M_J}$ refers to the orientation parameter corresponding to a molecule initially in the $|J, M_J\rangle$ stationary state. The function

$$P(J) = \exp\left[\frac{-BJ(J+1)}{k_B \mathrm{T}}\right] \tag{5.1.16}$$

is the Boltzmann distribution function associated with the rotational states. The rotational constant of the molecule is represented by $B = \hbar^2/(2I)$ and k_B is the Boltzmann constant. The partition function is denoted by

$$Z = \sum_{J=0}^{J_{max}} (2J+1)P(J). \tag{5.1.17}$$

5.1.1 Analytical approach

For a clear understanding of the time evolution of the system we develop in this section a two-level system approximation (TLSA). This approximation is based on the assumption that only the two lowest eigenstates are involved in the system evolution. The TLSA is in general of a limited validity, in particular it breaks down with increasing temperatures and/or for strong HCPs. Under appropriately chosen conditions, however, the TLSA provides a useful and comprehensive picture of the evolution of the system. In addition, as detailed below it is possible to deduce from this model analytical conditions for the optimal control of the molecular orientation.

Within the TLSA the complex vector $\mathbf{C}_{_M}(t)$ reduces to a two-dimensional spinor. Following the ideas of the GBVA, one can introduce the Bloch vector $\mathbf{B}(t)$ through the map Ξ [see Eq. (3.1.15)] and taking account of the fact that the Pauli matrices σ_i $(i = x, y, z)$ are the generators of the $SU(2)$ group. One then finds from Eqs. (5.1.11), (5.1.12), and the corresponding map Ξ from $\mathbb{C}^2$ to $\mathbb{R}^3$ that the action of the kth pulse on the system is determined, in the Bloch space, by the following relation [60, 61]:

$$\mathbf{B}(t_k) = \begin{pmatrix} 1 & 0 & 0 \\ 0 & \cos\alpha_k & -\sin\alpha_k \\ 0 & \sin\alpha_k & \cos\alpha_k \end{pmatrix} \mathbf{B}(t_k^-) \ , \tag{5.1.18}$$

where

$$\alpha_k = \frac{2\mu_0 \Delta p_k}{\hbar\sqrt{3}} \ , \tag{5.1.19}$$

and $t_k^- = t_k - \epsilon$ (with $\epsilon \to 0^+$) and t_k refer to the times just before and right after the kth pulse, respectively. On the other hand the field-free evolution of the system in the time intervals $t_k \le t < t_{k+1}$ is determined by

$$\mathbf{B}(t) = \begin{pmatrix} \cos\beta_k & -\sin\beta_k & 0 \\ \sin\beta_k & \cos\beta_k & 0 \\ 0 & 0 & 1 \end{pmatrix} \mathbf{B}(t_k) \ , \tag{5.1.20}$$

where

$$\beta_k = \frac{2\pi(t - t_k)}{\tau_{_{rot}}} \ , \tag{5.1.21}$$

and $\tau_{_{rot}}$ denotes the rotational period of the molecule [for details on the obtention of (5.1.18) and (5.1.20) see Appendix B]. Equations (5.1.18) and (5.1.20) offer a clear geometrical

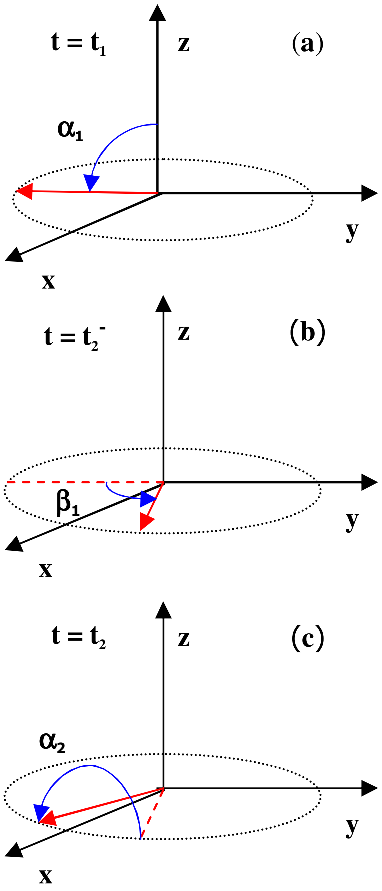

Figure 5.2: Geometrical illustration of the time-evolution of the system. (a) The Bloch vector is at $t = t_1 = 0$. (b) The Bloch vector is at $t = t_2^- = \frac{\tau_{rot}}{4} + \delta - \epsilon$ ($\delta \ll \tau_{rot}/4$, $\epsilon \to 0^+$). (c) The position of the Bloch vector at the time $t = t_2$.

interpretation of the evolution of the system. The action of the kth pulse represents an counterclockwise rotation of the Bloch vector **B** by an angle α_k round the x axis, while the field-free motion between the kth and the $(k+1)$th pulses amounts to rotating **B** counterclockwise by an angle β_k round the z axis.

Within the TLSA the orientation parameter [Eq. (5.1.13)] can be rewritten in terms of the Bloch vector as follows

$$\langle \cos\theta \rangle_M(t) = \frac{1}{\sqrt{3}} B_x(t) \quad . \tag{5.1.22}$$

In the Bloch space, the initial state of the system is given by the vector (0,0,1) [note that this vector is invariant to rotations round the z axis, i.e., it actually represents a stationary state], while the state of optimal orientation corresponds to the vector (1,0,0) [see Eq. (5.1.22)]. The process of inducing molecular orientation consists then in transforming the vector (0,0,1) into (1,0,0) through rotations around the x and z axes. One then searches for pulse parameters of field-induced rotations that leave quasi-invariant the Bloch vector (1,0,0) corresponding to the optimal molecular orientation. This simple geometrical interpretation leads to the procedure illustrated in Fig. 5.2 for inducing and maintaining the molecular orientation of a molecule initially in its rotational ground state. One applies, at $t = t_1^- = -\epsilon$ ($\epsilon \to 0^+$), an auxiliary pulse with a peak amplitude such that $\alpha_1 = \frac{\pi}{2}$ and the initial Bloch vector (0,0,1) evolves to (0,-1,0) [see Fig. 5.2 (a)]. After a subsequent time delay, at $t = t_2^- = \frac{\tau_{rot}}{4} + \delta - \epsilon$ ($0 < \delta < \frac{\tau_{rot}}{4}$; $\epsilon \to 0^+$), the Bloch vector evolves as shown in Fig. 5.2 (b) and the molecule is well oriented [note that now the vector $\mathbf{B}$ is close to the vector (1,0,0) corresponding to the optimal molecular orientation], i.e., at $t = t_2^-$ the observable $\langle\cos\theta\rangle_M(t)$ has reached the desired value. Following the ideas discussed in Chap. 4, we search for a procedure to induce quasiperiodic quasistationarity to the system. By applying at $t = t_2^-$ a second pulse with parameters such that $\alpha_2 = \pi$, the Bloch vector evolves as shown in Fig. 5.2 (c). Then upon a time delay 2δ, the Bloch vector returns to the position depicted in Fig. 5.2 (b), i.e., its evolution becomes cyclic: $\mathbf{B}(t_2^-) = \mathbf{B}(t_2^- + 2\delta)$. Iterating this procedure one can induce quasiperiodic cyclic evolution to the system and the Bloch vector will oscillate between the positions displayed in Figs. 5.2 (b) and (c) with a period $\mathcal{T} = 2\delta$. The solid angle Ω_γ corresponding to the closed path γ described by the Bloch vector on the sphere $\mathbb{S}^2$ during each evolution cycle can easily be obtained and the corresponding AA geometric phase is found to be given by

$$\phi_G = \frac{\Omega_\gamma}{2} = \frac{1}{2}\int_0^{\pi}\int_0^{(2\pi\delta)/\tau_{rot}} \sin\theta d\theta d\varphi = \frac{\pi}{2}\left(1 - \cos\left(\frac{2\pi\delta}{\tau_{rot}}\right)\right) \quad . \tag{5.1.23}$$

Now, if the parameter δ is chosen such that $\delta \ll \frac{\tau_{rot}}{4}$, the condition for quasistationarity [see (4.2.20)] is approximately fulfilled. It is worth noting, however, that in an actual physical situation there are some limitations on the possible values of the period $\mathcal{T}$ (and therefore on the parameter $\delta = \mathcal{T}/2$) imposed by the duration of the pulses (note that in the present case $\mathcal{T} = T$ and T has to be longer than the duration of each HCP together with the corresponding effective tail, in order to avoid the overlapping between consecutive pulses).

Following the scheme proposed above, quasiperiodic quasistationarity is induced to the system, the Bloch vector performs a cyclic evolution in a close vicinity of the vector $(1, 0, 0)$, and the molecule attains and maintains its maximal orientation $\langle\cos\theta\rangle \approx \frac{1}{\sqrt{3}}$ [see Eq. (5.1.22)] until the train of pulses is turned off [we note that for the quasiperiodic quasistationarity of $\langle\cos\theta\rangle$ to occurs it is necessary the train of pulses to lasts for a time longer than the corresponding deviation time τ_o that, in the present case, is related to the rotational period of the molecule as $\tau_o = \tau_{rot}$].

Summarizing, the TLSA leads to the following sequence of HCPs for a large sustainable molecular orientation: One applies, at first, an auxiliary pulse with a peak amplitude that provides the kick $\Delta p_1 = \frac{\sqrt{3}\hbar\pi}{4\mu_0}$ (i.e., $\alpha_1 = \pi/2$) and, after a time delay $t_2 - t_1 = \frac{\tau_{rot}}{4} + \delta$, a periodic train of HCPs with period $T \approx 2\delta$ and $\Delta p_k = 2\Delta p_1$ ($k > 1$). The value of δ can be arbitrarily chosen within the restriction $\delta \ll \frac{\tau_{rot}}{4}$ but not too small (to avoid the overlap of consecutive pulses).

The geometrical interpretation discussed above offers the following physical picture of the evolution of the system which serves as the basis for the control schemes proposed here (it will be shown below that this picture is not only valid for TLSA but, also viable for the general case). The application of an auxiliary HCP (or several auxiliary pulses as discussed in the following section) creates a rotational wave packet. Applying the external field the molecule begins to orientate along the field direction until it reaches a maximum orientation. We recall that the molecules here considered have a large moment of inertia. Therefore, once the maximum molecular orientation is achieved, the molecule reverses its rotational motion to orientates in the opposite direction. This process of reaching maximal orientation followed by orientation reversal is periodically repeated. This is because after the pulse has passed by, the molecule evolves in a field-free fashion. Strong molecular orientation is only achieved at time intervals close to the time at which the molecule reaches its optimal orientation. As a result of this behavior, if we subject the molecule only to a single pulse we cannot achieve a sustainable molecular orientation. In fact, within a rotational period, the time average of the orientation parameter vanishes [21, 25, 94].

The above picture of the creation and the time evolution of the molecular orientation changes if a second HCP is applied at the time when the molecule reaches the maximal orientation (due to the first HCP) and starts to reverse its rotational motion [cf. Fig. 5.2 (b)]. Provided the second pulse is strong enough a new reversal of the rotational wave packet motion is induced. Consequently, the molecule returns to its maximal orientation [cf. Fig. 5.2 (c)].

From the above we conclude that the application of several appropriately designed pulses renders possible the creation of sustainable molecular orientation lasting as long as the duration of the train of HCPs. The ideas behind this scheme are also valid in the general case when all the levels participate in the evolution of the system. The key question for practical implementation of the scheme is how to determine the parameters of the required pulses. A first hint for answering this question was provided by our discussion of the TLSA. However, as the TLSA is not valid for arbitrary values of the pulse parameters and is expected to fail especially when increasing temperatures, we also performed full numerical calculations for the optimization of the molecular orientation. This calculations are discussed in the following sections.

5.1.2 Numerical approach

In the general case, when subjecting the molecule to a strong HCP at finite temperature T, a large number of levels has to be included for a proper treatment of the time evolution of the system. An analytical approach becomes then intractable and one has to resort to full numerical methods. This section provides the details of the numerical model for optimizing the molecular orientation.

To obtain the wave function [Eq. (5.1.3)] one has to determine the expansion coefficients. Those are deduced from Eq. (5.1.12) between consecutive pulses and from the matching conditions Eq. (5.1.11) at the time steps when the pulses are applied. The quantities characterizing the molecular orientation are then evaluated using Eqs. (5.1.13) and (5.1.14). The highest relevant angular momentum value J_{max} of J is determined by inspecting the convergence condition

$$\sum_{J=0}^{J_{max}} \sum_{M_J=-J}^{J} |C_{J,M}|^2 \approx 1 \ , \tag{5.1.24}$$

which states that the angular momentum states beyond J_{max} are irrelevant.

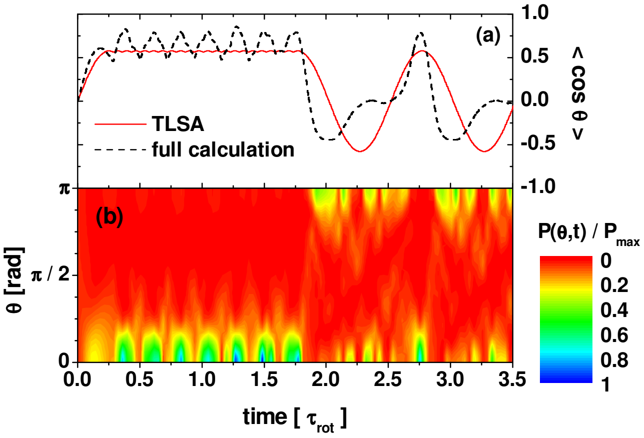

Figure 5.3: (a) Time dependence of the orientation parameter $\langle\cos\theta\rangle$ in units of the rotational period of the molecule. The pulse width is 1 ps ($\approx$ 0.0072 τ_{rot}). The optimal orientation pulse parameters are derived from the TLSA [$t_1 = 0$, $t_2 = 39.5$ ps ($\approx$ 0.29 τ_{rot}), $t_k = t_2 + (k-2)T$, $T = 10$ ps ($\approx$ 0.072 τ_{rot}), $F_1 = 93.5$ kV/cm, and $F_k = 187$ kV/cm ($k \geq 2$)]. The results of the TLSA (solid curve) are shown along with the full numerical calculations (dashed curve). (b) Numerical results (including all the spectrum) for the angular and time dependence of the probability density $P(\theta, t)$ normalized to its maximum value P_{max}. The pulse parameters are the same as in (a).

For the calculations we used the parameters corresponding to NaI molecules. This particular molecule is chosen as prototypical example for a polar molecule with a large moment of inertia (the rotational constant $B \approx 0.12$ cm^{-1}) and has a permanent dipole $\mu_0 = 9.2$ D. As stated in Sec. 5.1, for the treatment of the HCPs within the impulsive approximation it is essential the rotational period τ_{rot} to be much longer than the pulse durations ($\sim 0.5 - 1$ ps). This condition is well fulfilled for NaI since its rotational period is $\tau_{rot} = 138$ ps. Thus the impulsive approximation [Eq. (5.1.2)] is justified and used throughout the calculations. As done in Ref. [21], we assume sine-square HCPs with peak amplitudes F_k up to 600 kV/cm and durations in the range of $d \sim 0.5 - 1$ ps. The pulse areas are then obtained as $\Delta p_k = F_k d/2$. A reasonable choice for the ratio $\mathcal{R}$ of the pulse duration as compared to the time delay between them is essential. This choice has to be made in such a way as to avoid the overlap of consecutive pulses. In the present study we employ for this ratio a maximum of $\mathcal{R} = 1/8$.

5.2 Orienting NaI molecules

In this section we present the results of our calculations for the case of NaI molecules. The calculations were performed for the scheme provided by the TLSA in Sec. 5.1.1. Further schemes based on applying multiple auxiliary pulses and a subsequent train of HCPs for optimizing the molecular orientation were also numerically implemented and their corresponding results are discussed bellow.

In order to test the predictions of Sec. 5.1.1, we performed a full-fledge numerical calculation with the pulse parameters predicted by the TLSA. The results are shown in Fig. 5.3 (a), where the time dependence of the orientation parameter is displayed.

As clear from Fig. 5.3 (a), the TLSA (solid line) cannot reproduce quantitatively the full dynamics of the system (dashed line), but it is in qualitative agreement with the numerical calculation, showing that the scheme suggested in Sec. 5.1.1 for inducing an efficient and sustainable molecular orientation is essentially valid even when all the levels are incorporated in the system evolution. The results obtained within the TLSA [solid line in Fig. 5.3 (a)] show a strong induced quasistationarity of the molecular orientation (note that in this case the curve representing the time dependence of the orientation is practically flat during the time the system is driven by the train of HCPs). This behavior can be well understood from the fact that the period T of the train of pulses has been taken as $T = 10$ ps, i.e., $\delta = 5$ ps. Therefore, taking into account that for NaI molecules $\tau_{rot} = 138$ ps, one obtains from Eq. (5.1.23) that $\phi_G = 0.04$ rad, i.e., an AA geometric phase very close to zero, reflecting the strong quasistationarity of the induced molecular orientation.

A further useful quantity for the understanding of the time evolution of the system is the angular and time-resolved probability density $P(\theta, t)$ which is shown in Fig. 5.3 (b). Initially [before applying the first pulse $(t < 0)$], the probability density $P(\theta, t)$ is isotropically distributed, signifying the absence of orientation. After the application of the second pulse the angular distribution of $P(\theta, t)$ is squeezed in a localized region around $\theta = 0$ [cf. Fig. 5.3 (b)]. The strong localization (orientation) effect is time-dependent and lasts for $\tau_f \approx 250$ ps (i.e., $\tau_f \approx 1.8\ \tau_{rot}$). When the HCPs train is over the system evolves in a field-free manner with the rotational period of the molecule, regaining again its strong orientation at $t \approx \tau_f + \tau_{rot}$.

The TLSA guided us to the procedure of Fig. 5.3 which, compared to previous schemes (e.g. [21, 25, 92, 93, 94, 97, 98]), yields a strong and sustainable molecular orientation. On the other hand, the full numerical results indicate the possibility of achieving even stronger orientation when higher levels are included (see Fig. 5.3). Therefore, we envisage a second scheme based on applying two auxiliary pulses. Within this scheme we apply at first two auxiliary pulses for inducing strong orientation. The duration of the pulses is set to 1 ps ($\approx 0.0072\ \tau_{rot}$) and the time delay between them to 36 ps ($\approx 0.26\ \tau_{rot}$). Note that the time delay assumed is a few picosecond smaller than the value provided by the TLSA (39.5 ps) in order to take into account that when higher levels are included the orientation after the first pulse occurs faster than within the TLSA [see Fig. 5.3(a)]. The strengths F_1 and F_2 of the pulses are then numerically determined by imposing the condition $\langle \cos\theta \rangle > 0.8$. Several combinations obey this requirement, here we just show some of them in Fig. 5.4.

The results displayed in Fig. 5.4 are in agreement with those reported in Ref. [99], where an accumulative squeezing approach for inducing strong orientation was proposed. The scheme of Ref. [99] is based on the application of a sequence of pulses. Each pulse is applied when the molecule, after application of the previous pulse, reaches its maximum orientation (a similar behavior can be appreciated in Fig. 5.4). We note, however, that the

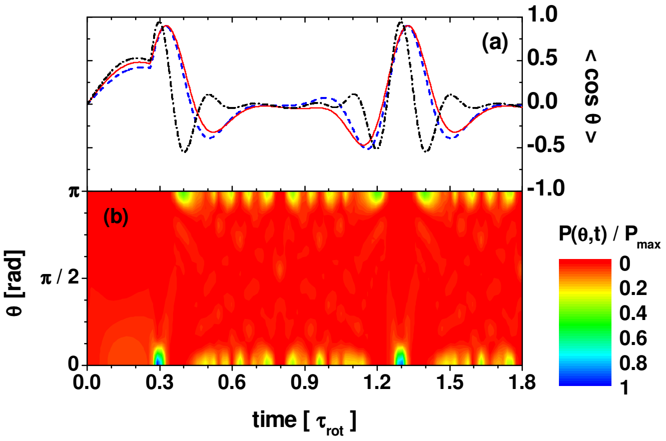

Figure 5.4: (a) Time dependence of the orientation parameter $\langle\cos\theta\rangle$ obtained with a first pulse applied at $t_1 = 0$ and a second one at $t_2 = 36$ ps ($\approx 0.26\ \tau_{rot}$) for different values of their strengths. Dashed line corresponds to $F_1 = 50$ kV/cm and $F_2 = 240$ kV/cm. Solid and dash-dotted lines correspond to $F_1 = 60$ kV/cm and $F_2 = 220$ kV/cm, and $F_1 = 70$ kV/cm and $F_2 = 420$ kV/cm, respectively. (b) Normalized angular distribution of the probability density corresponding to the dash-dotted line in (a) as a function of time and θ.

accumulative squeezing approach proposed in [99] requires the time delay between consecutive pulses to decrease exponentially with the number of pulses making the scheme too restrictive when a large number of pulses need to be considered (in an actual experimental situation the procedure will lead to the overlapping of the pulses). The authors of [99] proposed then to overcome this problem by the introduction of the τ_{rot} shift (during which the time average of the orientation is zero) between the pulses. Consequently, within the accumulative squeezing approach the molecular orientation is not sustainable (in the sense that between the successive times at which the molecule is well oriented, the time average of the orientation is zero). As suggested by the TLSA, to maintain the molecular orientation induced by the auxiliary pulses for times of the order of τ_{rot} or longer, the pulses have to be applied after the molecule has reversed its rotational motion, i.e., at certain delay time after the molecule reaches its optimal orientation.

Once the parameters of the two auxiliary pulses that lead to a strong orientation have been determined, a periodic train of HCPs which maintains the strong molecular orientation is applied. The optimal peak field and the period of the pulses are found by fixing the values of the pulse width (we assumed 1 ps) and setting the time t_3 of application of the train of HCPs close to the time at which the molecule, after application of the second auxiliary pulse, has reversed its rotational motion (i.e., a short time after the molecule reaches its maximum orientation). We then compute the time average of the orientation

$$Q = \frac{1}{(\tau_f - \tau_i)} \int_{\tau_i}^{\tau_f} \langle\cos\theta\rangle(t')dt' \ , \tag{5.2.1}$$

where τ_i and τ_f are the times at which the HCPs train is respectively applied and turned

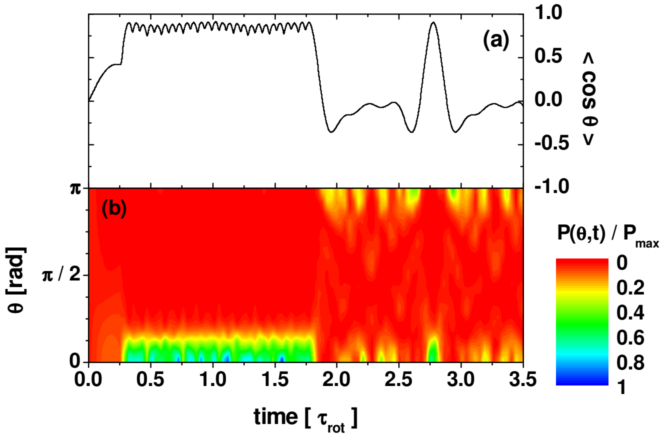

Figure 5.5: (a) Time dependence of the orientation parameter $\langle \cos\theta \rangle$ obtained with the field parameters $t_1 = 0$, $t_2 = 36$ ps ($\approx 0.26\ \tau_{rot}$), $t_3 = 49$ ps ($\approx 0.36\ \tau_{rot}$), $t_k = t_3 + (k-3)T$, $T = 8$ ps ($\approx 0.06\ \tau_{rot}$), $F_1 = 50$ kV/cm, $F_2 = 240$ kV/cm, and $F_k = 540$ kV/cm ($k \geq 3$). (b) The corresponding normalized angular distribution of the probability density as a function of time and θ.

off, and determine the values of the peak field and the period of the sequence of HCPs that lead to optimal orientation, i.e., those that maximize the averaged orientation Q.

The dynamics of the molecular orientation and the angular distribution corresponding to the maximum value of Q [see Eq. (5.2.1)] are displayed in Figs. 5.5 (a) and (b), respectively. The same qualitative behavior as in Fig. 5.3 is observed, but now the molecular orientation is stronger.

Generally, the orientation strength is destroyed at high temperatures T [25, 93, 94]. Thus, to achieve appreciable orientation at finite T we developed a three-auxiliary-pulses scheme. We use pulses with a duration of 0.5 ps ($\approx 0.0036\ \tau_{rot}$) separated by a delay time of 4 ps ($\approx 0.03\ \tau_{rot}$). The strengths of the first and the second auxiliary pulses are taken as $F_1 = 400$ kV/cm, and $F_2 = 200$ kV/cm. Following a similar procedure as for the two-auxiliary-pulses scheme, the optimization was performed with respect to the strength F_3 of the third auxiliary pulse while keeping the peaks of the subsequent train at $F_k = 600$ kV/cm ($k > 3$). To suppress the adverse effect of the thermal average on the molecular orientation, generally stronger pulses with shorter delay times are required. That is why we have taken the limit values (within the range of pulse parameters here considered) for the duration of the pulses and the time delay between them as well as for the peak amplitudes of the train of HCPs.

The results are depicted in Fig. 5.6, where the time dependence of the thermally averaged orientation is displayed for different values of the temperature. As shown in Fig. 5.6, within our scheme, a strong molecular orientation (compared to other methods [25, 93, 94]) can be achieved and maintained even at finite temperatures. It is worth noting that the fact that the orientation shown in Fig. 5.6 is maintained for a shorter interval of time than in the case of Fig. 5.5 is not a temperature effect. It is due to the fact that in Fig. 5.6 the period

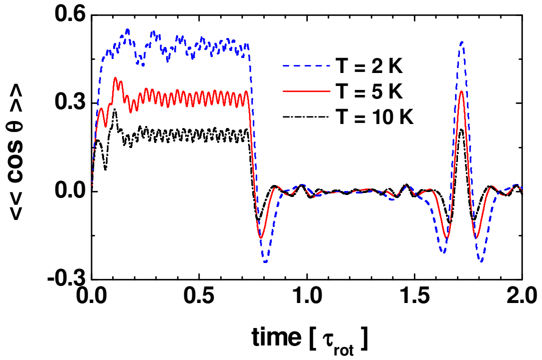

Figure 5.6: The thermal average ($\langle\langle \cos\theta \rangle\rangle$) of the orientation parameter versus the time at different temperatures T as depicted in the figure. HCPs are applied at times $t_l = (l-1)T$ [$T = 4$ ps ($\approx 0.03\ \tau_{rot}$), $l \geq 1$] with strengths $F_1 = 400$ kV/cm, $F_2 = 200$ kV/cm, $F_k = 600$ kV/cm ($k > 3$). The optimal values of F_3 are found to be about 375 kV/cm, 528 kV/cm, and 593.6 kV/cm for temperatures 2 K, 5 K, and 10 K, respectively.

of the pulses has been set to a half of the period used in Fig. 5.5 while keeping the same number of applied kicks. Therefore one can maintain the molecular orientation for longer times by applying more pulses.

Chapter 6

Control of electronic motion in double quantum wells

A variety of novel phenomena has been unravelled by studying the quantum dynamics of explicit time-dependent systems. In particular, the role of the time-dependent driving on the coherent tunnelling between two locally stable quantum wells has recently been investigated [45, 54, 55, 56, 100]. As an interesting result it has been found that an appropriately CW-laser driving can bring coherent tunnelling to an almost complete standstill. This driving induced phenomenon was termed coherent suppression of tunnelling [45, 54, 101] and yields other new quantum effects such as low frequency generation (LFG) and/or intense, nonperturbative harmonic generation in symmetric double quantum wells [45, 56, 100, 102]. Although these phenomena, as well as the possibility of controlling quantum coherence in double-well potentials [45, 54, 56, 100] and in two-level systems [45, 55, 102, 103] by using CW lasers have been extensively studied, only recently the possibility of a femtosecond control of the electronic motion in semiconductor double quantum wells driven by HCPs has been considered [67, 104, 105].

From the fundamental point of view it is interesting to investigate whether or not coherent suppression of tunnelling can be induced by a train of HCPs. In the case of symmetric double quantum wells driven by CW lasers, the coherent suppression of tunnelling is a direct consequence of the occurrence of accidental degeneracy of the quasienergies [45, 54, 100]. In fact, the requirement of accidental degeneracy of the quasienergies is usually referred to as a necessary condition for achieving coherent suppression of tunnelling [45, 54, 100, 103]. In the case of a train of HCPs as the driving field quasienergy degeneracy is not expected to occur because of the absence of well defined generalized parity of the Floquet modes, and the achievement of coherent suppression of tunnelling could be surprising at first sight. However, as we briefly commented in Chap. 4, the coherent suppression of tunnelling is just a particular case of induced quasistationarity. Then one can expect that coherent suppression of tunnelling induced by HCPs could occur through other than the quasienergy degeneracy mechanism [see conditions b) and c) in Sec. 4.3].

In the present chapter we perform a detailed study of the dynamical and emission properties of an electron in a semiconductor double quantum well driven by a train of

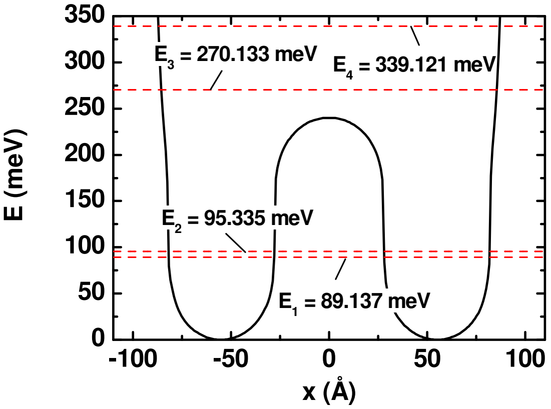

Figure 6.1: Electron confining potential. The central barrier hight is ∼ 240 meV. The well and barrier widths are ∼ 50 Å and ∼ 60 Å, respectively. Dashed lines indicate the lowest-energy levels.

HCPs. We show that a conveniently designed train of HCPs can indeed induce a strong localization of the electron in one of the wells by an efficient suppression of the tunnelling. The localization process can be controlled in the femtosecond scale. Therefore, the proposed scheme could be potentially useful for applications such as the designing of ultrafast switches [67, 104]. The emission spectrum is also investigated and phenomena such as LFG and half-harmonic generation (HHG) are also discussed.

6.1 General formulation

We consider a conduction electron confined in a typical $\mathrm{Al}_x\mathrm{Ga}_{1-x}\mathrm{As}$ based double quantum well. Within the parabolic band and the effective-mass approximations, the time-dependent Schrödinger equation describing the dynamics of the system under a train of HCPs can be written as

$$i\hbar\frac{\partial\Psi}{\partial t} = H\Psi \quad ; \quad H = H_0 + V_{conf} + V(z,t) \tag{6.1.1}$$

where H_0 represents the bare Hamiltonian, V_{conf} refers to the double-well confinement potential, and $V(z,t)$ corresponds to the interaction of the electron with the pulses. We use a symmetric shape for the confinement potential similar to that in [56, 100]. The central barrier hight is assumed to be about 240 meV and the well and barrier widths are, approximately, 50 Å and 60 Å, respectively (see Fig. 6.1). The electron effective mass $m^* = 0.067m_0$ is considered constant throughout the heterostructure. Effects of elastic scattering and electron-phonon interaction are neglected. For typical electron concentrations in high quality Ga(Al)As-GaAs heterostructures these effects lie in a scale of several picoseconds [106] that is longer than the time scale of interest in the present study.

The electron interaction with the train of strongly asymmetric pulses can be modelled by the potential

$$V(z,t) = -z \sum_{k=0}^{N-1} F_k U(t - t_p - kT) \ , \tag{6.1.2}$$

where

$$U(t) = \begin{cases} \exp\left[-\frac{t^2}{2\sigma^2}\right]\cos\Omega t & \text{if } -\frac{\pi}{2\Omega} \leq t < T - \frac{\pi}{2\Omega} \\ 0 & \text{otherwise} \end{cases} . \tag{6.1.3}$$

In Eqs. (6.1.2) and (6.1.3) F_k denotes the peak field of the kth pulse, $t_p = \frac{\pi}{2\Omega}$ corresponds to the time at which the positive tail of the first applied pulse is centered, T is the time between consecutive pulses, N is the number of applied pulses, and σ characterizes the width of the pulses. The parameter $\Omega = \frac{\pi}{3\sigma\sqrt{\ln 2}}$ in Eq. (6.1.3) guarantees a ratio 8:1 between the peak amplitudes of the positive and negative tails of the pulses. The duration d of the positive tail of each pulse is given by $d = 3\sigma\sqrt{\ln 2}$.

6.1.1 Numerical approach

The time-dependent Schrödinger equation [Eq. (6.1.1)] cannot be solved analytically, we therefore implemented a fast-Fourier-transform based numerical method as described in Sec. 3.3 for the propagation of the initial wave function in time. After computation of the time-dependent wave function $\Psi(z,t)$, we calculated the time-dependent probability

$$P_L(t) = \int_{-\infty}^{0} \Psi^*(z,t)\Psi(z,t)dz \tag{6.1.4}$$

and the average probability

$$\langle P_L \rangle_\tau = \frac{1}{\tau}\int_0^\tau P_L(t)dt \tag{6.1.5}$$

of finding the electron in the left well. The emission properties are studied through the quantity

$$I(\omega) = \left| \int_{-\infty}^{\infty} \mu(t)\exp[-i\omega t]dt \right| \ , \tag{6.1.6}$$

where $\mu(t) = \langle \Psi(z,t)|z|\Psi(z,t)\rangle$ is the time-dependent dipole moment. All calculations were performed with $\sigma = 20$ fs and $T = 100$ fs.

6.1.2 Analytical approach

For a better understanding of dependencies of the electron motion on the various parameters of the pulses we developed, in addition to the numerical scheme, a simple analytical approach that is capable of reproducing and explaining the main features of the numerical calculations. The analytical model is based on the observation that for the system under study the two lowest-energy levels are well separated from the other energy states (see Fig. 6.1). Hence, for a certain range of pulse parameters the system will behave, basically, as a two-level system. Although, the two-level system approximation (TLSA) introduces certain simplifications, the corresponding time-dependent Schrödinger equation with the interaction potential in

Eq. (6.1.2) cannot be solved analytically. However, further simplification is brought about by the fact that for ultrashort HCPs the duration of each pulse is much smaller than the typical characteristic time T_c of the undriven system (in the double quantum well studied here, we have, for example, $T_c \approx 665$ fs in the absence of the pulses, while the duration of the employed pulses is about 80 fs). As the width of the pulses is very small compared to the characteristic time of the undriven system, one can apply the impulsive approximation. Within the IA the kth actual pulse is replaced by an instantaneous kick that transfer the momentum

$$\Delta p_k = \int_{-\frac{\pi}{2\Omega}}^{T-\frac{\pi}{2\Omega}} F_k U(t) dt \tag{6.1.7}$$

to the system (see Sec. 2.3). The electron-pulses interaction can then be approximated as

$$V(z,t) \approx -z \sum_{k=0}^{N-1} \Delta p_k \delta(t - t_p - kT) \ , \tag{6.1.8}$$

where $\delta(x)$ represents the Dirac delta function. Note that the kth kick is applied at the same time the actual kth pulse reaches its maximum amplitude. Hence, the actual train of pulses [Eq. (6.1.2)] starts at $t = 0$, while within the IA the HCPs sequence [Eq. (6.1.8)] starts at $t = t_p$. For the sake of generality, in what follows we will denote by t_0 the time at which the train of pulses is turned on (i.e., $t_0 = 0$ for the exact calculation and $t_0 = t_p$ for the analytical approach) and in the case some confusion may appear we then specify the particular value of t_0.

We note that within the TLSA and the IA the time-dependent Schrödinger equation describing the dynamics of the electron in the double quantum well acquires the same structure than the Schrödinger equation treated in Sec. 5.1.1 for describing the two-level molecule. Therefore, in the present case the evolution of the system in the Bloch space is also determined by Eqs. (5.1.18) and (5.1.20) but now with the angles corresponding to the rotations induced by the kth pulse and the field-free evolution during the time interval $t \in [t_k, t_{k+1})$ given by

$$\alpha_k = \frac{2\mu_{12}\Delta p_k}{\hbar} \ , \tag{6.1.9}$$

and

$$\beta_k = \frac{2\pi(t - t_k)}{T_c} \ , \tag{6.1.10}$$

respectively. In (6.1.9) μ_{12} represents the dipole corresponding to the transitions between the two lowest eigenstates of the unperturbed system.

The probability $P_L(t)$ of finding the electron in the left well can be written, in terms of the Bloch vector, as follows

$$P_L(t) = \frac{1 - B_x(t)}{2} \ , \tag{6.1.11}$$

while the time-dependent dipole reads as

$$\mu(t) = \mu_{12} B_x(t) \ . \tag{6.1.12}$$

Eqs. (6.1.11) and (6.1.12) lead to

$$\mu(t) = -\mu_{12}\left[2P_L(t) - 1\right] \quad , \tag{6.1.13}$$

an expression that relates the dynamics of the electron motion [characterized by $P_L(t)$] to its emission properties [characterized by the Fourier transform of $\mu(t)$].

In the case of a quasiperiodic train of pulses, the study of the properties of the Floquet states and their quasienergies is of particular interest for understanding the dynamics of the system as well as its emission spectrum. Following the ideas of the FA (see Sec. 3.2) one can find without much effort that within the TLSA and the IA, the quasienergies are determined by

$$\varepsilon_\lambda = \epsilon_l + n\hbar\omega_0 \quad , \tag{6.1.14}$$

where $\lambda = (l, n)$ ($l = 1, 2$; $n = 0, \pm 1, \pm 2, ...$) and (see Appendix C)

$$\epsilon_1 = -\frac{\hbar\omega_0}{2\pi}\arccos(\cos\varphi\cos\vartheta) \quad ; \quad \epsilon_2 = -\epsilon_1 \quad , \tag{6.1.15}$$

with $\varphi = \frac{\mu_{12}\Delta p}{\hbar}$ and $\vartheta = \frac{\pi\omega_c}{\omega_0}$ ($\omega_c = \frac{2\pi}{T_c}$ is the characteristic frequency of the field-free system and $\omega_0 = \frac{2\pi}{T}$ is the frequency corresponding to the train of pulses). For an explicit treatment of periodically kicked two-level systems within the Floquet formalism see Appendix C.

In the coordinate representation, the Floquet modes $\Phi_l(z, t)$ satisfy the equation

$$\left(H - i\hbar\frac{\partial}{\partial t}\right)\Phi_l(z, t) = \epsilon_l\Phi_l(z, t) \quad . \tag{6.1.16}$$

We note that for HCPs the Eq. (6.1.16) is not invariant under the transformations ($z \rightarrow -z; t \rightarrow t + T/2$) as it is in the case of a CW laser. Consequently, the Floquet modes $\Phi_l(z, t)$ do not have well defined generalized parity. In such a situation we know from the von Neumann-Wigner theorem [48] that the existence of exact quasienergy crossings when a single system parameter is varied is no longer guaranteed and the quasienergies exhibit typically avoided crossings.

6.2 Coherent control of the electron dynamics

As the evolution of the wave function strongly depends on the initial conditions, we consider two possibilities for the initial wave function corresponding to initially localized (tunnelling initial condition) and initially delocalized (optical initial condition) states.

6.2.1 Tunnelling initial condition

In this case we consider an electron whose state at $t = 0$ is given by $|\Psi_0\rangle = (|1\rangle - |2\rangle)/\sqrt{2}$, where $|1\rangle$ and $|2\rangle$ are the two lowest-energy eigenstates of the electron in the absence of the pulses. This case corresponds to a particle trapped initially in the left well. As in this case the coherent suppression of tunnelling leads to the maintenance of the localization of the electron in the left well, in what follows we will refer to the coherent suppression of tunnelling just as *localization*.

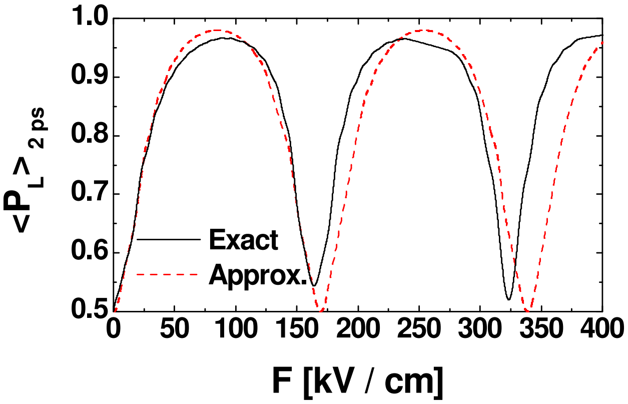

Figure 6.2: Time average of P_L as a function of the pulse strength for tunnelling initial condition.

The dependence of the average probability $\langle P_L \rangle$ of finding the electron in the left well on the pulse strength is displayed in Fig. (6.2) for the case of a quasiperiodic train of HCPs. The solid and dashed lines correspond to the full numerical calculation (including all the levels) and the analytical approximation, respectively. A good agreement between both calculations can be appreciated in the region of small pulse amplitudes. For strong pulses the TLSA is no longer valid and the differences between the analytical model and the exact numerical results become larger.

A remarkable fact is that, contrary to the case of a CW laser as a driving field, a train of HCPs can maintain the localization of the initially trapped particle in a wide range of pulse parameters. The existence of certain pulse amplitudes leading to optimal localization and delocalization can also be appreciated in Fig. (6.2). This behavior can be explained (within the analytical approximation) from the geometrical interpretation of the dynamics of the system in the Bloch space. In the Bloch space the tunnelling initial condition is represented by the vector $(-1, 0, 0)$. Before applying the first pulse, the vector **B** rotates counterclockwise around the z axis until the first pulse is applied at $t = t_p$. Just before the first kick, the vector **B** has then rotated an angle $\beta = \frac{2\pi t_p}{T_c}$ (see position 1 in Fig. 6.3). The first kick induces a rotation of **B** around the x axis. If the angle α of the kick-induced rotation is

$$\alpha = \frac{2\mu_{12}\Delta p}{\hbar} = (2n+1)\pi \qquad (n \in \mathbb{Z}) \quad , \tag{6.2.1}$$

then after the kick the vector **B** will be at position 2 (see Fig. 6.3), i.e., before the first pulse the particle was leaving the left well and now, after the pulse, the particle is returning to that well. If this procedure is iterated with $T = 2t_p$ and $t_p \ll T_c/4$ (this condition, as for the case discussed in Sec. 5.1.1, guarantees the achievement of quasistationarity) the vector **B** will remain oscillating in the vicinity of $(-1, 0, 0)$, i.e., the particle will remain localized to a large extent in the left well. We note that a similar situation in which **B** remains quasistationary in the vicinity of $(-1, 0, 0)$ occurs also if $T \neq 2t_p$ with $\max(T, t_p) \ll T_c/4$ (in fact, all the results shown in the present chapter correspond to the case $T > 2t_p$) but in

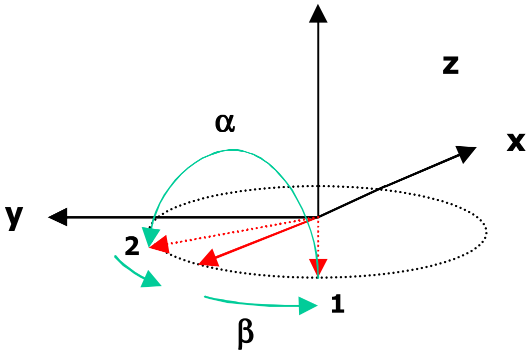

Figure 6.3: Geometrical interpretation of the localization condition, Eq. (6.2.1)

such a case sub-cycles can appear within each periodic cycle. Therefore, if $T \ll T_c/4$ (this condition prevents the delocalization of the particle during an evolution cycle), Eq. (6.2.1) represents a condition for determining the pulse parameters leading to the optimization of the electron localization in the left well. This behavior is illustrated in Fig. 6.4 (a), where the time dependence of the probability P_L of finding the electron in the left well is displayed for a pulse amplitude $F = 84.068$ kV/cm corresponding to $n = 0$ in Eq. (6.2.1). Solid and dashed lines correspond to the exact numerical calculations and to the analytical approximation, respectively (we stress that the exact numerical calculation is not a two-level system calculation but a full numerical solution of the Schrödinger equation, including all the levels of the system). If, on the contrary, the parameters of the pulse are such that

$$\alpha = \frac{2\mu_{12}\Delta p}{\hbar} = 2n\pi \qquad (n \in \mathbb{Z}) \ , \tag{6.2.2}$$

then after the pulse the vector **B** returns to position 1 (see Fig. 6.3), i.e., in this case the particle does not feel the field and behaves as in the field-free case, oscillating from one well to the other with a period approximately equal to the characteristic time of the unperturbed system. This situation is shown in Fig. 6.4 (b), where the probability of remaining in the left well as a function of time is shown for a pulse amplitude $F = 168.37$ kV/cm that corresponds to the case $n = 1$ in Eq. (6.2.2).

The dependence of the quasienergies (calculated within the analytical approximation) on the pulse strength is displayed in Fig. 6.5, showing that for the system here studied no crossing (and, therefore, no accidental degeneracy) of quasienergies occurs when a single system parameter (the pulse strength in the present case) is varied. This situation, as mentioned in the preceding section, is a consequence of the lack of well defined generalized parity of the Floquet modes.

The existence of localization in the absence of accidental degeneracy of the quasienergies can result surprising at first sight, since the existence of quasienergy crossings in the space of system parameters is usually regarded as a necessary condition for the achievement of coherent suppression of tunnelling [45, 54, 100, 103]. However, as discussed in Sec. 4.1, the actual necessary condition for inducing a sustainable localization (recall the coherent suppression of tunnelling is just a particular case of quasiperiodic quasistationarity) by a

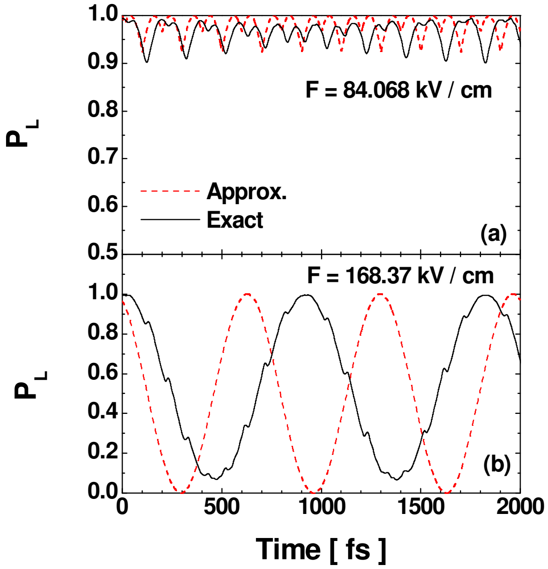

Figure 6.4: *Tunnelling initial condition.* (a) Time dependence of P_L for a pulse amplitude corresponding to $n = 0$ in the localization condition, Eq. (6.2.1). (b) Same as in (a) but for a pulse amplitude corresponding to $n = 1$ in the delocalization condition, Eq. (6.2.2).

quasiperiodic external field is the requirement of quasiperiodic cyclic evolution of the wave function of the system and, as was shown in Sec. 4.3, the existence of accidental degeneracy of the quasienergies is not the only mechanism that can lead to quasiperiodic cyclic evolution [see conditions a), b), and c) in Sec. 4.3]. For the system under investigation we found [see Eqs.(C.0.15) and (C.0.16) in Appendix C] that for $T = 2t_p$ and pulse amplitudes obeying Eq. (6.2.1) the localization mechanism is determined by the condition b) (see Sec. 4.3) for which the wave function of the system collapses into a pure Floquet state. In this case we obtain $A_1 = 0$ ($A_2 = 0$) for n even (odd) in Eq. (6.2.1).

Unlike for the case $T = 2t_p$, in the case $T > 2t_p$ each periodic cycle performed by the Bloch vector is composed of two sub-cycles with durations $2t_p$ and $2(T - t_p)$ as sketched in Fig. 6.6. In such a case the wave function of the system becomes cyclic quasiperiodic with period $\mathcal{T} = 2T$ and the localization mechanism corresponds to the condition c) (see Sec. 4.3) with $l = 2$. One can easily prove that the AA geometric phases corresponding to the first and second sub-cycles are given by

$$\phi_{G,1} = \frac{\pi}{2}\left[1 - \cos\left(\frac{2\pi t_p}{T_c}\right)\right] \quad , \tag{6.2.3}$$

and

$$\phi_{G,2} = \frac{\pi}{2}\left[1 - \cos\left(\frac{2\pi (T - t_p)}{T_c}\right)\right] \quad , \tag{6.2.4}$$

respectively. Thus, both sub-cycles obey the quasistationarity condition if $t_p \ll T_c/4$ and $(T - t_p) \ll T_c/4$. For $t_p = 25$ fs, $T = 100$ fs and $T_c = 665$ fs the values of the AA

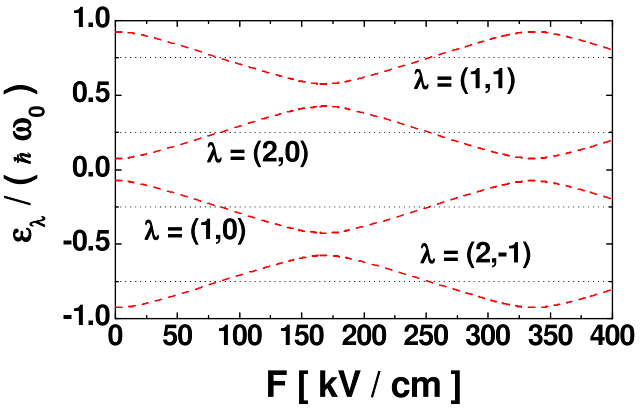

Figure 6.5: Dependence of the quasienergies on the pulse amplitude.

geometric phases obtained from Eqs. (6.2.3) and (6.2.4) are $\phi_{G,1} \approx 0.04$ and $\phi_{G,2} \approx 0.38$, respectively, reflecting the achievement of strong quasistationarity as shown in Fig. 6.4 (a). It can also be appreciated from Fig. 6.4 that each periodic cycle is indeed composed by two sub-cycles. One of the sub-cycles reflects stronger localization than the other as expected, since $\phi_{G,1} \ll \phi_{G,2}$.

A localization condition corresponding to the case $\mathcal{T} = 2T$ [equivalent to Eq. (6.2.1)] can be written, in terms of the quasienergies, as

$$\varepsilon_\lambda = \left(n \pm \frac{1}{2}\right)\frac{\hbar\omega_0}{2} \quad . \tag{6.2.5}$$

In obtaining Eq. (6.2.5) we took into account Eqs. (6.1.14) and (6.1.15).

The condition in Eq. (6.2.5) is represented in Fig. 6.5 by the intersection of the straight dotted lines with the quasienergies (dashed lines). The comparison of Figs. 6.2 and 6.5 confirms that Eq. (6.2.5) determines the pulse amplitudes corresponding to optimal localization.

Apart from the conditions a), b), and c) discussed in Sec. 4.3, the wave function of the system can be written as in Eq. (4.1.3) with $\mathcal{T} = T_c$ in the cases the system dynamics is similar to the field-free case (i.e., when the system behaves as *transparent* to the external field). We have found that this situation occurs if [67]

$$\epsilon_2 - \epsilon_1 = (1 - j)\hbar\omega_0 + (2j - 1)\hbar\omega_c \tag{6.2.6}$$

with $j = 0$ or $j = 1$. The condition in Eq. (6.2.6) leads to quasiperiodic cyclic evolution. It does not lead, however, to a sustainable localization, since the localization of the particle within one evolution cycle cannot be guaranteed (note that in this case $\mathcal{T} = T_c$ and the system behaves, essentially, as in the absence of external field) and quasistationarity cannot be achieved. In such a situation the periodic cycle described by $\mathbf{B}(t)$ on the sphere $\mathbb{S}^2$ is composed of $N + 1$ sub-cycles (with N the number of applied pulses within the periodic cycle). There are N sub-cycles corresponding to the N kick-induced rotations of $\mathbf{B}(t)$.

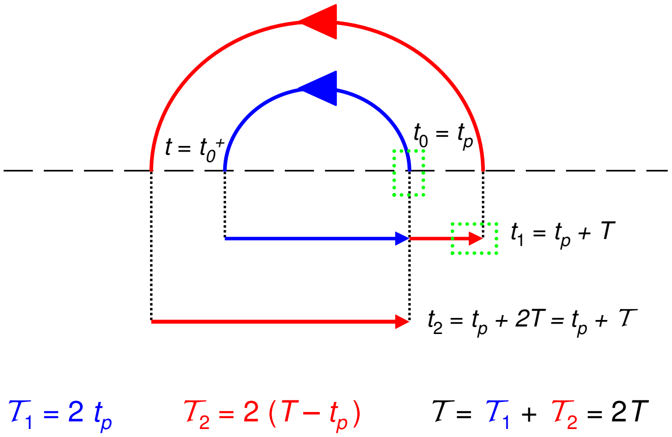

Figure 6.6: Sketch of the evolution of the Bloch vector for the case $T > 2t_p$ and pulse parameters obeying the localization condition Eq. (6.2.1). The horizontal dashed line represents the *equator* of the sphere $\mathbb{S}^2$. Solid lines represent the trajectory of the Bloch vector (note that the horizontal solid lines have been shifted for better visualization but they all lie on the *equator* line). The first sub-cycle (blue line) starts at $t = t_0$ and has a duration $\mathcal{T}_1$. The second sub-cycle (red line) starts at $t = 2t_p$ and has a duration $\mathcal{T}_2$. The duration of the periodic cycle is $\mathcal{T} = \mathcal{T}_1 + \mathcal{T}_2$ and is completed at $t = t_2 = t_p + \mathcal{T}$. The centers of the green rectangles correspond to the times of application of the HCPs.

Recall that under the condition (6.2.6) each kick rotates the vector $\mathbf{B}(t)$ by an angle $\alpha = 2n\pi$ [see Eq. (6.2.2)] round the x axis. The other sub-cycle corresponds to the *equator* (assuming the north and south poles lie in the z axis) of $\mathbb{S}^2$, and therefore to a solid angle $\Omega = 2\pi$. The AA geometric phase acquired by the wave function within this *equatorial* sub-cycle is then equal to π and the condition for quasistationarity is not fulfilled. Consequently, no quasistationarity is induced and the suppression of tunnelling is not achieved. In fact, Eq. (6.2.6) corresponds to avoided crossings of the quasienergies (see Fig. 6.5) and leads to optimal delocalization, as can be appreciated from the comparison of Figs. 6.2 and 6.5 [i.e., Eq. (6.2.6) constitutes a delocalization condition, equivalent to Eq. (6.2.2) with n odd (even) corresponding to $j = 0$ ($j = 1$)].

The IA introduced in the analytical model neglects the finite duration of the actual pulses, hence the duration of the evolution cycles corresponding to the actual system becomes longer that in the case of the analytical approach. Note, for example, that within the analytical approach the pulse induced rotation of the Bloch vector from position 1 to position 2 in Fig. 6.3 occurs instantaneously, while the corresponding evolution in the actual system lasts a finite time and, therefore, the evolution cycle for the actual system is longer. The differences in the evolution cycle durations originate then a dephasing between both models, as can be seen in Fig. 6.4.

After performing a procedure similar to that used in [100], we found that the emission spectrum [Eq. (6.1.6)] is determined by

$$I(\omega) = |I_1(\omega) + I_2(\omega) + I_3(\omega)| \quad , \qquad (6.2.7)$$

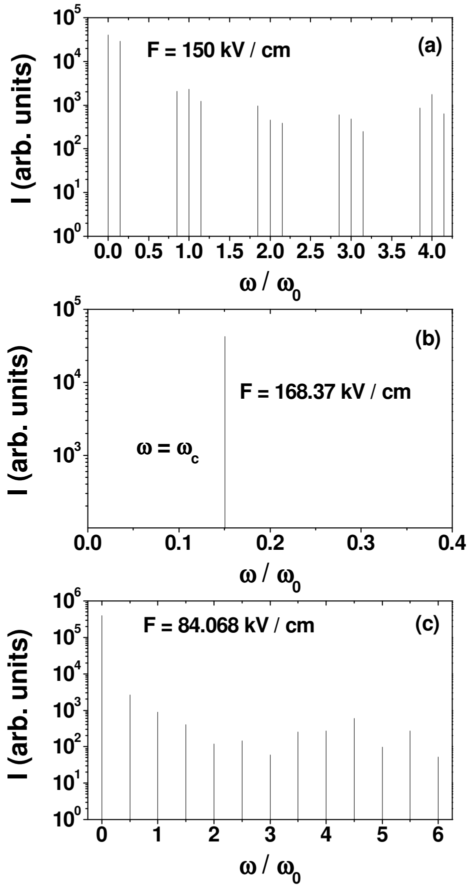

Figure 6.7: Emission spectrum for different values of the pulse strength.

where

$$I_1(\omega) = 2\pi \sum_{l=1}^{2} \sum_{m,n=-\infty}^{\infty} \Big[|A_l|^2 \\ \times \int_{-\infty}^{\infty} b_{ln}^*(z)\; z\; b_{lm}(z) dz\; \delta[(m-n)\omega_0 - \omega] \Big] \ , \tag{6.2.8}$$

$$I_2(\omega) = 2\pi A_1 A_2^* \sum_{m,n=-\infty}^{\infty} \Big[\int_{-\infty}^{\infty} b_{2n}^*(z)\; z\; b_{1m}(z) dz \\ \times\ \delta[(m-n)\omega_0 + (\epsilon_2 - \epsilon_1)/\hbar - \omega] \Big] \ , \tag{6.2.9}$$

and

$$I_3(\omega) = 2\pi A_2 A_1^* \sum_{m,n=-\infty}^{\infty} \Big[\int_{-\infty}^{\infty} b_{1n}^*(z)\; z\; b_{2m}(z) dz \\ \times\ \delta[(m-n)\omega_0 + (\epsilon_1 - \epsilon_2)/\hbar - \omega] \Big] \ . \tag{6.2.10}$$

In Eqs. (6.2.8) - (6.2.10) A_l represents the expansion coefficients in Eq. (3.2.9) (see also Appendix C) and $b_{ln}(z)$ are the coefficients of the Fourier expansion of the lth Floquet mode, i.e.,

$$\Phi_l(z,t) = \sum_{n=-\infty}^{\infty} b_{ln}(z) e^{in\omega_0 t} \quad ; \quad l = 1, 2 \ . \tag{6.2.11}$$

Unlike for the case of a CW laser as the driving field, in the present case the coefficients $b_{ln}(z)$ do not have well-defined parity. Therefore, no selection rules for the integrals in Eqs. (6.2.8) - (6.2.10) can be stated and the emission spectrum is composed, in general, by a static component at $\omega = 0$ [corresponding to $m = n$ in Eq. (6.2.8)], integer harmonics at $\omega = (m-n)\omega_0$ [corresponding to $m \neq n$ in Eq. (6.2.8)], a bandhead at $\omega = (\epsilon_2 - \epsilon_1)/\hbar$ [corresponding to $m = n$ in Eq. (6.2.9)], and doublets at $\omega = (m-n)\omega_0 \pm (\epsilon_2 - \epsilon_1)/\hbar$ [corresponding to $m \neq n$ in Eqs. (6.2.9) and (6.2.10)] around the integer harmonics. One can design the emission spectrum by using Eq. (6.1.15) for the estimation of the appropriate pulse parameters.

The emission spectrum (vertical lines represent the emission peaks) obtained through exact numerical calculations for different values of the pulse strength is shown in Fig. 6.7. The general case in which the four kind of emission lines are present is shown in Fig. 6.7 (a), where the phenomena of low-frequency generation (LFG) is also quite apparent. Because of the absence of accidental degeneracy of the quasienergies there is a lower limit for the LFG determined by the lowest value of the difference $\epsilon_2 - \epsilon_1$ (note that this lowest value corresponds precisely to the characteristic frequency ω_c of the undriven system), i.e., at the pulse parameters leading to optimal delocalization (see Figs. 6.2 and 6.5). Under the condition of optimal delocalization only the line corresponding to LFG (that in this limit coincides with ω_c) survives, while the other lines collapse, i.e., the system behaves as

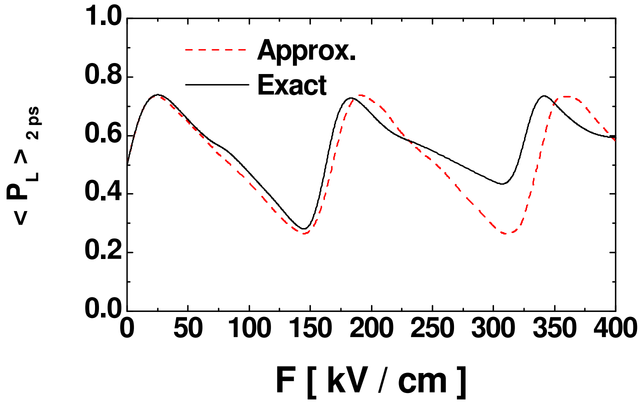

Figure 6.8: Time average of P_L as a function of the pulse strength for optical initial condition.

transparent to the external field [see Fig. 6.7 (b)]. On the contrary, when $\epsilon_2 - \epsilon_1 = \hbar\omega_0/2$, the doublets coincide at odd multiples of $\omega_0/2$. This situation corresponds to the process of optimal localization and the corresponding emission spectrum is displayed in Fig. 6.7 (c), where half-harmonic generation [i.e., at $\omega = n\omega_0/2$ $(n = 0, 1, 2, 3, ...)$] can be clearly appreciated. As clear from Eq. (6.1.13), the large static component present in Fig. 6.7 (c) is a manifestation of the strong localization effects [note also that in the case of optimal delocalization displayed in Fig. 6.7 (b) the static component vanishes].

6.2.2 Optical initial condition

Although the preceding case is widely treated in the literature, in practice, the more realistic situation is that the initial state corresponds to the ground state of the field-free system. Therefore, in the present case we consider this particularly important situation. Because of the symmetry of the double-well heterostructure, before applying the pulses, the particle is completely delocalized, with the same probability of being in the left or right well. This situation is represented by the vector (0,0,1) in the Bloch space [note that the vector (0,0,1) actually corresponds to a stationary state, since it is invariant to rotations around the z axis]. On the basis of the analytical approach one can find several strategies for inducing the electron localization with a quasiperiodic train of HCPs. By setting, for example, $T = T_c/4$ and pulse amplitudes such that

$$\frac{2\mu\Delta p}{\hbar} = (4n+1)\frac{\pi}{2} \quad , \quad (n \in \mathbb{Z}) \ , \tag{6.2.12}$$

the Bloch vector will follows periodically the cycle A-B-C-D-A [here A (B) represents the positive direction of the z (y) axis and C (D) the negative direction of the x (y) axis] and the electron will be localized in the left well. As we are specially interested in the case $T < T_c/4$ we also studied the possibility of inducing electron localization for that case. Following the geometrical interpretation of the evolution of the system one can find (although now the situation is less intuitive) that for $T < T_c/4$ the Bloch vector performs

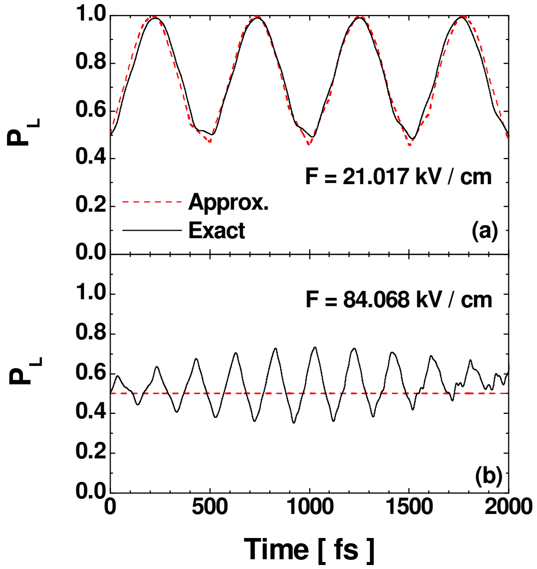

Figure 6.9: *Optical initial condition.* (a) Time dependence of P_L for a pulse amplitude corresponding to $n = 0$ in the localization condition, Eq. (6.2.13). (b) Same as in (a) but for a pulse amplitude corresponding to $n = 1$ in the delocalization condition, Eq. (6.2.14).

closed circuits corresponding to localization in the left (right) well if the pulse amplitudes obey the relation

$$\frac{2\mu\Delta p}{\hbar} = (2n+1)\frac{\pi}{2} + (-1)^{n+1}\frac{\pi}{4} \quad ; \quad n \in \mathbb{Z} \quad , \tag{6.2.13}$$

with n even (odd). On the other hand, for $T < T_c/4$ and pulse amplitudes such that

$$\frac{2\mu\Delta p}{\hbar} = n\pi \quad ; \quad n \in \mathbb{Z} \tag{6.2.14}$$

the electron will remain delocalized.

The average probability $\langle P_L \rangle_{2\mathrm{ps}}$ as a function of the pulse amplitude is displayed in Fig. 6.8 for the case $T = 100$ fs $< T_c/4$. Solid and dashed lines correspond to the exact numerical calculations and to the analytical approximation, respectively. It is clear from Fig. 6.8 that the initially delocalized electron can be steered to one well or to the other by choosing an appropriate value for the pulse amplitudes. A similar effect is achieved by changing the direction of the pulses. The time dependence of the probability of finding the electron in the left well is shown in Figs. 6.9 (a) and (b) for pulse amplitudes obeying Eqs. (6.2.13) and (6.2.14), respectively.

The process of inducing the electron localization of an initially delocalized electron by using a train of uniform quasiperiodic HCPs is not highly efficient (compare Figs. 6.2 and 6.8). Therefore we consider the possibility of optimizing the localization process by applying at first an auxiliary HCP and, after an appropriate time delay, a quasi periodic train of HCPs.

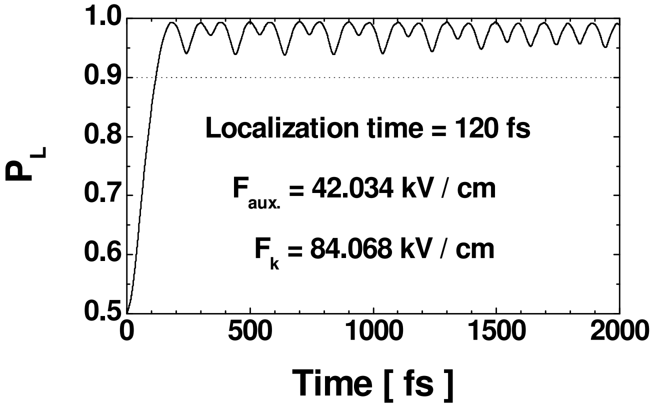

Figure 6.10: Optimal localization process for the case of optical initial condition.

By application of an auxiliary pulse with peak amplitude F_{aux} such that the condition $\frac{2\mu\Delta p_{aux}}{\hbar} = \frac{\pi}{2}$ holds [this pulse will rotate the Bloch vector from its initial direction (0,0,1) into (0,1,0)] and after a subsequent time delay $\tau = \frac{T_c}{4} + \delta$ ($\delta \ll T_c/4$), the Bloch vector of the system evolves to the position 1 in Fig. 6.3. One can then induce a strong localization of the electron in the left well by applying a train of HCPs with period $T \approx 2\delta$ and obeying the localization condition, Eq. (6.2.1). Thus, the first pulse pushes the electron into the left well and the subsequent train of HCPs maintains the particle localization in that well.

The results corresponding to the exact numerical calculations are shown in Fig. 6.10. One can see from Fig. 6.10 that a strong localization of the initially delocalized electron can be achieved in times of the order of hundreds of femtoseconds. This finding is in sharp contrast to the case when CW lasers are used as driving fields [56, 100], where it has not been possible to achieve such a strong localization and, in addition, the time needed for the control of the electron motion is found to be on the order of few picoseconds [56, 100]. Thus, the use of HCPs for controlling the electron motion in symmetric double quantum wells can be potentially useful for applications in designing electro-optical devices such as efficient ultrafast switches.

Chapter 7

HCPs induced currents in ballistic mesoscopic rings

Mesoscopic systems have been the object of considerable attention in the last decades because of their technological applications and their unique properties (see, for example, Refs. [107, 108, 109, 110, 111]). Of particular interest are the mesoscopic systems with ring-confining geometries. At low enough temperature, the phase coherence length of electrons in a mesoscopic ring (MR) can be considerably large compared to the size of the ring and the interference effects become important. As a manifestation of the interference effects, when a MR is threaded by a magnetic field, the thermodynamic properties of the system become periodic functions of the magnetic flux. The flux dependence of the free energy then leads to the existence of the so-called persistent currents [111, 112, 113, 114, 115, 116] and to the Aharonov-Bohm conductance oscillations [107].

The properties of persistent currents generated in MRs threaded by a static magnetic field have been studied in details. In particular, the electron-electron interaction [117, 118, 119], impurity scattering [117], and disorder [115, 118] effects on the persistent currents have been considered by various researchers. Persistent currents in carbon nanotube based rings have recently been studied [120]. Several experiments in which persistent currents have been measured, have also been reported [121, 122, 123, 124].

The dynamical effects produced by a time-dependent electric field acting on a MR threaded by a static magnetic field have been investigated in Refs. [125, 126, 127, 128], where the existence of a stationary non-equilibrium current has been theoretically demonstrated. The direct non-equilibrium current is a consequence of the nonlinear effects and is an odd function of the static magnetic flux (as for the case of persistent currents) that, consequently, vanishes if the static magnetic flux is zero [126, 127, 128]. Further investigations concerning the dynamical properties of MRs subject to external CW laser fields have also been reported [129, 130, 131].

In the present chapter we investigate the dynamics of non-interacting electrons confined in a ballistic thin MR subject to linearly polarized HCPs. We show that the application of a linearly polarized HCP on a ballistic thin MR induces a polarization that persists even after the HCP has passed by. Although once the HCP has passed by, the attenuated external field is not strictly zero, it is, however, too weak (see Chap. 2) as to produce any appreciable change in the evolution of the system, that will behave, essentially, as in the zero field case. For this reason we also refer to the postpulse polarization as a field-free polarization. In general, the applied HCP delivers an impulsive momentum transfer (or *kick*) to the system inducing postpulse, time-dependent charge oscillations that will last as long as the coherence is preserved. No current is induced, however, in the ring when a single linearly polarized HCP is applied. As one can expect from an intuitive point of view, the application of a single linearly polarized pulse does not destroy the clockwise-counterclockwise symmetry of the paths in the ring and the total current vanishes. This situation changes qualitatively, if a second HCP polarized in a direction other than the polarization direction of the first pulse is applied after the ring has been subject to the first HCP. In such a case the second HCP brakes the clockwise-counterclockwise symmetry and a non-equilibrium current is generated in the ring as will be shown in the following sections.

7.1 Postpulse polarization of mesoscopic rings

We consider a gas of non-interacting particles confined to an isolated 1D mesoscopic ring at low temperature (T ≈ 0 K). Despite the relative simplicity of this model, it has been shown to provide the main physical features in the description of thin MRs in the ballistic regime [111, 112, 113, 114, 115, 116, 123, 129]. A linearly polarized HCP is applied in the x direction at $t = t_1$. The duration of the pulse is assumed to be much shorter than the ballistic time τ_F a particle at the Fermi level requires for completing one turn along the ring (note that this condition is experimentally feasible since for typical ballistic rings τ_F is of the order of several tens of picoseconds [123, 132] and, as discussed in Chap. 2, HCPs as short as 1 ps can be generated with modern techniques). Consequently, one can safely treat the interaction of the system with the HCP within the impulsive approximation.

The Schrödinger equation describing the evolution of the system is given by

$$i\hbar\frac{\partial\Psi}{\partial t} = \left[-\frac{\hbar^2}{2m^*\rho_0^2}\frac{\partial^2}{\partial\theta^2} - q\rho_0\varepsilon_1(t)\cos\theta\right]\Psi \ , \tag{7.1.1}$$

where

$$\varepsilon_1(t) = p_1\delta(t-t_1) \ . \tag{7.1.2}$$

In Eqs. (7.1.1) and (7.1.2) ρ_0 represents the radius of the ring, $\delta(x)$ denotes the Dirac δ function, θ is the polar angle, and m^* and q are the effective mass and charge of the carriers, respectively. The pulse is applied at $t = t_1$ and transfers a momentum denoted by p_1 (p_1 is given by the area of the actual pulse) to the system (see Chap. 2). From now on we will assume $t = t_1 = 0$.

The solutions of Eq. (7.1.1) obey the following matching condition (see Appendix B)

$$\Psi(\theta, t=0^+) = \Psi(\theta, t=0^-)e^{i\alpha_1\cos\theta} \ , \tag{7.1.3}$$

where $\alpha_1 = q\rho_0 p_1/\hbar$ and $t = 0^-$ and $t = 0^+$ refer to the time just before and right after the application of the pulse, respectively.

The solution of Eq. (7.1.1) corresponding to a particle that is initially in the m_0th state can be written on the basis of the stationary eigenstates as

$$\Psi_{m_0}(\theta,t) = \frac{1}{\sqrt{2\pi}} \sum_{m=-\infty}^{\infty} C_m(m_0,t) e^{im\theta} e^{-i\frac{E_m t}{\hbar}} \quad , \tag{7.1.4}$$

where

$$E_m = \frac{\hbar^2 m^2}{2m^* \rho_0^2} \quad , \quad m = 0, \pm 1, \pm 2, ... \tag{7.1.5}$$

are the eigenenergies of the unperturbed states.

Taking into account the matching condition (7.1.3) and after applying the expansion theorem one finds that the expansion coefficients are given by

$$C_m(m_0,t) = \begin{cases} \delta_{m,m_0} & \text{for } t \leq 0 \\ i^{m_0 - m} J_{m-m_0}(\alpha_1) & \text{for } t > 0 \end{cases} \quad , \tag{7.1.6}$$

with $J_l(x)$ representing the Bessel functions and $\delta_{m,n}$ is the Kronecker symbol. In obtaining (7.1.6) the identity (D.0.1) was considered.

The energy spectrum of the particle is rearranged after the application of the pulse. The energy corresponding to a particle initially in the m_0th state is given by

$$E_{m_0}(t) = \langle \Psi_{m_0}(\theta,t) | H | \Psi_{m_0}(\theta,t) \rangle = i\hbar \left\langle \Psi_{m_0}(\theta,t) \left| \frac{\partial}{\partial t} \right| \Psi_{m_0}(\theta,t) \right\rangle \quad . \tag{7.1.7}$$

The substitution of Eqs. (7.1.4) - (7.1.6) in (7.1.7) leads to a postpulse energy (i.e., for $t > 0$),

$$E_{m_0}(t>0) = \frac{\hbar^2}{2m^* \rho_0^2} \sum_{m=-\infty}^{\infty} \left[m J_{m_0 - m}(\alpha_1) \right]^2 \quad . \tag{7.1.8}$$

The infinite sum involved in (7.1.8) can be performed exactly [see Eq. (D.0.3) in Appendix D] and the energy corresponding to a particle initially in the m_0th state is given by

$$E_{m_0}(t) = \begin{cases} \frac{\hbar^2 m_0^2}{2m^* \rho_0^2} & \text{for } t \leq 0 \\ \frac{\hbar^2}{2m^* \rho_0^2} \left(m_0^2 + \frac{\alpha_1^2}{2} \right) & \text{for } t > 0 \end{cases} \quad , \tag{7.1.9}$$

i.e., the HCP shifts the unperturbed energy spectrum by an amount that scales quadratically with the strength of the pulse and does not depend on the size of the ring. The initial degeneracy is therefore preserved after the pulse is applied. We remark that Eq. (7.1.9) is only valid for times much shorter than the duration of the complete pulse.

It is not difficult to prove from Eqs. (7.1.4) - (7.1.6) that $\Psi_{m_0}(\theta,t) = \Psi_{-m_0}(-\theta,t)$ i.e., the clockwise-counterclockwise symmetry is preserved after the application of the pulse, and therefore, currents carried by particles initially in the m_0 and $-m_0$ states compensate each other. This fact together with the degeneracy of the states [see Eq. (7.1.9)] confirms the intuitive expectation that no total current will be induced in the ring.

In order to characterize the degree of polarization in the direction of the pulse (i.e., along the x axis), we introduce the localization parameter

$$\langle\cos\theta\rangle_{m_0}(t) = \int_0^{2\pi} |\Psi_{m_0}(\theta,t)|^2 \cos\theta d\theta \ . \tag{7.1.10}$$

This parameter [analogue to the parameter commonly used for characterizing molecular orientation (see Sec. 5.1)] constitutes a measure of how strong a particle initially in the m_0th state localizes in the x direction. The parameter $\langle\cos\theta\rangle_{m_0}(t)$ varies in the interval $[-1, 1]$, taking the extreme values -1 and 1 when the particle is perfectly localized at the angles $\theta = \pi$ and $\theta = 0$, respectively. Note, however, that $\langle\cos\theta\rangle_{m_0}(t) = 0$ does not necessary mean that the particle is localized at $\theta = \pm\pi/2$. In such a case one only can say that the localization of the particle is symmetric with respect to the y axis, i.e., that the polarization in the x direction vanishes. Note also that the dipole moment on the x axis corresponding to a particle initially in the m_0th stationary state is proportional to $\langle\cos\theta\rangle_{m_0}(t)$ and, more precisely, is given by

$$\mu_{m_0}(t) = q\rho_0\langle\cos\theta\rangle_{m_0}(t) \ . \tag{7.1.11}$$

After some mathematical manipulations one can obtain from Eqs. (7.1.4) - (7.1.6) and (7.1.10) the following relation

$$\langle\cos\theta\rangle_{m0}(t) = \Theta(t)\alpha_1 h(\Omega) \sin\left[\frac{2\pi t}{\tau_p}\right] \cos\left[\frac{4\pi m_0 t}{\tau_p}\right] \ , \tag{7.1.12}$$

where $\Theta(x)$ denotes the Heaviside step function,

$$\Omega = \alpha_1\sqrt{2 - 2\cos[4\pi t/\tau_p]} \quad ; \quad \tau_p = \frac{4\pi m^* \rho_0^2}{\hbar} \ , \tag{7.1.13}$$

and

$$h(\Omega) = J_0(\Omega) + J_2(\Omega) \ . \tag{7.1.14}$$

In obtaining (7.1.12) we took into account Eq. (D.0.4).

From Eq. (7.1.12) it results $\langle\cos\theta\rangle_{m_0}(t) = \langle\cos\theta\rangle_{-m_0}(t)$. Therefore, the contributions of particles initially in the m_0 and $-m_0$ states to the polarization interferes constructively and a non-vanishing total polarization is generated.

The total dipole moment on the x axis induced in the ring is given by

$$\mu(t) = \sum_{m_0,\sigma} f(m_0, t)\mu_{m_0}(t) \ , \tag{7.1.15}$$

where σ refers to the spin of the particle, f represents the non-equilibrium distribution function, and $\mu_{m_0}(t)$ is given by Eq. (7.1.11). At low temperatures and for relatively weak pulses ($\frac{\hbar^2\alpha_1^2}{4m^*\rho_0^2} \ll E_F$), the non-equilibrium distribution function can be calculated within the relaxation time approximation [133, 134].

Within the relaxation time approximation, the non-equilibrium distribution function is determined by the Boltzmann equation:

$$\frac{\partial f(m_0, t)}{\partial t} = -\frac{f(m_0, t) - n_F(m_0)}{\tau_{rel}} \ , \tag{7.1.16}$$

where τ_{rel} represents the relaxation time and

$$n_F(m_0) = \left[1 + \exp\left(\frac{E_{m_0}(t) - \eta_0}{k_B \mathrm{T}}\right)\right]^{-1} \tag{7.1.17}$$

denotes the Fermi-Dirac distribution function corresponding to the equilibrium. In the equation above T, k_B, and η_0 represent the temperature, the Boltzmann constant and the chemical potential, respectively.

The Eq. (7.1.16) has to be complemented with the boundary condition specifying the value of the distribution function right after the application of the pulse,

$$f(m_0, 0^+) = n_F^{(1)}(m_0) = \left[1 + \exp\left(\frac{E_{m_0}(0^+) - \eta_1}{k_B \mathrm{T}}\right)\right]^{-1} \quad . \tag{7.1.18}$$

The values of the chemical potentials η_0 and η_1 depends on the physical nature of the system. If the ring is connected to a reservoir of particles, for example, the chemical potential is fixed and $\eta_0 = \eta_1$. In the particular case of our interest, in which the MR is isolated, the chemical potentials η_0 and η_1 have to be calculated, however, by requiring the number of particles N in the ring to be a constant. Thus, for a given isolated ring with N particles, η_0 is a function of the temperature, while η_1 depends on both the temperature and the pulse amplitude.

It is worth noting that in the case of an isolated MR the relaxation mechanism has to include, necessarily, inelastic scattering. The interaction of the carriers with the phonons is then crucial for the estimation of τ_{rel}. Here, however, we consider, for simplicity, τ_{rel} as a phenomenological parameter.

The Eq. (7.1.16) with initial condition (7.1.18) can be integrated over the time duration of the complete pulse for an arbitrary time-dependence of $n_F(E_{m_0}(t))$. After solving (7.1.16), taking into account that for times much shorter than the duration of the complete pulse (i.e., the time scale of our interest here) $E_{m_0}(t)$ is approximately given by (7.1.9), and considering that the value of the dipole moment before the application of the pulse (i.e., its equilibrium value) is zero, one can rewrite (7.1.15) as follows,

$$\mu(t) = e^{-\frac{t}{\tau_{rel}}} \sum_{m_0,\sigma} n_F^{(1)}(m_0)\mu_{m_0}(t) \quad . \tag{7.1.19}$$

At zero temperature only the lowest-lying states are occupied. In such a case the sum in Eq. (7.1.19) can be performed analytically by taking into account the dependence of the filling of the levels bellow the Fermi level on whether the carriers are spinless or spin-$\frac{1}{2}$ particles as well as on the number N of particles in the ring.

In the case of spinless particles at T = 0 K the filling of the levels bellow the Fermi level depends on whether there is an odd or even number of particles in the ring (we remark that we are considering an isolated ring and therefore the number of particles is a constant). In the case N is an odd number all the occupied levels are completely filled [see Fig. 7.1 (a)] and Eq. (7.1.19) reduces to

$$\mu(t) = e^{-\frac{t}{\tau_{rel}}} \sum_{m_0=-\frac{(N-1)}{2}}^{\frac{(N-1)}{2}} \mu_{m_0}(t) \quad . \tag{7.1.20}$$

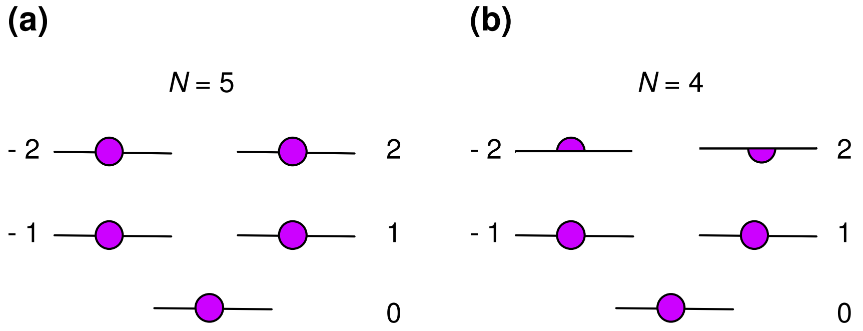

Figure 7.1: Filling of the energy levels at T = 0 K for the case of N spinless particles. a) N is an odd number and all the occupied levels are completely filled. b) N is an even number and, because of the energy degeneracy, the highest occupied levels are half-filled.

The substitution of (7.1.11) and (7.1.12) in (7.1.20) leads to the following expression

$$\mu_o(N,t) = -\Theta(t) q \alpha_1 \rho_0 h(\Omega) \sin\left[\frac{2\pi N t}{\tau_p}\right] e^{-\frac{t}{\tau_{rel}}} \ , \tag{7.1.21}$$

for the dipole moment corresponding to an odd number of spinless particles in the ring.

In the case of an even number of spinless particles, because of the energy degeneracy [see Eq. (7.1.9)], the highest occupied levels are half-filled [see Fig. (7.1)]. Consequently, in such a case (7.1.19) reduces to

$$\mu(t) = e^{-\frac{t}{\tau_{rel}}} \sum_{m_0=-\frac{(N-2)}{2}}^{\frac{(N-2)}{2}} \mu_{m_0}(t) + \frac{1}{2}\left[\mu_{-\frac{N}{2}}(t) + \mu_{\frac{N}{2}}(t)\right] \ . \tag{7.1.22}$$

Taking into account (7.1.11), (7.1.12) and (7.1.22) one then obtains that the dipole moment corresponding to the case of an even number of spinless particles in the ring is given by

$$\mu_e(N,t) = -\Theta(t) q \alpha_1 \rho_0 h(\Omega) \sin\left[\frac{2\pi N t}{\tau_p}\right] \cos\left[\frac{2\pi t}{\tau_p}\right] e^{-\frac{t}{\tau_{rel}}} . \tag{7.1.23}$$

For the case of spin-$\frac{1}{2}$ particles the induced dipole moment can be written as

$$\mu^{\sigma}(t) = \mu^{\uparrow}(t) + \mu^{\downarrow}(t) \ , \tag{7.1.24}$$

where $\mu^{\uparrow}(t)$ and $\mu^{\downarrow}(t)$ refer to the contribution from the spin up and spin down configurations, respectively. Four cases regarding the number of particles in the ring need to be considered separately. The situation is shown in Fig. 7.2, where the filling of the levels by spin-up (red circles and semicircles) and spin-down (blue circles and semicircles) particles is sketched. The comparison between Figs. 7.1 and 7.2 reveals the possibility of expressing the dipole moment corresponding to the case of spin-$\frac{1}{2}$ particles as a function of the dipole moment corresponding to the spinless particles case (see also Ref. [135]). We now study in details the four cases of interest.

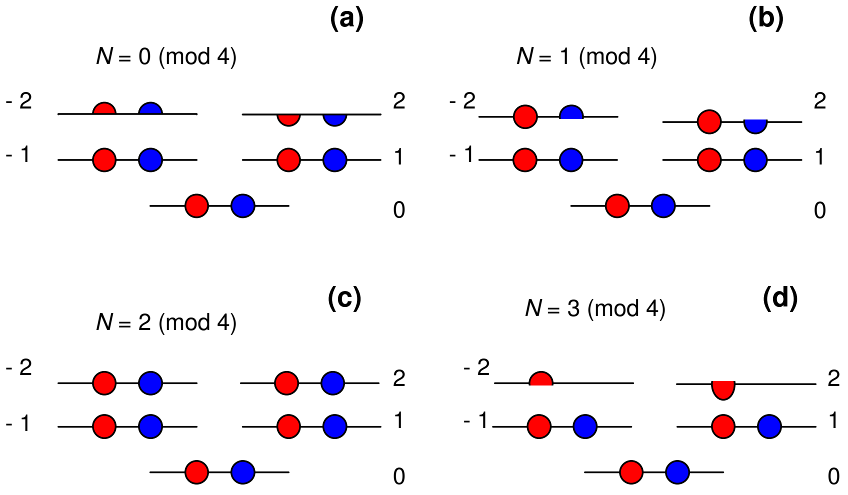

Figure 7.2: Filling of the energy levels at T = 0 K for the case of N spin-$\frac{1}{2}$ particles. Red and blue circles and semicircles correspond to spin-up and spin-down particles, respectively. a), b), c), and d) correspond to the cases $N = 0$ (mod 4), $N = 1$ (mod 4), $N = 2$ (mod 4), and $N = 3$ (mod 4) particles.

1) *An even number of pairs, i.e.,* $N = 0$ (mod 4)

In such a case one easily obtain from the comparison of Figs. 7.1 and 7.2 (a) that the contributions to the dipole moment resulting from up spins and down spins are

$$\mu^{\uparrow}(N,t) = \mu^{\downarrow}(N,t) = \mu_e(N/2,t) \quad , \tag{7.1.25}$$

i.e., they are identical and each is equal to the dipole moment corresponding to the case of $N/2$ spinless particles (note that $N/2$ is even).

2) *An even number of pairs plus an extra particle, i.e.,* $N = 1$ (mod 4)

From the comparison of Figs. 7.1 and 7.2 (b) it results that

$$\mu^{\uparrow}(N,t) = \mu_o((N+1)/2,t) \quad ; \quad \mu^{\downarrow}(N,t) = \mu_e((N-1)/2,t) \quad . \tag{7.1.26}$$

3) *An odd number of pairs, i.e.,* $N = 2$ (mod 4)

It results from the comparison of Figs. 7.1 and 7.2 (c) that

$$\mu^{\uparrow}(N,t) = \mu^{\downarrow}(N,t) = \mu_o(N/2,t) \quad , \tag{7.1.27}$$

i.e., they are identical and each is equal to the dipole moment corresponding to the case of $N/2$ spinless particles (note that $N/2$ is odd).

4) *An odd number of pairs plus an extra particle, i.e.,* $N = 3$ (mod 4)

From the comparison of Figs. 7.1 and 7.2 (d) one obtains that

$$\mu^{\uparrow}(N,t) = \mu_e((N+1)/2,t) \quad ; \quad \mu^{\downarrow}(N,t) = \mu_o((N-1)/2,t) \quad . \tag{7.1.28}$$

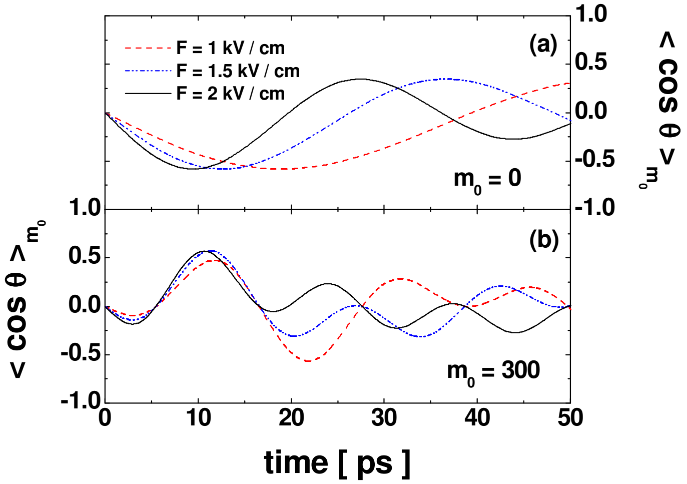

Figure 7.3: Time dependence of the localization parameter $\langle \cos\theta \rangle_{m_0}$.

Taking into account the four cases above discussed, one obtains from Eq. (7.1.24) that for the case of spin-$\frac{1}{2}$ particles, the total induced dipole moment $\mu^\sigma(t)$ can be expressed in terms of spinless case dipole moments [Eqs. (7.1.21), (7.1.23)] as follows

$$\mu^\sigma = \begin{cases} 2\mu_e(\frac{N}{2},t) & \text{if } N = 0 \pmod 4 \\ \mu_o(\frac{N+1}{2},t) + \mu_e(\frac{N-1}{2},t) & \text{if } N = 1 \pmod 4 \\ 2\mu_o(\frac{N}{2},t) & \text{if } N = 2 \pmod 4 \\ \mu_e(\frac{N+1}{2},t) + \mu_o(\frac{N-1}{2},t) & \text{if } N = 3 \pmod 4 \end{cases} . \tag{7.1.29}$$

At low temperatures, if the MR is thin enough and contains a large number of electrons, all the close-lying states corresponding to the ground state of the system belong to different angular momentum and as a result of the angular momentum conservation, the Coulomb interaction cannot couple them. That is why the effects of the electron-electron interaction in thin MRs (in the ground state) are usually irrelevant [116, 119]. When the HCP hits the MR, the system is promoted into an excited state and starts to relax after the HCP has passed by. The relaxation of the system can occur through various mechanisms, e.g., electron-electron inelastic scattering, electron-phonon scattering, etc. Here the relaxation processes are introduced phenomenologically through the relaxation time τ_{rel} that is assumed as a parameter.

In order to have an estimation of the dependence of the induced polarization on the different parameters of the system we performed calculations for a ballistic GaAs-AlGaAs ring similar to that used in the experiment reported in Ref. [123] with $\rho_0 = 1.35\ \mu$m, electron effective mass $m^* = 0.067 m_e$, and $N = 1400$. A Sine-square HCP with time duration of 1 ps was assumed. Zero temperature was considered in all calculations.

The time dependence of the localization parameter $\langle \cos\theta \rangle_{m_0}$ corresponding to the ground state ($m_0 = 0$) is displayed in Fig. 7.3 (a) for different values of the amplitude F of the HCP. As can be clearly appreciated in the figure, a particle initially in the ground

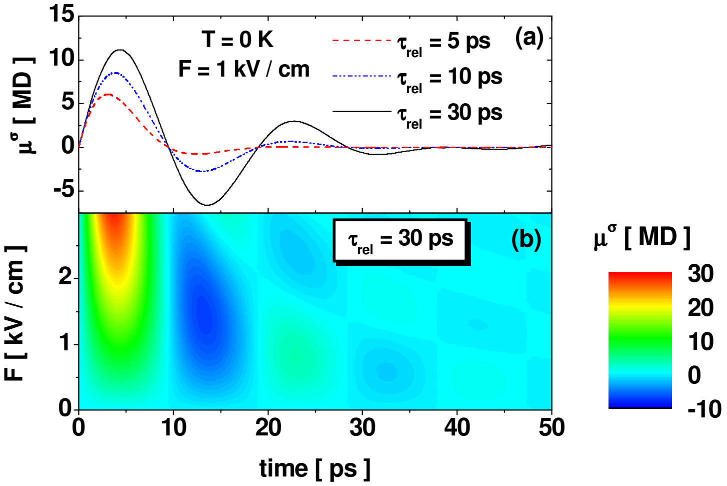

Figure 7.4: Time dependence of the dipole moment μ^σ corresponding to the case of spin-$\frac{1}{2}$ particles for different values of the relaxation time τ_{rel} (a) and with varying the pulse strength F (b).

stationary state reaches its maximum localization around $\theta = \pi$ after a time of the order of 20 ps for a peak field $F = 1$ kV/cm. However, when stronger fields are applied, the localization of the particle oscillates faster, and for the case of $F = 2$ kV/cm the particle localizes around the angles $\theta = \pi$ and $\theta = 0$ after times of about 8 and 27 ps, respectively. This behavior is comprehensible, since stronger pulses induce larger momentum change and enhance the energy of electronic states [cf. Eq. (7.1.9)] leading thus to faster oscillations in the charge-density localization parameter $\langle \cos\theta \rangle_{m_0}$ with increasing F. From these arguments it is also clear that, if the carrier is initially in a high-angular-momentum state, the localization $\langle \cos\theta \rangle_{m_0}$ will have an oscillatory behavior, even for small fields. This situation is illustrated in Fig.7.3 (b), in which case $m_0 = 300$. From Fig.7.3 (b), it is also evident that stronger fields are helpful to achieve swiftly a certain degree of directional localization of the charge distribution. However, a strong field does not necessarily means stronger localization. It is important to note that the localization parameter $\langle \cos\theta \rangle_{m_0}$ is strictly periodic with a period determined by τ_p [see Eq. (7.1.12)]. However, since $\tau_p \approx 13.26$ ns is much longer than the typical relaxation time τ_{rel}, the field-free (postpulse) charge oscillations decay before the τ_p periodic dependence becomes apparent.

Using the relaxation time approximation we present the time dependence of the total dipole moment μ^σ for different values of τ_{rel} and for varying pulse amplitudes in Figs. 7.4 (a) and (b), respectively. A field-free *mesoscopic* polarization is generated within 10 ps after the application of the pulse (note that μ^σ is depicted in units of 10^6 D). The maximum absolute value of the postpulse dipole moment decreases when shortening the relaxation time [see Fig. 7.4 (a)]. The postpulse polarization, however, is still appreciable within a typical range of values of τ_{rel} in ballistic semiconductor MRs [109, 110, 111] as shown in Fig. 7.4 (a). On the other hand, the dipole moment increases with the pulse strength but the time within which it is created decreases with stronger fields [see Fig. 7.4 (b)]. Thus

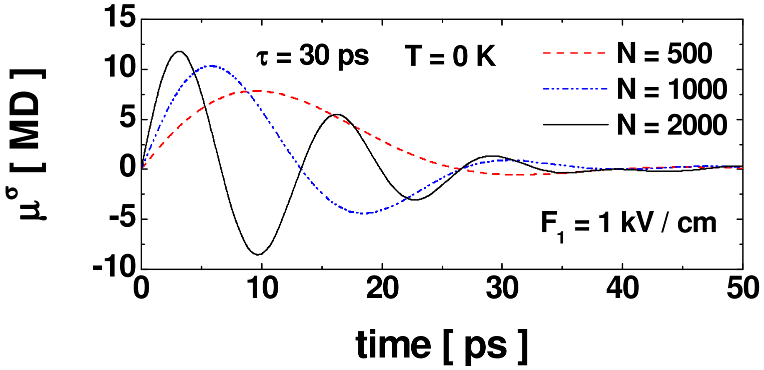

Figure 7.5: Time dependence of the dipole moment μ^{σ} corresponding to the case of spin-$\frac{1}{2}$ particles for different values of the number of particles N in the ring.

the amount and duration of the induced dipole moment can, to a certain extent, be tuned by applying an appropriately designed HCP. In principle, the postpulse polarization and dipole moment can be enhanced considerably by increasing the field amplitude beyond the values shown in Fig. 7.4. Here, we use relatively weak pulses to ensure that the energy delivered to the system is much smaller than E_F. Stronger excitations results in shorter relaxation times and hence the postpulses polarization and dipole moment will decay faster. The time dependence of the postpulse dipole moment corresponding to an even number of spin-$\frac{1}{2}$ carriers, shows a damped oscillating behavior with nodes [see Eqs. (7.1.21), (7.1.23), and (7.1.29)] at $t = \frac{n\tau_p}{N}$ (with n an integer number) and at those values of t for which $h(\Omega) = 0$. Therefore the duration of the first half-cycle of the polarization (note that this cycle gives the strongest polarization, since the dipole moment is exponentially damped by the relaxation of the system) depends, essentially, on the number of carriers in the ring. This situation can be clearly appreciated in Fig. 7.5, where the time evolution of the induced dipole moment is displayed for different values of the number of particles in the ring.

We remark that the charge polarization effect depicted in Figs. 7.4 and 7.5 emerges after the HCP has passed by and hence it occurs in a nearly field-free environment. This fact offers a unique opportunity for studying relaxation processes in the absence of external perturbations and differs, qualitatively, from the case when a *stationary* polarization is induced by a dc electric field.

It is worth noting that the polarization of the MR can be sustained for longer times if it is subject to a train of HCPs. For example, by applying a periodic train of HCPs (with a period longer than the relaxation time) the behavior of the polarization shown in Fig. 7.4 can be periodically repeated as many times as the number of applied pulses. Because of the periodic charge oscillations thus induced, the driven MR can result in a source of electromagnetic radiation whose characteristics can be controlled (to a certain extent) by appropriately designing the sequence of HCPs [136, 137].

From the obtained results and taking into account that all the system parameters utilized in our investigation are in a range experimentally feasible nowadays, we believe that the predicted field-free polarization could, in principle, be experimentally detected with modern techniques. Since the optical absorption properties of a system strongly depend on its charge polarization, the postpulse polarization of the ring could be monitored by performing a pump-probe experiment analogous to that reported in Ref. [138]. In our case the HCP would play the role of the pump pulse inducing the ring charge polarization. A second delayed probe femtosecond pulse is then applied to monitor in time the absorption properties of the system (by varying the time delay between the pump and the probe fields). It is worth noting, however, that the nature of the postpulse polarization here discussed is qualitatively different to that on which the experiment in Ref. [138] is based. In the present case the postpulse polarization strongly depends on the amount of momentum transferred to the system by the pulse. That is the reason why a HCP should be employed as the pump pulse instead of a nearly time symmetric femtosecond pulse as was used in Ref. [138] (note that a time symmetric pulse transfer no momentum to the system).

Concerning the dimensionality of the ring it is instructive to analyze whether the results of the single channel 1D model here studied can offer a qualitatively correct picture of the electron dynamics in more realistic thin, ballistic MRs involving a small number of channels. For these rings and weak fields, the angular and radial motions are adiabatically decoupled [139] and the decisive effect of including the different radial channels is a lowering of the Fermi energy compared to the Fermi energy of the single-channel case. We expect that the peak of the polarization will increase when other channels are included [139], since the system will be more easily excited (a similar situation occurs for the case of persistent currents, where the peak current scales as the square root of the number of channels [114, 123]). On the other hand, lowering E_F is accompanied by a reduction of the angular velocity of the particles near the Fermi level and, consequently, one could expect the time oscillations of the single-channel polarization to occur in a slower time scale when the different radial channels are included [139].

As mentioned above, the lack of total current in the ring is a consequence of the fact that a single pulse is unable to destroy the energy degeneracy and the clockwise-counterclockwise symmetry of the wave function. However, one can intuitively expect that if a second HCP is applied (in a direction different than x in order to brake down the clockwise-anticlockwise symmetry) after a certain delay time from the application of the first pulse, a non-vanishing postpulses current will be induced in the ring [140]. The possibility of inducing currents in a ballistic MR subject to a two counterpropagating orthogonal, linearly polarized HCPs is investigated in the following section.

7.2 Field-free currents in mesoscopic rings

Let us investigate now the dynamics of a ballistic MR similar to the one studied in the preceding section, but now subject to the action of two counterpropagating orthogonal, linearly polarized HCPs . Such pulses, as was discussed in Sec. 2.2, can be experimentally generated with nowadays techniques.

The time-dependent Schrödinger equation describing the dynamics of the system is given by

$$i\hbar\frac{\partial\Psi}{\partial t} = \left[-\frac{\hbar^2}{2m^*\rho_0^2}\frac{\partial^2}{\partial\theta^2} - q\rho_0[\varepsilon_1(t)\cos\theta + \varepsilon_2(t)\sin\theta]\right]\Psi \ , \tag{7.2.1}$$

where

$$\varepsilon_k(t) = p_k\delta(t-t_k) \quad ; \quad k = 1,2 \quad . \tag{7.2.2}$$

The time of application of the kth pulse and the momentum it transfers to the system (i.e., the area of the actual pulse) are denoted by t_k and p_k, respectively. From now on we will assume the first and second pulses are applied at $t = t_1 = 0$ and $t = t_2 = \tau$, respectively, i.e., τ represents the time delay between the two pulses.

The solutions of (7.2.1) obey the matching conditions (see Appendix B)

$$\Psi(\theta, t_1^+) = \Psi(\theta, t_1^-)e^{i\alpha_1\cos\theta} \quad ; \quad \Psi(\theta, t_2^+) = \Psi(\theta, t_2^-)e^{i\alpha_2\sin\theta} \ , \tag{7.2.3}$$

where $\alpha_k = e\rho_0 p_k/\hbar$ and t_k^- and t_k^+ refer to the time just before and right after the application of the kth pulse.

The wave function corresponding to a particle initially in the m_0th stationary state can be expanded as in (7.1.4). Taking into account that before, between, and after the pulses the system evolves in a field-free fashion and after application of the matching conditions (7.2.3), we found, through the expansion theorem that the expansion coefficients are given by

$$C_m(m_0, t) = \begin{cases} \delta_{m,m_0} & \text{for } t \leq 0 \\ i^{m_0-m}J_{m-m_0}(\alpha_1) & \text{for } 0 < t \leq \tau \\ \sum_{n=-\infty}^{\infty} i^{m_0-n}J_{n-m_0}(\alpha_1)J_{m-n}(\alpha_2)e^{-\frac{i}{\hbar}(E_n-E_m)\tau} & \text{for } t > \tau \end{cases} . \tag{7.2.4}$$

In obtaining (7.2.4), the identities (D.0.1) and (D.0.2) were considered and it was assumed that during the time interval $0 < t \leq \tau$ the coherence of the wave function is preserved. Consequently, for consistency, the time delay τ between the pulses has to be shorter than the relaxation time of the system.

The Eq. (7.1.6), corresponding to the case in which a single pulse is applied, is easily obtained from (7.2.4) by taking into account that $J_{m-n}(\alpha_2 \to 0) = \delta_{m,n}$.

The energy spectrum of a particle initially in the m_0th state can be calculated from Eqs.(7.1.4), (7.1.5), (7.1.7), and (7.2.4). After some mathematical manipulations, we obtained

$$E_{m_0}(t) = \begin{cases} \frac{\hbar^2 m_0^2}{2m^*\rho_0^2} & \text{for } t \leq 0 \\ \frac{\hbar^2}{2m^*\rho_0^2}\left(m_0^2 + \frac{\alpha_1^2}{2}\right) & \text{for } 0 < t \leq \tau \\ \epsilon_1(m_0) + \epsilon_2(m_0) + \epsilon_3(m_0) & \text{for } t > \tau \end{cases} , \tag{7.2.5}$$

where

$$\epsilon_1(m_0) = \frac{\hbar^2}{2m^*\rho_0^2}\left(m_0^2 + \frac{\alpha_1^2}{2} + \frac{\alpha_2^2}{2}\right) \ , \tag{7.2.6}$$

$$\epsilon_2(m_0) = \frac{\hbar^2}{2m^*\rho_0^2}\,\frac{\alpha_2^2}{2}\,J_2(\vartheta)\cos\left(8\pi m_0\frac{\tau}{\tau_p}\right) \ , \tag{7.2.7}$$

with

$$\vartheta = 2\alpha_1 \sin\left(4\pi\frac{\tau}{\tau_p}\right) \quad , \tag{7.2.8}$$

and

$$\epsilon_3(m_0) = -\frac{\hbar^2}{2m^*\rho_0^2}\alpha_1\alpha_2\left[g_+(m_0) - g_-(m_0)\right] \quad , \tag{7.2.9}$$

with

$$g_\pm(m_0) = \left[\left(m_0 \mp \frac{1}{2}\right)J_0(\varphi) + \left(m_0 \pm \frac{1}{2}\right)J_2(\varphi)\right]\sin\left[2\pi(2m_0 \mp 1)\frac{\tau}{\tau_p}\right] \quad , \tag{7.2.10}$$

and

$$\varphi = 2\alpha_1 \sin\left(2\pi\frac{\tau}{\tau_p}\right) \quad . \tag{7.2.11}$$

In obtaining Eqs. (7.2.6) - (7.2.11) the identities (D.0.3), (D.0.5), and (D.0.6) were used.

Two aspects regarding the energy spectrum (7.2.5) deserve to be commented. The first one is that in the case a single pulse is applied (i.e., $\alpha_2 = 0$), Eq. (7.2.5) reduces to Eq. (7.1.9) as it must be. The second one concerns to the fact that $\epsilon_1(m_0) = \epsilon_1(-m_0)$, $\epsilon_2(m_0) = \epsilon_2(-m_0)$, and $\epsilon_3(m_0) = -\epsilon_3(-m_0)$. Consequently, the initially degenerated energy levels $E_{\pm m_0}(t \leq \tau)$ split into $E_{\pm m_0}(t > \tau) = \epsilon_1(m_0) + \epsilon_2(m_0) \pm \epsilon_3(m_0)$, i.e., $E_{m_0}(t > \tau) \neq E_{-m_0}(t > \tau)$, and the initial energy degeneracy is destroyed after the application of the second pulse.

It results from Eqs. (7.1.4) and (7.2.4) that $\Psi_{m_0}^{(t\leq\tau)}(\theta,t) = \Psi_{-m_0}^{(t\leq\tau)}(-\theta,t)$. Consequently, the first pulse does not destroy the clockwise-counterclockwise symmetry and the currents curried by particles initially in the m_0 and $-m_0$ states compensate each other. As the energy degeneracy of $\pm m_0$ states is preserved for $t \leq \tau$, no current is expected to be induced by the first pulse. This situation changes, however, after the application of the second pulse, when the clockwise-counterclockwise symmetry is broken $[\Psi_{m_0}^{(t>\tau)}(\theta,t) \neq \Psi_{-m_0}^{(t>\tau)}(-\theta,t)]$ and a total non-vanishing current is induced. Note that in order to brake the clockwise-counterclockwise symmetry, the pulses have to be polarized in different directions.

The total current induced in the ring is given by

$$I(t) = \sum_{m_0,\sigma} f(m_0,t) I_{m_0}(t) \quad , \tag{7.2.12}$$

where $f(m_0,t)$ denotes the non-equilibrium distribution function,

$$I_{m_0}(t) = \int_0^{2\pi} j_{m_0}(\theta,t)d\theta \tag{7.2.13}$$

[with $j_{m_0}(\theta,t)$, the corresponding density current] is the current carried by a particle initially in the m_0th stationary state. After some mathematical manipulations and taking into account Eqs. (D.0.4) and (D.0.8) we found that

$$I_{m_0}(t) = \begin{cases} I_{m_0}^{(0)} & \text{for } t \leq 0 \\ I_{m_0}^{(0)} & \text{for } 0 < t \leq \tau \\ I_{m_0}^{(0)} + I_{m_0}^{(1)} & \text{for } t > \tau \end{cases} \quad , \tag{7.2.14}$$

where

$$I^{(0)}_{m_0} = \frac{q\hbar m_0}{m^* \rho_0^2} \quad , \tag{7.2.15}$$

and

$$I^{(1)}_{m_0} = \frac{q\hbar}{m^* \rho_0^2}\, \alpha_1 \alpha_2 \;\; [J_0(\varphi) + J_2(\varphi)] \sin\left(2\pi \frac{\tau}{\tau_p}\right) \cos\left(4\pi m_0 \frac{\tau}{\tau_p}\right) \tag{7.2.16}$$

with φ given by Eq. (7.2.11).

By comparing Eqs. (7.1.11) - (7.1.14) with (7.2.16) one can easily see that

$$I^{(1)}_{m_0} = \frac{\hbar}{m^* \rho_0^3}\, \alpha_2 \; \mu_{m_0}(\tau) \quad . \tag{7.2.17}$$

Thus, for $t > \tau$ the current carried by a particle initially in the m_0th stationary state depends on the corresponding dipole moment $\mu_{m_0}(\tau)$ right before the application of the second pulse.

It is clear from (7.2.5) and (7.2.14) that $E_{m_0}(t \leq \tau) = E_{-m_0}(t \leq \tau)$ and $I_{m_0}(t \leq \tau) + I_{-m_0}(t \leq \tau) = 0$. Consequently, the total current $I(t \leq \tau) = 0$, as was discussed above.

The non-equilibrium distribution function $f(m_0, t)$ can be calculated, within the relaxation time approximation, as done in the preceding section. However, unlike for the case in which a single pulse is applied, when the two orthogonal, linearly polarized HCPs are applied the energy levels are redistributed in a non-trivial way and the boundary conditions for determining the non-equilibrium distribution function depends on the relaxation processes between the different system states.

Before the application of the first pulse ($t \leq 0$) the energy levels are degenerated. At T = 0 K only the lowest energy levels are occupied. We will refer to this equilibrium state as the state A. After the application of the first pulse, in the time interval $0 < t \leq \tau$, the initial energy levels are just shifted. Therefore the degeneracy, ordering and occupation of the energy levels are preserved when the system evolves from $t \leq 0$ to $0 < t \leq \tau$. The state of the system in the time interval $0 < t \leq \tau$ will be referred to as the state B. Right after the application of the second pulse the system state B evolves into an excited state that will be denoted by C. The non-equilibrium state C is reached at $t = \tau^+$ and its energy levels are, in general, non-degenerated and rearranged in a new ordering. The occupation of the energy levels is, however, preserved during the system evolution from the state B to the state C. Depending on the nature of the system two different relaxation processes involving carrier relaxation between different coherent one-particle states or from a coherent to a stationary one-particle state could, in principle, occur after the system has reached the non-equilibrium state C. If the time the system requires for relaxing from the state C to the state D (with D denoting the system state resulting from the same energy levels configuration as state C but with the particles occupying the lowest energy levels only) is longer than the time the coherence of the wave functions is preserved, then the system will relax directly from the system state C to the initial equilibrium state A with a rate characterized by a relaxation time τ_{rel}. If, on the contrary, the coherence of the wave functions is preserved for a long enough time, the system can relax with a rate determined by τ'_{rel} from the state C to state D, and then, from state D to the initial equilibrium state A with a relaxation rate characterized by τ''_{rel}. For a better understanding of the notation used for the system states

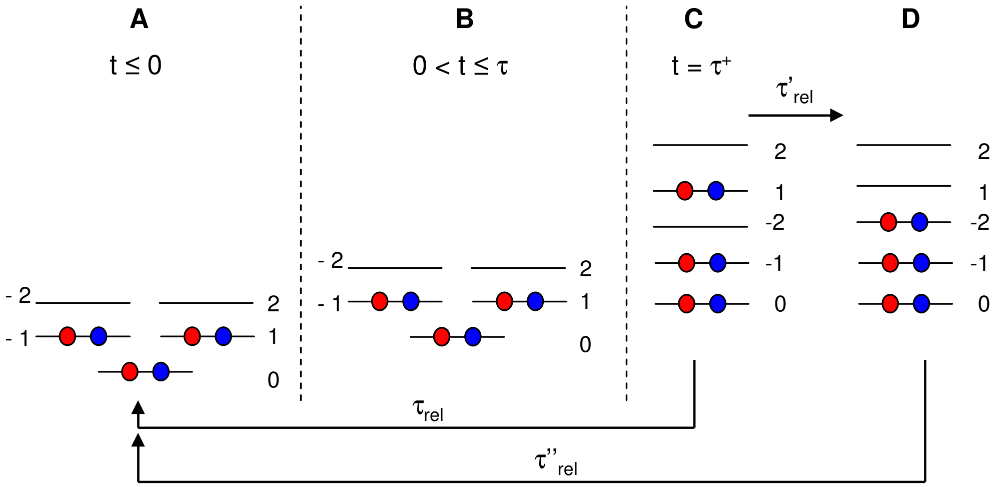

Figure 7.6: Schematics of the time evolution of ordering and occupation of the energy levels at T = 0 K. If $\tau_{rel} < \tau'_{rel}$, the system state evolves in the sequence A-B-C-A. If, on the contrary, $\tau_{rel} > \tau'_{rel}$, the evolution of the system state occurs according to the sequence A-B-C-D-A.

and the different relaxation processes, we shown in Fig. 7.6 a qualitative representation of a possible time evolution of the system state for the case of $N = 6$ spin-$\frac{1}{2}$ particles.

Although all the relaxation mechanisms (C-A, C-D, and D-A) have to be inelastic, there is a significant difference between the intermediate relaxation process C-D (involving transitions between different coherent one-particle states) and the relaxation to the equilibrium C-A and D-A (involving transitions from a coherent to a stationary one-particle state). We note that, in general, the relaxation from the state C to D involves transitions of the type $m_0 \to -m'_0$ with $|m_0|$ close to $|m'_0|$. For a particle in a state with a large value of $|m_0|$ such a transition can occur only if the carrier loses small energy and large momentum simultaneously. Thus, while the intermediate relaxation process C-D requires the existence of inelastic backscattering mechanisms involving small energy and large momentum transfers (for example, the simultaneous scattering by impurities and phonons or the electron-electron scattering), the relaxation to the equilibrium (C-A and D-A) does not require such mechanisms and could, indeed, occur through phonon scattering only.

The determination of whether the system evolves through the sequences A-B-C-A or A-B-C-D-A, depending of the system parameters is an interesting issue that requires the evaluation of the different relaxation times by including the corresponding scattering mechanisms. Such an investigation is currently under way and here we limit our analysis just to the study of the two possible processes separately and assume the involved relaxation times as given parameters.

We firstly study the case in which the state of the system evolves through the sequence A-B-C-A. Following a procedure similar to that used in the preceding section we found from Eqs. (7.2.12), (7.2.14), and (7.2.17) that, within the relaxation time approximation,

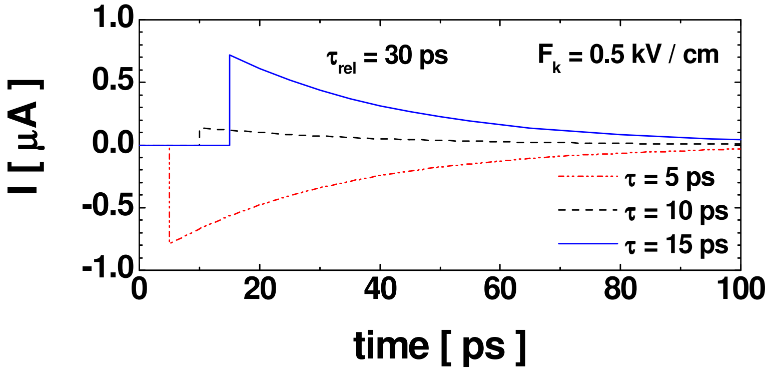

Figure 7.7: Time dependence of the induced current (corresponding to the case in which the system state evolves through the sequence A-B-C-A) for different values of the time delay τ.

the total current induced in the ring is given by

$$I(t) = \frac{\hbar}{m^* \rho_0^3}\, \alpha_2\, \Theta(t-\tau) e^{-\frac{(t-\tau)}{\tau_{rel}}} \sum_{m_0,\sigma} n_F^{(1)}(m_0) \mu_{m_0}(\tau) \quad . \tag{7.2.18}$$

In the obtention of (7.2.18) we have also taken into account that at T = 0 K the contribution to the total current corresponding to the sum of $I_{m_0}^{(0)}$ over the occupied states vanishes. From the comparison of Eqs. (7.1.19) and (7.2.18) one obtains that

$$I(t) = \frac{\hbar}{m^* \rho_0^3}\, \alpha_2\, \Theta(t-\tau) e^{-\frac{(t-2\tau)}{\tau_{rel}}} \mu(\tau) \quad . \tag{7.2.19}$$

Thus the total current induced in the ring depends on the total dipole moment right before the application of the second pulse. Analytical expressions for evaluating the total current $I(t)$ in the different cases of spinless and spin-$\frac{1}{2}$ particles can be obtained by substituting the corresponding analytical expressions for $\mu(t)$ given in the preceding section.

The time dependence of the postpulses induced current corresponding to spin-$\frac{1}{2}$ particles in a ballistic MR with the same characteristics that the one studied in the preceding section is displayed in Fig. 7.7 for different values of the time delay τ, pulse amplitudes $F_k = 0.5$ kV/cm ($k = 1, 2$), $\tau_{rel} = 30$ ps, and T = 0 K. The *instantaneous* rising of the current right after the application of the second pulse (see Fig. 7.7) is just a consequence of the assumed impulsive approximation and have the meaning that, as for the duration of the pulses, the actual current rising time is much shorter than the ballistic time τ_F a particle at the Fermi level (in the absence of the external field) requires for a turn along the ring.

For time delays between the pulses such that $\tau \ll \tau_p$ (a condition that holds in the time domain of our interest since $\tau_p = 13.26$ ns) and for the relatively weak pulses here considered, the behavior of the peak current I_p as a function of τ is mainly dominated by the sine oscillations with nodes at $\tau = \frac{n\tau_p}{N}$ [see Eqs. (7.1.21), (7.1.23), (7.1.29), and (7.2.19)], with n being a positive integer. Thus the sign of the peak current can be controlled by

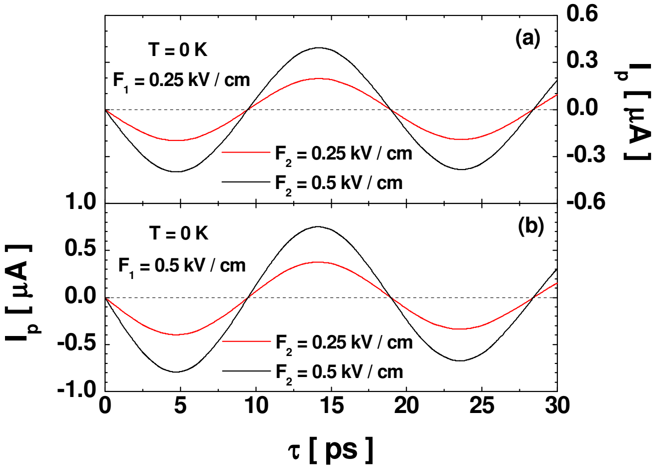

Figure 7.8: Peak current I_p (corresponding to the state C) as a function of the time delay τ.

choosing the appropriate value of τ. This situation can be clearly appreciated in Fig. 7.8, where the dependence of the peak of the induced current on the delay time τ between the pulses is displayed for the case of spin-$\frac{1}{2}$ particles and different combinations of the pulse amplitudes F_k ($k = 1, 2$). Note also that even for the weak fields here considered, the peak of the induced current can be more than one order of magnitude greater than the persistent currents (~ 5 nA) measured in ballistic MRs [123].

In the case the coherence time is longer than the time the system needs for relaxing from the state C to the state D (see Fig. 7.6), the evolution of the system state occurs according to the sequence A-B-C-D-A. In such a case one finds, within the relaxation time approximation, that the total current in the ring within the time interval $\tau < t \leq (\tau + t')$ [here t' ($t' > \tau'_{rel}$) represents the time the system needs for completely relaxing from state C to state D] is given by

$$I(t) = \frac{\hbar}{m^* \rho_0^3}\, \alpha_2\, \Theta(t-\tau) e^{-\frac{(t-2\tau)}{\tau'_{rel}}} \mu(\tau) + \left(1 - e^{-\frac{(t-\tau)}{\tau'_{rel}}}\right) \left(I^{(0)}(t) + I^{(1)}(t)\right) \quad , \tag{7.2.20}$$

where

$$I^{(0)}(t) = \frac{q\hbar}{m^* \rho_0^2} \Theta(t-\tau) \sum_{m_0, \sigma} n_F^{(2)}(m_0) m_0 \quad , \tag{7.2.21}$$

$$I^{(1)}(t) = \frac{\hbar}{m^* \rho_0^3}\, \alpha_2\, \Theta(t-\tau) \sum_{m_0, \sigma} n_F^{(2)}(m_0) \mu_{m_0}(\tau) \quad , \tag{7.2.22}$$

and

$$n_F^{(2)}(m_0) = \left[1 + \exp\left(\frac{E_{m_0}(t > \tau) - \eta_2}{k_B \mathrm{T}}\right)\right]^{-1} \quad . \tag{7.2.23}$$

In Eq. (7.2.23) η_2 represents the chemical potential corresponding to the system state D and has to be calculated from the condition that the number of particles in the isolated MR is a constant.

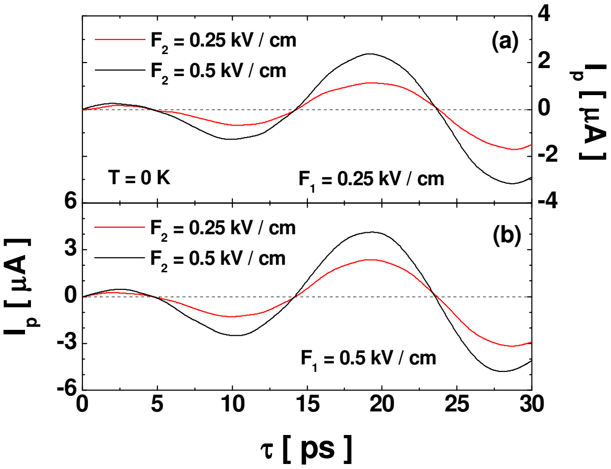

Figure 7.9: Peak current I_p (corresponding to the state D) as a function of the time delay τ.

It is worth noting that the system state D corresponds to a non-trivial rearrangement of the initial energy levels induced by the second applied pulse. Such energy levels configuration depends sensitively on the system and pulse parameters. Consequently, in the general case (even at T = 0 K) the sums involved in Eqs. (7.2.21) and (7.2.22) have to be performed numerically. We note also that unlike in the case the system state evolves in the sequence A-B-C-A, in the present case the contribution to the current corresponding to the sum of I_{m_0} over all the occupied state does not vanish in general [see Eq. (7.2.21)]. This fact opens the possibility of the existence of a non-zero total current in the ring even when at the time of application of the second pulse the ring is unpolarized. In such a case the total current constitutes a consequence of the inelastic backscattering processes that lead the system to relax into the state D.

Once the system has completely relaxed to the system state D at $t = \tau + t'$ it begins to relax to the equilibrium state A with a relaxation time τ''_{rel}. Within the relaxation time approximation the total current for $t > \tau + t'$ is found to be given by

$$I(t) = e^{-\frac{(t-\tau-t')}{\tau''_{rel}}} \left(I^{(0)}(t) + I^{(1)}(t) \right) \quad ; \quad t > \tau + t' \ . \tag{7.2.24}$$

The peak current I_p corresponding to the system state D (i.e., at $t = \tau + t'$) as a function of the time delay τ between the application of the HCPs, is displayed in Fig. 7.9 for different combinations of the pulse amplitudes F_k $(k = 1, 2)$. From the comparison of Figs. 7.8 and 7.9 one can see that the peak current can increase in near one order of magnitude due to the inelastic backscattering processes (we recall that to reach the state D, the system has to relax, necessarily, through inelastic backscattering mechanisms involving small energy and large momentum transfers). Thus, in contrast to the usual destructive effects produced by inelastic scattering in mesoscopic phenomena, in the present case the inelastic scattering could lead to a significative increase in the peak of the postpulses current. A similar effect

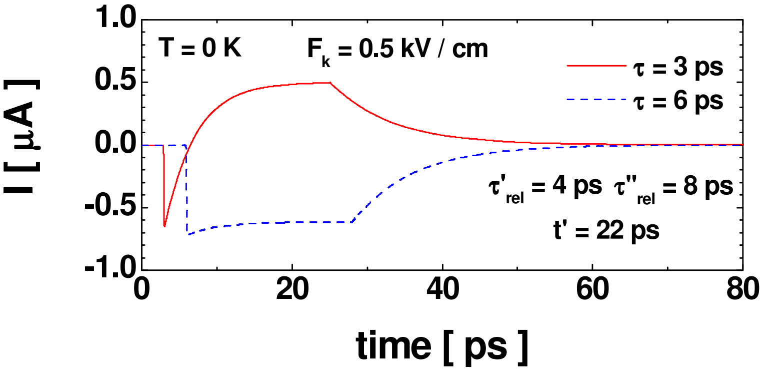

Figure 7.10: Time dependence of the postpulses current (corresponding to the case in which the system state evolves through the sequence A-B-C-D-A) for different values of the time delay τ.

was found in Ref. [132], where the possibility of observing constructive effects produced by inelastic scattering in a MR threaded by a time-dependent magnetic field was investigated.

The time dependence of the postpulses induced current corresponding to the case in which the system state follows the time evolution sequence A-B-C-D-A is shown in Fig. 7.10 for different values of the time delay τ. As it can be appreciated from Fig. 7.10, the time dependence of the postpulses current can acquire different behaviors by changing the time delay τ. Note that in the case the system evolution follows the sequence A-B-C-D-A, by changing the values of τ one can change not only the sign of the induced current in the ring [as for the A-B-C-A case (see Fig. 7.7)] but it is also possible to induce a current that changes its sign during the relaxation processes.

The postpulses current $I(t)$ induced in the ring generates a field-free magnetization $M(t)$ that can be calculated through the relation $M(t) = \pi\rho_0^2 I(t)$. A direct estimation of the field-free magnetization M of the ring can be easily obtained from the curves corresponding to the current by taking into account that for the ring parameters here considered a current of 1 μA corresponds to a magnetization of 112.27 eV/Tesla.

It is worth to stress that the proposed model gives only a qualitative idea of the relaxation processes and therefore of the precise time dependence of the postpulses current. Hence, such processes require a more detailed study. Nevertheless, we believe the obtained values for the peak currents constitutes a good approximation for think ballistic MRs at low temperature. We note that the assumed zero-temperature approximation is also expected to be accurate within the range of temperature commonly considered in actual experimental situations (measurements of persistent currents in MR, for example, are commonly performed at temperatures of the order of a few tents of mK [121, 122, 123, 124]).

From the obtained results and taking into account that all the system parameters (ring and pulse parameters as well as the amplitude of the postpulses current and magnetization) utilized in our investigation are in a range experimentally feasible nowadays, we believe that the predicted field-free current could be experimentally detected with modern techniques. The crossed HCPs can be generated in a way similar to that discussed in Sec. 2.2 and

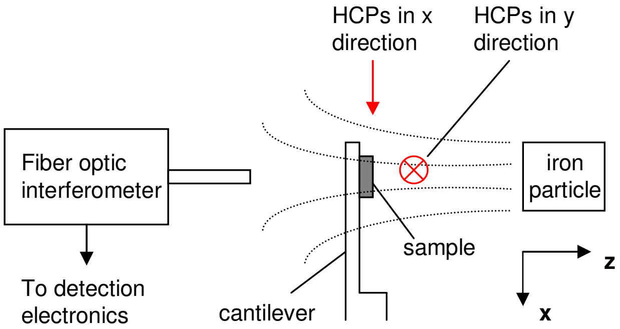

Figure 7.11: A representative experiment for measuring the postpulses induced current and magnetization of a ballistic thin MR.

the induced postpulses current (or magnetization) could be detected by employing the same experimental techniques used in Ref. [123], where low-temperature measurements of persistent currents (even weaker than the obtained in the present study) for a ballistic MR with similar characteristics than the one considered in our calculations were performed.

Various applications could result from the effects investigated in the present section. As the amplitude and time dependence of the postpulses current depends on the characteristics of the relaxation processes, estimations of the relaxation times as well as information about the role of the different scattering mechanism on the destruction of the coherence could be obtained by measuring the induced current (or magnetization).

We also note that although within the two-pulses procedure investigated in this work one expects the postpulses current and magnetization to decay after a relaxation time, it is in principle possible to induce sustainable currents by applying two orthogonal, linearly polarized periodic trains of HCPs. By controlling the parameters of the HCPs the time dependence of the induced current could be designed over a time of the order of the duration of the train of pulses. In particular, for crossed trains of HCPs with period longer than the relaxation time of the system, it could be possible to create periodic trains of pulsed currents (and a time-dependent magnetization) whose characteristics can be controlled by appropriately designing the sequence of HCPs. The time-dependent magnetization thus generated in the MR could be useful for applications in designing micro-electromechanical actuators. As an example, we show in Fig. 7.11 a schematic representation of a possible experimental realization of a micro-electromechanical actuator that could serve for monitoring the magnetization induced by the HCPs. The sample (containing the MR) is placed on a cantilever. An iron particle mounted on a piezoelectric translator is positioned at a distance d from the sample. The magnetized iron particle produces an inhomogeneous magnetic field (dotted lines). In the absence of the pulses, the system is in equilibrium and the magnetization of the ring is zero. By applying two crossed trains of HCPs an oscillating magnetization is induced in the ring. The oscillating magnetization in presence of the inhomogeneous field of the iron particle generates an oscillating magnetic force and causes the cantilever to vibrate. By measuring the vibration amplitude (it can be done with the use of a fiber optic interferometer and a lock-in amplifier [141, 142]) the time dependence of the induced magnetic force (and, consequently, of the magnetization and the current) can be monitored. We note that the experimental situation here described is quite similar to that discussed in Refs. [141, 142]. If one neglects the effects of the iron particle on the quantum states of the ring, the order of the z component of the generated magnetic force can be estimated directly from the results obtained for the peak current (see Figs. 7.8 and 7.9). As done in Ref. [141], we assume the value $\partial B_z/\partial z \simeq 600$ Tesla/m for the magnetic field gradient created by the iron particle. One then obtains that a current of 0.1 μA (or a magnetization of 11.27 eV/Tesla for the ring here studied) corresponds to a force of about 11×10^{-16} N, a force that is in the range of sensitivity of nowadays experimental apparatuses [141, 142].

Chapter 8

Conclusions

In the present work we have investigated the possibility of controlling the quantum dynamics of different physical systems driven by half-cycle electromagnetic pulses.

General methods such as the generalized Bloch vector approach, the Floquet formalism, and a numerical algorithm based on the splitting operator approach have been used throughout our study of the dynamics of driven quantum systems. The combination of these methods constitutes a powerful tool for describing the time evolution of quantum systems as well as for the analysis of different strategies that can lead to an efficient control of the dynamics of a given quantum system. The sustainability in time of the control process is another important issue that has been addressed in the present work through the introduction of the definition of *quasistationarity* of a time-dependent quantum state. The definition of quasistationarity is shown to be particularly useful since it allows us to treat phenomena such as the coherent suppression of tunnelling, dynamical localization, and sustainable molecular orientation in a general and unified way. Necessary and sufficient conditions for inducing quasiperiodic quasistationarity to a time-dependent quantum system are found within the generalized Bloch vector approach and the Floquet formalism. It is shown also that the Aharonov-Anandan geometric phase plays an important role in achieving quasiperiodic quasistationarity, and in fact, it can be used as a measure of the degree of quasistationarity of a time-dependent quantum system that evolves cyclically.

When a physical system is subject to the action of a highly asymmetric mono-cycle pulse, its HCP can deliver a non-zero momentum transfer to the system over a time much longer than the duration of the HCP. This peculiarity of the HCPs has opened new possibilities for the experimental realization of kicked quantum systems and for the efficient control of the dynamics of quantum systems in the non-adiabatic regime. In particular, we have shown in the present work that subjecting a diatomic molecule to a conveniently designed train of HCPs can result in a strong and sustainable molecular orientation without disturbing the electronic and vibrational modes of the molecule. Explicit calculations were performed for the NaI molecule showing that the molecular orientation obtained within our scheme is stronger than that obtained with previous methods and that it is robust to thermal average up to temperatures of about 10 K.

We have also studied the dynamics and emission properties of an electron in a double quantum well driven by a train of HCPs. Phenomena such as the low-frequency generation, half-harmonic generation, and the coherent suppression of tunnelling in the absence of accidental quasienergy degeneracy were shown to occur and were discussed in detail within the concept of quasiperiodic quasistationarity. We performed calculations for the case of a typical $\mathrm{Al}_x\mathrm{Ga}_{1-x}\mathrm{As}$ based double quantum well. The obtained results show that when the system is driven by an appropriately designed train of HCPs, a strong localization (in one of the two wells) of an initially delocalized electron can be achieved in a fast and efficient way.

The study of mesoscopic systems constitutes an issue of great interest in physics because of their technological applications and their unique properties. In the present work we report about the first investigation of the dynamical properties of electrons confined in a ballistic thin MR and subject to linearly polarized HCPs. We showed that at low temperatures the application of a single linearly polarized HCP on a ballistic thin MR induces a polarization in the ring that persists even after the HCP has passed by, i.e., under field-free conditions. The dependence of the field-free polarization induced in the ring on the pulse parameters was investigated. We also showed that subjecting a ballistic thin MR to a sequence of two orthogonal, linearly polarized HCPs can result in the generation of a non-equilibrium field-free current (and a magnetization) in the ring that lasts as long as the coherence of the wave functions of the carriers is preserved. Some potential applications and the possibility of experimentally detecting the field-free current and magnetization were also discussed.

Zusammenfassung

Wird ein Quantensystem einem zeitabhängigen externen Feld ausgesetzt, tritt eine Vielzahl von Phänomenen auf, die innerhalb der gewöhnlichen stationären Quantenmechanik nicht zugänglich sind. Zudem lassen sich diese Phänomene oftmals durch die gezielte Anwendung geeigneter Felder kontrollieren und manipulieren. Moderne opto-elektronische Geräte, Laser-kontrollierte chemische Reaktionen sowie die Erzeugung von verschränkten Zuständen zum Einsatz in der Quanteninformatik sind nur einige Beispiele der Anwendungsmöglichkeiten resultierend aus einer effizienten Kontrolle der Quantendynamik.

Wird ein Quantensystem einem Halb-Zyklus-Puls (half-cycle pulse, HCP) ausgesetzt, können Effekte auftreten, die sich aufgrund der hoch asymmetrischen Eigenschaften des HCP in ihrer Qualität deutlich von denen unterscheiden, die beobachtbar sind, wenn ein kontinuierlicher Laser (CW lasers) oder fast symmetrische Laserpulse verwendet werden. In der vorliegenden Arbeit untersuchen wir Möglichkeiten zur Kontrolle der Dynamik von Quantensystemen durch den Einsatz von HCPs. Insbesondere betrachten wir die Dynamik von drei physikalischen Systemen.

Das erste hier betrachtete Quantensystem besteht aus einem polaren zweiatomigen Molekül angetrieben von einer Sequenz von HCPs. Basierend auf einem einfachen analytischen Modell haben wir die Charakteristika und Parameter der HCPs bestimmt, die eine starke und dauerhafte nicht-adiabatische Orientierung der molekularen Achse veranlassen können. Zusätzlich wurde eine Optimierung des Kontrollprozesses für das NaI-Molekül mit Hilfe von voll-numerischen Berechungen durchgeführt. Die Ergebnisse zeigen, dass die innerhalb unseres Schemas erlangte molekulare Orientierung stärker ist als bei herkömmlichen Methoden und dass sie gegenüber Temperaturschwankungen bis zu ca. 10 K stabil bleibt.

Das zweite physikalische System, welches in dieser Arbeit untersucht wird, ist die Quantendynamik eines in einem symmetrischen Doppel-Quantentrog eingeschlossenen Elektrons, das zudem von HCPs zeitlich angetrieben wird. Unterliegt solch ein System einer Sequenz von HCPs, können sowohl die Bewegung als auch das Emissionsspektrum des Elektrons auf einer Femtosekunden-Zeitskala verändert werden. Einige interessante Phänomene wie die Emission von Strahlung niedriger Frequenzen sowie die kohärente Unterdrückung des Tunnelprozesses in Abwesenheit der Entartung der Quasi-Energien werden vorhergesagt.

Schließlich untersuchen wir die dynamischen Eigenschaften eines dünnen ballistischen mesoskopischen Rings (MR) in Anwesenheit von HCPs. Wir zeigen, dass die Anwendung eines einzelnen HCPs auf einen ballistischen MR zu einer ultraschnellen Erzeugung einer Polarisation der Ladungsdichte im Ring führt. Wird ein dünner ballistischer MR der Wirkung von zwei orthogonal und linear polarisierten HCPs ausgesetzt, kann im Ungleichgewicht ein Strom im Ring induziert werden. Der induzierte Strom hält an, solange die Kohärenz der Ladungsträger erhalten bleibt. Einige potentielle Anwendungen und die Möglichkeit des experimentellen Nachweises dieses Stromes werden erläutert.

Appendix A

Products: Definitions and properties.

Different kind of products involving vectors and matrices are used throughout this dissertation.

The standard product between two matrices A and B is represented, as usually, by AB, i.e., without any *product* symbol between them.

A *dot* product between two vector-like objects $\mathbf{X}$ and $\mathbf{Y}$ is defined as

$$\mathbf{X} \cdot \mathbf{Y} = X_j Y_j \ , \tag{A.0.1}$$

where X_j and Y_j represent the jth component of $\mathbf{X}$ and $\mathbf{Y}$, respectively. We refer to $\mathbf{X}$ and $\mathbf{Y}$ as vector-like objects because they can be vectors (in the usual sense) or vectors whose components are matrices. In the particular case $\mathbf{X}$ and $\mathbf{Y}$ are both vectors, the *dot* product as defined in (A.0.1) reduces to the standard scalar product between two vectors [note that in Eq. (A.0.1), and in what follows, we adopt the Einstein's summation convention].

The SU(N) group has $N_{_D} = \dim[\mathrm{SU}(N)] = N^2 - 1$ generators that we denote by $\mathcal{F}_j$ ($j = 1, 2, ..., N_{_D}$). The generators $\mathcal{F}_j$ satisfy the following commutation

$$[\mathcal{F}_j, \mathcal{F}_k] = 2i f_{jkl} \mathcal{F}_l \tag{A.0.2}$$

and anticommutation

$$\{\mathcal{F}_j, \mathcal{F}_k\} = \frac{4}{N} \delta_{jk} \mathcal{I}_{_N} + 2 d_{jkl} \mathcal{F}_l \tag{A.0.3}$$

relations, respectively. In the equations above,

$$f_{jkl} = -\frac{i}{4} \mathrm{Tr}\left([\mathcal{F}_j, \mathcal{F}_k] \, \mathcal{F}_l \right) \tag{A.0.4}$$

and

$$d_{jkl} = \frac{1}{4} \mathrm{Tr}\left(\{\mathcal{F}_j, \mathcal{F}_k\} \, \mathcal{F}_l \right) \tag{A.0.5}$$

are the asymmetric and symmetric structure constants of the Lie algebra of SU(N) and $\mathcal{I}_{_N}$ represents the $(N \times N)$ unit matrix. By summing Eqs. (A.0.2) and (A.0.3) one obtains the following relation

$$\mathcal{F}_j \mathcal{F}_k = \frac{2}{N}\delta_{jk}\mathcal{I}_{_N} + (d_{jkl} + i f_{jkl})\mathcal{F}_l \ \ . \tag{A.0.6}$$

Inner products involving the structure constants are introduced for vectors in $\mathbb{R}^{N_D}$ as follows. Let the vectors $\mathbf{X}, \mathbf{Y} \in \mathbb{R}^{N_D}$, then the *wedge* product $\mathbf{X} \wedge \mathbf{Y}$ is a vector in $\mathbb{R}^{N_D}$ with components given by

$$(\mathbf{X} \wedge \mathbf{Y})_j = f_{jkl} X_k Y_l \ \ , \tag{A.0.7}$$

and the *star* product $\mathbf{X} \star \mathbf{Y}$ is a vector in $\mathbb{R}^{N_D}$ with components

$$(\mathbf{X} \star \mathbf{Y})_j = d_{jkl} X_k Y_l \ \ . \tag{A.0.8}$$

In the particular case of SU(2) the *wedge* product as defined in (A.0.7) reduces to the standard vector product, while the *star* product vanishes for any two vectors in $\mathbb{R}^3$.

Taking into account the symmetry properties of the structure constants, one can easily verify that for $\mathbf{X}, \mathbf{Y}, \mathbf{Z} \in \mathbb{R}^{N_D}$, the following properties hold:

1) $\mathbf{X} \star \mathbf{Y} = \mathbf{Y} \star \mathbf{X}$
2) $\mathbf{X} \cdot (\mathbf{Y} \star \mathbf{Z}) = \mathbf{Y} \cdot (\mathbf{X} \star \mathbf{Z}) = \mathbf{Z} \cdot (\mathbf{X} \star \mathbf{Y})$
3) $(\mathbf{X} \wedge \mathbf{Y}) = -\mathbf{Y} \wedge \mathbf{X} \ \Rightarrow \ (\mathbf{X} \wedge \mathbf{X}) = 0$
4) $\mathbf{X} \cdot (\mathbf{Y} \wedge \mathbf{Z}) = \mathbf{Y} \cdot (\mathbf{Z} \wedge \mathbf{X}) = \mathbf{Z} \cdot (\mathbf{X} \wedge \mathbf{Y})$
5) $\mathbf{X} \wedge (\mathbf{Y} \star \mathbf{Z}) = \mathbf{Y} \star (\mathbf{X} \wedge \mathbf{Z}) + \mathbf{Z} \star (\mathbf{X} \wedge \mathbf{Y})$
6) $\mathbf{X} \wedge (\mathbf{Y} \wedge \mathbf{Z}) = \mathbf{Y} \wedge (\mathbf{X} \wedge \mathbf{Z}) - \mathbf{Z} \wedge (\mathbf{X} \wedge \mathbf{Y})$

In obtaining the properties 5) and 6) we used the identities

$$f_{jkl} d_{lmn} + f_{nkl} d_{lmj} + f_{mkl} d_{jln} = 0 \tag{A.0.9}$$

and

$$f_{jkl} f_{lmn} + f_{mkl} f_{lnj} + f_{jml} f_{lnk} = 0 \ \ . \tag{A.0.10}$$

Let $\mathbf{X}, \mathbf{Y} \in \mathbb{R}^{N_D}$ and let $\hat{\mathcal{F}}$ be a *vector* whose components are the generators of SU(N), i.e., $\hat{\mathcal{F}} = (\mathcal{F}_1, \mathcal{F}_2, ..., \mathcal{F}_{N_D})$, then from Eq. (A.0.1) we can write

$$\left(\mathbf{X} \cdot \hat{\mathcal{F}}\right)\left(\mathbf{Y} \cdot \hat{\mathcal{F}}\right) = X_j \mathcal{F}_j Y_k \mathcal{F}_k = X_j Y_k \mathcal{F}_j \mathcal{F}_k \ \ . \tag{A.0.11}$$

By substituting Eq. (A.0.6) in (A.0.11) and having into consideration that the structure constants d_{jkl} and f_{jkl} are completely symmetric and antisymmetric, respectively, under the permutation of any two subindexes, one obtains the following identity relation:

$$\left(\mathbf{X} \cdot \hat{\mathcal{F}}\right)\left(\mathbf{Y} \cdot \hat{\mathcal{F}}\right) = \frac{2}{N}\mathcal{I}_{_N}(\mathbf{X} \cdot \mathbf{Y}) + ((\mathbf{X} \star \mathbf{Y}) + i(\mathbf{X} \wedge \mathbf{Y})) \cdot \hat{\mathcal{F}} \ \ . \tag{A.0.12}$$

Appendix B

Solving the TDSE for kicked systems

We are interested in solving the time-dependent Schrödinger equation (TDSE),

$$i\hbar\frac{\partial\Psi}{\partial t} = \left(H - \mathbf{r}.\mathbf{e}\sum_{k=1}^{N_0}\Delta p_k\delta(t-t_k)\right)\Psi \ \ , \tag{B.0.1}$$

corresponding, within the impulsive and dipole approximations, to a quantum system interacting with a train of N_0 HCPs. We have assumed, for simplicity, that all the pulses are linearly polarized in the same direction (determined by the unit vector $\mathbf{e}$).

For an N-level system, the solutions of (B.0.1) can be expanded on the eigenfunctions $\Psi_n^{(0)}(r)$ of the unperturbed system (that are assumed to be known) as follows:

$$\Psi(r,t) = \sum_{n=1}^{N} C_n(t)\Psi_n^{(0)}(r) \ \ . \tag{B.0.2}$$

The substitution of (B.0.2) into (B.0.1) leads to the following system of differential equations for determining the expansion coefficients,

$$i\hbar\frac{\partial\mathbf{C}(t)}{\partial t} = \mathcal{E}\mathbf{C}(t) - \mathcal{W}\sum_{k=1}^{N_0}\Delta p_k\delta(t-t_k)\mathbf{C}(t) \ \ , \tag{B.0.3}$$

where $\mathbf{C}(t)$ is a vector whose components are the expansion coefficients, i.e., $\mathbf{C}(t) = (C_{_1}(t), C_{_2}(t), ..., C_{_N}(t))^T$, the matrix $\mathcal{W}$ is composed of the elements

$$W_{ij} = \langle\Psi_i^{(0)}|\mathbf{r}.\mathbf{e}|\Psi_j^{(0)}\rangle \ \ , \tag{B.0.4}$$

and

$$\mathcal{E} = \mathrm{diag}\left(E_1^{(0)}, E_2^{(0)}, ..., E_N^{(0)}\right) \ \ , \tag{B.0.5}$$

with $E_n^{(0)}$ representing the eigenenergies of the stationary states.

Let assume that the kth kick is applied at $t = t_k^- = t_k - \epsilon$ ($\epsilon \to 0$) and finishes at $t = t_k$. As between consecutive kicks the system evolves in a field-free manner, the integration of (B.0.3) in the time intervals $t_k \leq t < t_{k+1}$ can be easily performed and leads to the following continuous time propagation of the wave function,

$$\mathbf{C}(t) = e^{-\frac{1}{\hbar}\mathcal{E}(t-t_k)}\mathbf{C}^{(k)}(t) \quad ; \quad t_k \leq t < t_{k+1} \ , \tag{B.0.6}$$

where we used the notation $\mathbf{C}^{(k)}(t) = \mathbf{C}(t_k)$. For a complete description of the evolution of $\mathbf{C}(t)$ one needs to complement Eq. (B.0.6) with appropriate matching conditions relating the values of the vector $\mathbf{C}(t)$ just before and right after each pulse. For the obtention of these matching conditions one can be tempted to directly integrate (B.0.3) by making use of the sifting property of the Dirac δ function [143, 144]. However, the use of the sifting property is inappropriate since the vector $\mathbf{C}(t)$ has discontinuities at the time of application of each kick (for a detailed discussion see [145]). One can overcome such a problem by introducing the area $a(t)$ of the δ function as a new variable. The advantage of doing that is that although $\mathbf{C}(t)$ is not a continuous function of time, it is a continuous function of the area $a(t)$ [145].

The Dirac δ function can be represented as

$$\delta(t - t_k) = \begin{cases} \lim\limits_{\epsilon \to 0} \frac{1}{\epsilon} & \text{for } t_k^- < t \leq t_k \\ 0 & \text{elsewhere} \end{cases} \ , \tag{B.0.7}$$

and the area of the δ function as a function of time can be written, in the interval $t_k^- < t \leq t_k$, as

$$a(t) = \int_{t_k - \epsilon}^{t} \delta(t' - t_k) dt' = \frac{(t - t_k + \epsilon)}{\epsilon} \quad . \tag{B.0.8}$$

Thus, right before and after the kth pulse we have $a(t_k^-) = 0$ and $a(t_k) = 1$, respectively. In terms of the new variable $a(t)$, and after performing the limit $\epsilon \to 0$, the Schrödinger equation in the vicinity of $t = t_k$ reduces to

$$i\hbar \frac{\partial \mathbf{C}^{(k)}(a)}{\partial a} = -\mathcal{W}\Delta p_k \mathbf{C}^{(k)}(a) \ , \tag{B.0.9}$$

whose general solution is given by

$$\mathbf{C}^{(k)}(a) = e^{\frac{i}{\hbar} a \mathcal{W}\Delta p_k}\mathbf{C}^{(k)}(0) \ . \tag{B.0.10}$$

Taking into account that $\mathbf{C}^{(k)}(a = 0) = \mathbf{C}(t_k^-)$ and $\mathbf{C}^{(k)}(a = 1) = \mathbf{C}(t_k)$, we obtain from (B.0.10) the following matching condition:

$$\mathbf{C}(t_k) = e^{\frac{i}{\hbar}\mathcal{W}\Delta p_k}\mathbf{C}(t_k^-) \ , \tag{B.0.11}$$

that relates the values of the vector $\mathbf{C}(t)$ just before and right after the application of the kth kick. Then, by combining (B.0.6) and (B.0.11) it results the following stroboscopic map from $t = t_k$ to $t = t_{k+1}$,

$$\mathbf{C}(t_{k+1}) = e^{i\frac{\mathcal{W}\Delta p_k}{\hbar}} e^{-\frac{i}{\hbar}\mathcal{E}(t_{k+1}-t_k)}\mathbf{C}(t_k) \quad . \tag{B.0.12}$$

For a two-level system Eq. (B.0.6) can be rewritten as

$$\mathbf{C}(t) = \begin{pmatrix} e^{\frac{i}{2}\omega_c(t-t_k)} & 0 \\ 0 & e^{-\frac{i}{2}\omega_c(t-t_k)} \end{pmatrix} \mathbf{C}(t_k) \quad ; \quad t_k \le t < t_{k+1} \ , \tag{B.0.13}$$

where we have introduced the characteristic frequency $\omega_c = \frac{E_2^{(0)} - E_1^{(0)}}{\hbar}$. On the other hand , if the two-level system is such that $\mathcal{W}$ is traceless, one can rewrite (B.0.12) as

$$\mathbf{C}(t_k) = e^{\frac{i\Delta p_k}{\hbar}\mathbf{Q}\cdot\hat{\sigma}}\mathbf{C}(t_k^-) \ , \tag{B.0.14}$$

where $\hat{\sigma} = (\sigma_x, \sigma_y, \sigma_z)$ with σ_i $(i = x, y, z)$ denoting the Pauli matrices and $\mathbf{Q} = (Q_x, Q_y, Q_z)$ with Q_i $(i = x, y, z)$ representing the coefficients of the expansion

$$\mathcal{W} = \sum_i Q_i \sigma_i \ . \tag{B.0.15}$$

In the particular case $\mathcal{W} = -\mu\sigma_x$ with μ a real number (note that the cases discussed in Secs. 5.1.1 and 6.1.2 correspond to this particular situation with $\mu = \mu_0/\sqrt{3}$ and $\mu = \mu_{12}$, respectively), the relation (B.0.14) reduces to

$$\mathbf{C}(t_k) = \begin{pmatrix} \cos\left(\frac{\mu\Delta p_k}{\hbar}\right) & i\sin\left(\frac{\mu\Delta p_k}{\hbar}\right) \\ i\sin\left(\frac{\mu\Delta p_k}{\hbar}\right) & \cos\left(\frac{\mu\Delta p_k}{\hbar}\right) \end{pmatrix} \mathbf{C}(t_k^-) \ . \tag{B.0.16}$$

By performing the transition to the generalized Bloch space through the transformation $\mathbf{B}(t) = \mathbf{C}^\dagger(t)\hat{\sigma}\mathbf{C}(t)$, one easily obtain from (B.0.13) that the field-free evolution of the Bloch vector between consecutive kicks is determined by

$$\mathbf{B}(t) = \begin{pmatrix} \cos\beta_k & -\sin\beta_k & 0 \\ \sin\beta_k & \cos\beta_k & 0 \\ 0 & 0 & 1 \end{pmatrix} \mathbf{B}(t_k) \quad ; \quad t_k \le t < t_{k+1} \ , \tag{B.0.17}$$

where

$$\beta_k = \omega_c(t - t_k) \ . \tag{B.0.18}$$

On the other hand, we obtain from Eq. (B.0.16) that the action of the kth kick on the system is determined, in the Bloch space, by the relation

$$\mathbf{B}(t_k) = \begin{pmatrix} 1 & 0 & 0 \\ 0 & \cos\alpha_k & -\sin\alpha_k \\ 0 & \sin\alpha_k & \cos\alpha_k \end{pmatrix} \mathbf{B}(t_k^-) \ , \tag{B.0.19}$$

where

$$\alpha_k = \frac{2\mu\Delta p_k}{\hbar} \ . \tag{B.0.20}$$

In the cases $\mu = \mu_0/\sqrt{3}$ and $\mu = \mu_{12}$, Eqs. (B.0.17) and (B.0.19) reduce to the corresponding expressions utilized in Secs. 5.1.1 and 6.1.2, respectively.

Appendix C

Floquet analysis of a kicked two-level system

We consider the two-level system studied in Sec. 6.1.2 for the case of a quasiperiodic train of kicks with period T as the driving field.

From Eqs. (B.0.13) and (B.0.16) one can easily obtain that if a kick is applied at $t = t_0$, then

$$\mathbf{C}(t_0 + T) = U(t_0 + T, t_0)\mathbf{C}(t_0) \ , \tag{C.0.1}$$

with the one-period evolution operator given by

$$U(t_0 + T, t_0) = \left(\begin{array}{cc} u_{11} & u_{12} \\ u_{21} & u_{22} \end{array} \right) \ , \tag{C.0.2}$$

where

$$u_{11} = e^{\frac{i}{2}\omega_c T} \cos\left(\frac{\mu_{12}\Delta p_k}{\hbar}\right) \quad ; \quad u_{22} = u_{11}^* \ , \tag{C.0.3}$$

and

$$u_{12} = ie^{\frac{i}{2}\omega_c T} \sin\left(\frac{\mu_{12}\Delta p_k}{\hbar}\right) \quad ; \quad u_{21} = -u_{12}^* \ . \tag{C.0.4}$$

The Floquet modes $\Phi_\lambda(t_0)$ and the quasienergies ε_λ are the corresponding eigenvectors and eigenvalues of the following eigenvalue problem [see Eq. (3.2.12)],

$$U(t_0 + T, t_0)\Phi_\lambda(t_0) = e^{-\frac{i}{\hbar}\varepsilon_\lambda T}\Phi_\lambda(t_0) \ . \tag{C.0.5}$$

Taking into account Eqs. (C.0.2) - (C.0.5) it is not difficult to find that the quasienergies corresponding to the first Brillouin zone are determined by

$$\epsilon_1 = -\frac{\hbar}{T} \arccos\left[\cos\left(\frac{\mu_{12}\Delta p_k}{\hbar}\right)\cos\left(\frac{\omega_c T}{2}\right)\right] \quad ; \quad \epsilon_2 = -\epsilon_1 \ . \tag{C.0.6}$$

On the other hand, for the case $u_{12} = -u_{21}^* \neq 0$ (in the opposite case the problem is trivial, since the evolution operator becomes diagonal) the corresponding Floquet modes are found to be given by

$$\Phi_1(t_0) = \frac{1}{\sqrt{|u_{12}|^2 + |\kappa_1 - u_{11}|^2}} \begin{pmatrix} u_{12} \\ \kappa_1 - u_{11} \end{pmatrix} \quad , \tag{C.0.7}$$

and

$$\Phi_2(t_0) = \frac{1}{\sqrt{|u_{21}|^2 + |\kappa_2 - u_{22}|^2}} \begin{pmatrix} \kappa_2 - u_{22} \\ u_{21} \end{pmatrix} \quad , \tag{C.0.8}$$

where $\kappa_l = \exp(-i\epsilon_l T/\hbar)$ $(l = 1, 2)$.

If the system parameters are such that the localization condition [see Eq. (6.2.1)]

$$\frac{\mu_{12}\Delta p}{\hbar} = (2n+1)\frac{\pi}{2} \qquad (n \in \mathcal{Z}) \ , \tag{C.0.9}$$

is fulfilled, then Eqs. (C.0.6) - (C.0.8) reduce to

$$\epsilon_1 = -\frac{\hbar\omega_0}{4} \quad ; \quad \epsilon_2 = \frac{\hbar\omega_0}{4} \quad ; \quad \omega_0 = \frac{2\pi}{T} \ , \tag{C.0.10}$$

$$\Phi_1(t_0) = \frac{i}{\sqrt{2}} \begin{pmatrix} (-1)^n e^{\frac{i}{2}\omega_c T} \\ 1 \end{pmatrix} \quad , \tag{C.0.11}$$

and

$$\Phi_2(t_0) = -\frac{i}{\sqrt{2}} \begin{pmatrix} 1 \\ (-1)^{n+1} e^{-\frac{i}{2}\omega_c T} \end{pmatrix} \quad , \tag{C.0.12}$$

respectively.

The vector $\mathbf{C}(t)$ determining the evolution of the wave function is given, at stroboscopic times, by [see Eq. (3.2.9)]

$$\mathbf{C}(t_0 + kT) = A_1 e^{-\frac{i}{\hbar}\epsilon_1(t_0+kT))}\Phi_1(t_0) + A_2 e^{-\frac{i}{\hbar}\epsilon_2(t_0+kT))}\Phi_2(t_0) \ . \tag{C.0.13}$$

The expansion coefficients A_l are determined by [see Eq. (3.2.10)],

$$A_l = e^{\frac{i}{\hbar}\epsilon_l t_0}\Phi_l^\dagger(t_0)\mathbf{C}(t_0) \quad ; \quad l = 1, 2. \tag{C.0.14}$$

In the case of tunnelling initial condition (see Sec. 6.2.1) and under the localization condition (C.0.9) the expansion coefficients are given by

$$A_1 = \frac{i}{2} e^{\frac{i}{\hbar}\epsilon_1 t_0} \left[(-1)^{n+1} e^{\frac{i}{2}\omega_c(t_0 - T)} + e^{-\frac{i}{2}\omega_c t_0} \right] \quad , \tag{C.0.15}$$

and

$$A_2 = \frac{i}{2} e^{\frac{i}{\hbar}\epsilon_2 t_0} \left[(-1)^n e^{-\frac{i}{2}\omega_c(t_0 - T)} + e^{\frac{i}{2}\omega_c t_0} \right] \quad . \tag{C.0.16}$$

Appendix D

Sums involving Bessel functions

Here we present some mathematical identities that result useful for the calculations performed in Chap. 7.

In all the following identities $m, n \in \mathbb{Z}$ and $a, b \in \mathbb{R}$.

$$\int_0^{2\pi} e^{im\theta} e^{ia\cos\theta} d\theta = 2\pi i^m J_m(a) = 2\pi i^m J_{-m}(-a) \ . \tag{D.0.1}$$

$$\int_0^{2\pi} e^{im\theta} e^{ia\sin\theta} d\theta = 2\pi J_{-m}(a) = 2\pi J_m(-a) \ . \tag{D.0.2}$$

$$\sum_{m=-\infty}^{\infty} [mJ_{n-m}(a)]^2 = n^2 + \frac{a^2}{2} \ . \tag{D.0.3}$$

$$\sum_{m=-\infty}^{\infty} J_m(a)J_{m+1}(a) \left\{ \begin{array}{c} \cos mb \\ \sin mb \end{array} \right\} = J_1(\omega) \left\{ \begin{array}{c} \sqrt{\frac{1-\cos b}{2}} \\ \frac{\sin b}{\sqrt{2(1-\cos b)}} \end{array} \right\} \ . \tag{D.0.4}$$

$$\sum_{m=-\infty}^{\infty} J_{n-m}(a)J_{n-m-2}(a)\cos[(m+1)b] = -J_2(\omega)\cos(nb) \tag{D.0.5}$$

In Eqs. (D.0.4) and (D.0.5) $\omega = a\sqrt{2-2\cos b}$.

$$\sum_{m=-\infty}^{\infty} (2m+1)J_{n-m}(a)J_{n-m-1}(a)\sin[(2m+1)b] = a[g_+(n) - g_-(n)] \ , \tag{D.0.6}$$

where

$$g_\pm(n) = \left[\left(n \mp \frac{1}{2}\right) J_0(\varphi) + \left(n \pm \frac{1}{2}\right) J_2(\varphi)\right] \sin\left[(2n \mp 1)b\right] \ , \tag{D.0.7}$$

and $\varphi = 2a\sin(b)$.

$$\sum_{m=-\infty}^{\infty} m\left[J_{m-n}(a)\right]^2 = n \ . \tag{D.0.8}$$

All the identities above were obtained, after some mathematical manipulations, from identities reported in [146]. In addition we also proved numerically their validity.

Bibliography

[1] M. D. Perry *et al.*, Opt. Lett. **24**, 160 (1999).

[2] J. Squier, F. Salin, G. Mourou, and D. Harter, Opt. Lett. **16**, 324 (1991).

[3] V. Krainov and M. B. Smirnov, Phys. Rep. **370**, 237 (2002).

[4] E. Hertz *et al.*, Phys. Rev. A **64**, 051801 (2001).

[5] M. Hentschel *et al.*, Nature **414**, 509 (2001).

[6] D. You, R. R. Jones, and P. H. Bucksbaum, Opt. Lett. **18**, 290 (1993).

[7] R. R. Jones, D. You, and P. H. Bucksbaum, Phys. Rev. Lett. **70**, 1236 (1993).

[8] J. G. Zeibel, *Manipulating wavepacket dynamics with half-cycle pulses*, Ph. D. thesis (Dpt. of Physics, University of Virginia, 2003), available at http://landau1.phys.virginia.edu/research/groups/jones/.

[9] T. J. Bensky, G. Haefler, and R. R. Jones, Phys. Rev. Lett. **79**, 2018 (1997).

[10] A. E. Kaplan, Phys. Rev. Lett. **73**, 1243 (1994).

[11] A. E. Kaplan and P. L. Shkolnikov, Phys. Rev. Lett. **75**, 2316 (1995).

[12] A. E. Kaplan, S. F. Straub, and P. L. Shkolnikov, J. Opt. Soc. Am. B **14**, 3013 (1997).

[13] V. P. Kalosha and J. Herrmann, Phys. Rev. Lett. **83**, 544 (1999).

[14] R. R. Jones, Phys. Rev. Lett. **76**, 3927 (1996).

[15] A. Wetzels, A. Gürtel, H. G. Muller, and L. D. Noordam, Eur. Phys. J. D **14**, 157 (2001).

[16] M. T. Frey *et al.*, Phys. Rev. A **59**, 1434 (1999).

[17] B. E. Tannian *et al.*, Phys. Rev. A **62**, 043402 (2000).

[18] C. O. Reinhold, J. Burgdörfer, M. T. Frey, and F. B. Dunning, Phys. Rev. Lett. **79**, 5226 (1997).

[19] C. O. Reinhold *et al.*, J. Phys. B **34**, L551 (2001).

[20] A. Bugacov, B. Piraux, M. Pont, and R. Shakeshaft, Phys. Rev. A **51**, 4877 (1995).

[21] C. Dion, A. Keller, and O. Atabek, Eur. Phys. J. D **14**, 249 (2001).

[22] S. Yoshida *et al.*, Phys. Rev. A **58**, 2229 (1998).

[23] E. Persson *et al.*, Phys. Rev. A (in press).

[24] B. E. Tannian *et al.*, Phys. Rev. A **64**, 021404 (2001).

[25] M. Machholm and N. E. Henriksen, Phys. Rev. Lett. **87**, 193001 (2001).

[26] F. Bloch, Phys. Rev. **70**, 460 (1946).

[27] C. P. Slichter, *Principle of Magnetic Resonance*, 3th eddition (Springer, Berlin, 1992).

[28] R. P. Feynman, F. L. Vernon, Jr., and R. W. Hellwarth, J. Appl. Phys. **28**, 49 (1957).

[29] L. Allen and J. H. Eberly, *Optical Resonance and Two-level Atoms* (Wiley, New York, 1975).

[30] F. T. Hioe and J. H. Eberly, Phys. Rev. Lett. **47**, 838 (1981).

[31] F. T. Hioe, Phys. Rev. A **26**, 1466 (1982).

[32] F. T. Hioe, Phys. Rev. A **28**, 879 (1983).

[33] W. Greiner and B. Müller, *Quantum Mechanics (Symmetries)*, 2nd edditon (Springer, Berlin, 1994).

[34] *Geometric Phase in Physics*, ed. by A. Shapere and F. Wilczek (World Scientific, Singapore, 1989).

[35] A. Bohm *et al.*, *The Geometric Phase in Quantum Systems* (Springer, Berlin, 2003).

[36] B. Y. Hou and B. Y. Hou, *Differential Geometry for Physicists* (World Scientific, Singapore, 1997).

[37] Arvind, K. S. Mallesh, and N. Mukunda, J. Phys. A **30**, 2417 (1997).

[38] L. Jakóbczyk and M. Siennicki, Phys. Lett. A **286**, 383 (2001).

[39] N. Mukunda and R. Simon, Ann. Phys. (N.Y.) **228**, 205 (1993).

[40] A. Matos-Abiague and J. Berakdar (unpublished).

[41] J. H. Shirley, Phys. Rev. **138**, B979 (1965).

[42] W. R. Salzman, Phys. Rev. A **10**, 461 (1974).

[43] S. R. Barone and M. A. Narcowich, Phys. Rev. A **15**, 1109 (1977).

[44] K. F. Milfeld and R. E. Wyatt, Phys. Rev. A **27**, 72 (1983).

[45] M. Grifoni and P. Hänggi, Phys. Rep. **304**, 229 (1998).

[46] A. N. Seleznyova, J. Phys. A **26**, 981 (1993).

[47] Y. Aharonov and J. Anandan, Phys. Rev. Lett. **58**, 1593 (1987).

[48] J. von Neumann and E. Wigner, Physik. Z. **30**, 467 (1929).

[49] R. Heather and H. Metiu, J. Chem. Phys. **86**, 5009 (1987).

[50] J. A. Fleck, Jr., J. R. .Morris, and M. D. Feit, Appl. Phys. **10**, 129 (1976).

[51] M. D. Feit, J. A. Fleck, Jr., and A. Steiger, J. Comput. Phys. **47**, 42 (1982).

[52] M. D. Feit and J. A. Fleck, Jr., J. Chem. Phys. **80**, 2578 (1984).

[53] E. O. Brigham, *The Fast Fourier Transform*, (Prentice-Hall, 1974).

[54] F. Grossmann, T. Dittrich, P. Jung, and P. Hänggi, Phys. Rev. Lett. **67**, 561 (1991).

[55] J. Gómez Llorente and J. Plata, Phys. Rev. A **45**, R6958 (1992).

[56] R. Bavli and H. Metiu, Phys. Rev. Lett. **69**, 229 (1998).

[57] A. Sacchetti, J. Phys. A **34**, 10293 (2001).

[58] A. A. Ignatov, K. F. Renk, and E. P. Dodin, Phys. Rev. Lett. **70**, 1996 (1993).

[59] D. H. Dunlap and V. M. Kenkre, Phys. Rev. B **37**, 6622 (1988).

[60] A. Matos-Abiague and J. Berakdar, Chem. Phys. Lett. **382**, 475 (2003).

[61] A. Matos-Abiague and J. Berakdar, Phys. Rev. A **68**, 063411 (2003).

[62] D. J. Moore, Phys. Rep. **210**, 1 (1991).

[63] J. Anandan and L. Stodolsky, Phys. Rev. D **35**, 2597 (1987).

[64] S. L. Zhu, Z. D. Wang, and Y. D. Zhang, Phys. Rev. B **61**, 1142 (2000).

[65] T. F. Jordan, Phys. Rev. A **38**, 1590 (1988).

[66] A. K. Pati, Phys. Rev. A **52**, 2576 (1995).

[67] A. Matos-Abiague and J. Berakdar, Phys. Rev. B **69**, 155304 (2004).

[68] R. P. Feynman, Phys. Rev. **56**, 340 (1939).

[69] L. A. Wu, Phys. Rev. A **50**, 5317 (1994).

[70] K. H. Kramer and R. B. Bernstein, J. Chem. Phys. **40**, 200 (1964).

[71] P. R. Brooks and M. E. Jones, J. Chem. Phys. **45**, 3449 (1966).

[72] P. R. Brooks, Science **193**, 11 (1976).

[73] R. B. Bernstein, J. Chem. Phys. **82**, 3656 (1985).

[74] R. B. Bernstein, D. R. Herschbach, and R. D. Levine, J. Phys. Chem. **91**, 5365 (1987).

[75] H. J. Loesch and A. Remscheid, J. Phys. Chem. **95**, 8194 (1991).

[76] H. J. Loesch and A. Remscheid, J. Chem. Phys. **93**, 4779 (1990).

[77] H. J. Loesch, Annu. Rev. Phys. Chem. **46**, 555 (1995).

[78] H. Sakai *et al.*, Phys. Rev. Lett. **90**, 083001 (2003).

[79] Special issue on *Stereodynamics of Chemical Reactions*, J. Phys. Chem. A **101**, 7461 (1997).

[80] F. J. Aoiz *et al.*, Chem. Phys. Lett. **289**, 132 (1998).

[81] T. Seideman, M. Yu. Ivanonv, and P. B. Corkum, Phys. Rev. Lett. **75**, 2819 (1995).

[82] E. Constant, H. Stapelfeldt, and P. B. Corkum, Phys. Rev. Lett. **76**, 4140 (1996).

[83] C. M. Dion *et al.*, J. Chem. Phys. **105**, 9083 (1996).

[84] T. Seideman, Phys. Rev. A **56**, R17 (1997).

[85] M. G. Tenner, E. W. Kuipers, A. W. Kleyn, and S. Stolte, J. Chem. Phys. **94**, 5197 (1991).

[86] H. Stapelfeldt and T. Seideman, Rev. Mod. Phys. **75**, 543 (2003).

[87] H. Stapelfeldt, H. Sakai, E. Constant, P. B. Corkum, Phys. Rev. Lett. **79**, 2787 (1997).

[88] B. Friedrich and D. R. Herschbach, Nature **353**, 412 (1991).

[89] B. Friedrich and D. R. Herschbach, Phys. Rev. Lett. **474**, 4623 (1995).

[90] C. M. Dion, A. Keller, O. Atabek, and A. D. Bandrauk, Phys. Rev. A **59**, 1382 (1999).

[91] B. Friedrich and D. R. Herschbach, J. Chem. Phys. **111**, 6157 (1999).

[92] L. Cai, J. Marango and B. Friedrich, Phys. Rev. Lett. **86**, 775 (2001).

[93] T. Kanai and H. Sakai, J. Chem. Phys. **115**, 5492 (2001).

[94] A. B. Haj-Yedder *et al.*, Phys. Rev. A **66**, 063401 (2002).

[95] M. Machholm, J. Chem. Phys. **115**, 10724 (2001).

[96] D. A. Varshalovich, A. N. Moskalev, and V. K. Khersonskii, *Quantum Theory of Angular Momentum* (World Scientific, Singapore, 1989).

[97] M. J. J. Vrakking and S. Stolte, Chem. Phys. Lett. **271**, 209 (1997).

[98] O. Atabek, C. M. Dion, and A. B. Haj-Yedder, J. Phys. B **36**, 4667 (2003).

[99] I. Sh. Averbukh and R. Arvieu, Phys. Rev. Lett. **87**, 163601 (2001).

[100] R. Bavli and H. Metiu, Phys. Rev. A **47**, 3299 (1993).

[101] F. Grossmann, P. Jung, T. Dittrich and P. Hänggi, Z. Phys. B **84**, 315 (1991).

[102] Y. Dakhnovskii and R. Bavli, Phys. Rev. B **48**, 11010 (1993).

[103] J. Shao and P. Hänggi, Phys. Rev. A **56**, R4397 (1997).

[104] A. Matos-Abiague and J. Berakdar, Appl. Phys. Lett. **84**, 2346 (2004).

[105] A. Matos-Abiague and J. Berakdar (to be published in Phys. Scr.).

[106] G. Bastard, *Wave mechanics applied to semiconductor heterostructures* (Les éditions de physique, Les Ulis Cedex, 1996).

[107] S. A. Washburn and R. A. Webb, Adv. Phys. **35**, 375 (1986).

[108] *Mesoscopic Phenomena in Solids*, ed. by B. L. Altshuler, P. A. Lee, and R. A. Webb (North-Holland, Amsterdam, 1991).

[109] *Transport Phenomena in Mesoscopic Systems*, ed. by H. Fukuyama and T. Ando (Springer, Heidelberg, 1992).

[110] *Quantum coherence and decoherence*, ed. by Y. A. Ono and K. Fujikawa (North-Holland, Amsterdam, 1999).

[111] Y. Imry, *Introduction to mesoscopic physics*, Scnd. edition (University press, Oxford, 2002).

[112] M. Büttiker, Y. Imry, and R. Landauer, Phys. Lett. A **96**, 365 (1983).

[113] R. Landauer and M. Büttiker, Phys. Rev. Lett. **54**, 2049 (1985).

[114] H. F. Cheung, Y. Gefen, E. K. Riedel, and W. H. Shih, Phys. Rev. B **37**, 6050 (1988).

[115] J. F. Weisz, R. Kishore, and F. V. Kusmartser, Phys. Rev. B **49**, 8126 (1994).

[116] C. W. Tan and J. C. Inkson, Phys. Rev. B **60**, 5626 (1999).

[117] A. Müller-Groeling and H. A. Weidenmüller, Phys. Rev. B **49**, 4752 (1994).

[118] G. Bouzerar, D. Poiblanc, and G. Montambaux, Phys. Rev. B **49**, 8258 (1994).

[119] T. Chakraborty and P. Pietiläinen, Phys. Rev. B **50**, 8460 (1994).

[120] S. Latil, S. Roche, and A. Rubio, Phys. Rev. B **67**, 165420 (2003).

[121] L. P. Lévy, G. Dolan, J. Dunsmuir, and H. Bouchiat, Phys. Rev. Lett. **64**, 2074 (1990).

[122] V. Chandrasekhar *et al.*, Phys. Rev. Lett. **67**, 3578 (1991).

[123] D. Mailly, C. Chapelier, and A. Benoit, Phys. Rev. Lett. **70**, 2020 (1993).

[124] W. Rabaud *et al.*, Phys. Rev. Lett. **86**, 3124 (2001).

[125] K. B. Efetov, Phys. Rev. Lett. **66**, 2794 (1991).

[126] V. E. Kravtsov and V. I. Yudson, Phys. Rev. Lett. **70**, 210 (1993).

[127] O. L. Chalaev and V. E. Kravtsov, Phys. Rev. Lett. **89**, 176601 (2002).

[128] P. Kopietz and A. Völker, Eur. Phys. J. B **3**, 397 (1998).

[129] M. Moskalets and M. Büttiker, Phys. Rev. B **66**, 245321 (2002).

[130] K. Yakubo and J. Ohe, Physica E **18**, 97 (2003).

[131] G. M. Genking and G. A. Vugalter, Phys. Lett. A **189**, 415 (1994).

[132] T. Swahn *et al.*, Phys. Rev. Lett. **73**, 162 (1994).

[133] J. M. Ziman, *Principles of the Theory of Solids*, Scnd. edition (University press, Cambridge, 1998).

[134] W. Jones and N. H. March, *Theoretical Solid State Physiscs*, Vol. 2 (Dover Publications, New York, 1985).

[135] D. Loss and P. Goldbart, Phys. Rev. B **43**, 13762 (1991).

[136] A. Matos-Abiague and J. Berakdar, Phys. Lett. A **330**, 113 (2004).

[137] A. Matos-Abiague and J. Berakdar, Phys. Rev. B **70**, 195338 (2004).

[138] R. Huber *et al.*, Nature **414**, 286 (2001).

[139] A. Matos-Abiague and J. Berakdar, Eurohys. Lett. **69**, 277 (2005).

[140] A. Matos-Abiague and J. Berakdar (unpublished).

[141] D. Rugar *et al.*, Science **264**, 1560 (1994).

[142] J. A. Sidles *et al.* Rev. Mod. Phys. **67**, 249 (1995).

[143] M. Klews and W. Schweizer, Phys. Rev. A **64**, 053403 (2001).

[144] B. Y. Ou, X. G. Zhao, and S. G. Chen, Phys. Lett. A **248**, 377 (1998).

[145] A. Matos-Abiague and K. A. Kouzakov, Phys. Rev. A **68**, 017401 (2003).

[146] *Handbook of Mathematical functions*, ed. by M. Abramowitz and I. Stegun (Dover Publications, New York, 1972).

Erklärung

Hiermit ekläre ich, daß ich die vorliegende Dissertation selbständig un ohne fremde Hilfe verfaßt, andere als die angegebenen Quellen und Hilfsmittel nicht benutzt, und die den benutzten Werken wörtlich oder inhaltlich entnommenen Stellen als solche kenntlich gemacht habe. Die Dissertation wurde bisher an keiner anderen Universität oder Hochschule vorgelegt.

Halle (Saale), den 16 März 2004.

Alex Matos Abiague

Curriculum Vitae

Personal data:

Name: Alex Matos Abiague
Date of birth: December 06, 1969
Place of birth: Santiago de Cuba, Cuba
Marital status: Married

Education:

Sept. 1975 - June 1981:
Primary school “Chiqui Gómez Lubian”, Santa Clara, Cuba.

Sept. 1981 - July 1984:
Secondary school “Fe del Valle”, Santa Clara, Cuba.

Sept. 1984 - July 1987:
High school “Capitán Roberto Rodríguez”, Santa Clara, Cuba.

Sept. 1987 - July 1988:
Diploma of technical Bulgarian language, Facultad Preparatoria, Havana, Cuba.

Sept. 1988 - July 1990:
Faculty of Physics at the University Kliment Ohridski, Sofia, Bulgaria.

Sept. 1990 - July 1993:
Faculty of Natural Sciences and Mathematics at the “Universidad de Oriente”, Santiago de Cuba, Cuba. Degree in Physics with the thesis: *Polaron effect in semiconductor quantum wells.*

June 2001 - June 2004:
Ph. D. candidate at Max-Planck-Institut für Mikrostrukturphysik, Halle (Saale), Germany. Supervisor: PD Dr. Jamal Berakdar.

Work experience:

Sept. 1993 - July 1995:
Teaching assistant at the Department of Physics, Universidad de Oriente, Santiago de Cuba, Cuba. Teaching: Analytic Geometry and Linear Algebra, and Mathematical Methods of Physics I.

Sept. 1995 - Dec. 1999:

Instructor at the Department of Physics, Universidad de Oriente, Santiago de Cuba, Cuba. Teaching: Analytic Geometry and Linear Algebra, and Mathematical Methods of Physics II.

Sept. 1996 - July 1999:

Research/Teaching assistant at the Department of Theoretical Physics, University of Havana, Havana, Cuba. Research: Excitons and shallow impurities in semiconductor heterostructures. Teaching: Analytic Geometry and Linear Algebra.

List of Publications

1. Fractional-dimensional space and applications in quantum-confined semiconducting heterostructures. M. de Dios-Leyva, A. Bruno-Alfonso, A. Matos-Abiague and L. E. Oliveira, J. Appl. Phys. **82** (6) 3155 (1997).

2. Excitonic and shallow-donor states in semiconducting quantum wells: a fractional-dimensional space approach. M. de Dios-Leyva, A. Bruno-Alfonso, A. Matos-Abiague and L. E. Oliveira, J. Phys.: Condens. Matter **9**, 8477 (1997).

3. Fractional-dimensional approach for excitons in $\mathrm{GaAs} - \mathrm{Ga}_{1-x}\mathrm{Al}_x\mathrm{As}$ quantum wells. A. Matos-Abiague, L. E. Oliveira and M. de Dios-Leyva, Phys. Rev. B **58**, 4072 (1998).

4. Excitons and shallow impurities in semiconductor heterostructures. L. E. Oliveira, A. Matos-Abiague, E. Reyes-Gómez, and M. de Dios-Leyva, in *Condensed Matter Theories*, Vol. 14, ed. by D. J. Ernst, I. E. Perakis, and A. S. Umar (Nova Science, New York, 2000).

5. On polar optical vibrational quantum excitations in semiconductor nanostructures. A. Matos-Abiague, Rev. Mex. Fis. **45**, 581 (1999).

6. The fractional-dimensional space approach: excitons and shallow impurities in semiconductor low-dimensional systems. E. Reyes-Gómez, A. Matos-Abiague, M. de Dios-Leyva and L. E. Oliveira, Phys. Status Solidi B **220**, 71 (2000).

7. Excitons and shallow impurities in $\mathrm{GaAs} - \mathrm{Ga}_{1-x}\mathrm{Al}_x\mathrm{As}$ semiconductor heterostructures within a fractional-dimensional space approach: Magnetic-field effects. E. Reyes-Gómez, A. Matos-Abiague, C. A. Perdomo-Leiva, M. de Dios-Leyva, and L. E. Oliveira, Phys. Rev. B **61**, 13104 (2000).

8. Exciton states and diamagnetic shifts in symmetric coupled double $\mathrm{GaAs}-\mathrm{Ga}_{1-x}\mathrm{Al}_x\mathrm{As}$ quantum wells within the fractional-dimensional approach. A. Matos-Abiague, L. E. Oliveira, and M. de Dios-Leyva, J. Phys.: Condens. Matter **12**, 5691 (2000).

9. Fractional dimensional momentum operator for a system of one degree of freedom. A. Matos-Abiague, Physica Scripta **62**, 106 (2000).

10. Free particle in fractional-dimensional space. A. Matos-Abiague, Bulgarian Journal of Physics **27**, 54 (2000).

11. A fractional-dimensional space approach to the study of shallow-donor states in symmetric-coupled $\mathrm{GaAs} - \mathrm{Ga}_{1-x}\mathrm{Al}_x\mathrm{As}$ multiple quantum wells. A. Matos-Abiague, L. E. Oliveira and M. de Dios-Leyva, Physica B **296**, 342 (2001).

12. Bose-like oscillator in fractional-dimensional space. A. Matos-Abiague, J. Phys. A: Math. Gen. **34**, 3125 (2001).

13. The fractional-dimensional space approach to MBE-grown quantum-sized semiconductor low-dimensional systems. E. Reyes-Gómez, A. Matos-Abiague, M. de Dios-Leyva, and L. E. Oliveira, J. Cryst. Growth **227**, 77 (2001).

14. Shallow-donor states in $\mathrm{GaAs} - \mathrm{Ga}_{1-x}\mathrm{Al}_x\mathrm{As}$ multiple quantum wells: a fractional-dimensional space approach. A. Matos-Abiague, M. de Dios-Leyva, and L. E. Oliveira, Bulgarian Journal of Physics **27**, Supplement 2, 1 (2000).

15. Deformation of quantum mechanics in fractional-dimensional space. A. Matos-Abiague, J. Phys. A: Math. Gen. **34**, 11059 (2001).

16. Fractional-dimensional space approach for parabolic-confined polarons. A. Matos-Abiague, Semicond. Sci. Technol. **17**, 150 (2002).

17. Polaron effect in $\mathrm{GaAs}-\mathrm{Ga}_{1-x}\mathrm{Al}_x\mathrm{As}$ quantum wells: a fractional-dimensional space approach. A. Matos-Abiague, Phys. Rev. B **65**, 165321 (2002).

18. A fractional-dimensional space approach to the polaron effect in quantum wells. A. Matos-Abiague, J. Phys.: Condens. Matter **14**, 4543 (2002).

19. Fractional-dimensional polaron corrections in asymmetric $\mathrm{GaAs}-\mathrm{Ga}_{1-x}\mathrm{Al}_x\mathrm{As}$ quantum wells. R. L. Rodríguez Suárez and A. Matos-Abiague, Physica E **18**, 485 (2003).

20. Ultrafast control of the electronic motion in quantum well structures. A. Matos-Abiague and J. Berakdar, Appl. Phys. Lett. **84**, 2346 (2004).

21. Comment on “Three-dimensional kicked hydrogen atom”. A. Matos-Abiague and K. A. Kouzakov, Phys. Rev. A **68**, 017401 (2003).

22. Controlling the orientation of polar molecules by half-cycle pulses. A. Matos-Abiague and J. Berakdar, Chem. Phys. Lett. **382**, 475 (2003).

23. Sustainable orientation of polar molecules induced by half-cycle pulses. A. Matos-Abiague and J. Berakdar, Phys. Rev. A **68**, 063411 (2003).

24. Femtosecond control of electronic motion in semiconductor double quantum wells. A. Matos-Abiague and J. Berakdar, Phys. Rev. B **69**, 155304 (2004).

25. Emission spectrum of an electron in a double quantum well driven by ultrashort half-cycle pulses. A. Matos-Abiague and J. Berakdar (to be published in Physica Scripta).

26. Excitonic polarons in confined systems. A. Thilagam and A. Matos-Abiague, J. Phys.: Condens. Matter **16**, 3981 (2004).

27. Emission spectrum of a mesoscopic ring driven by fast unipolar pulses. A. Matos-Abiague and J. Berakdar, Phys. Lett. A **330**, 113 (2004).

28. Field-free charge polarization of mesoscopic rings. A. Matos-Abiague and J. Berakdar, Phys. Rev. B **70**, 195338 (2004).

29. Ultrafast build-up of polarization in mesoscopic rings. A. Matos-Abiague and J. Berakdar, Europhys. Lett. **69**, 277 (2005).

30. Photo-induced charge currents in mesoscopic rings. A. Matos-Abiague and J. Berakdar (accepted in Phys. Rev. Lett.).